Electronic Supplementary Material (ESI) for Physical Chemistry Chemical Physics.

Electronic Supplementary Information

Atomic-Scale Insights in the Interplay of Chemical Composition and Chirality in Two-Dimensional Chiral Perovskites

Guilherme K. Inui,*,† Rafael Besse,*,‡ José E. González,*,† and Juarez L. F. Da Silva*,†

†*São Carlos Institute of Chemistry, University of São Paulo, P.O. Box* 780, 13560-970, *São Carlos, SP, Brazil*

‡*University of Brasília, Institute of Physics, Brasília,* 70919-970, *Brazil*

E-mail: guiinui@gmail.com; rafael.besse@gmail.com; jegonzalezmireles@gmail.com; juarez_dasilva@iqsc.usp.br

Contents

1 Introduction

The electronic supplementary information file includes detailed computational methodologies, convergence assessments, and additional details on structural, energetic, and electronic attributes. Provides additional data on the analysis of lattice parameters, unit cell volumes, effective coordination numbers (ECN), mean bond distances, energy per atom, band gaps, and properties derived from density-related electrostatic and chemical analyses. Furthermore, it provides additional data on the density of states, band structures, and band offsets.

2 Additional Computational Details

Table S1: Technical computational details of the Projector Augmented Wave (PAW) - Perdew–Burke–Ernzerhof projectors. Information of atom name, PAW projector name and date, recommended plane wave cutoff energy, ENMAX (eV), number of valence electrons, Z_{val}, and valence electronic configuration.

Element	PAW projector	ENMIN	ENMAX	Z_{val}	Valence
H	H_GW 21Apr2008	250.000	300.000	1	$1s^1$
C	C_GW_new 19Mar2012	310.494	413.992	4	$2s^2 2p^2$
N	N_GW_new 19Mar2012	315.677	420.902	5	$2s^2 2p^3$
Cl	Cl_GW 19Mar2012	196.854	262.472	7	$3s^2 3p^5$
Ge	Ge_sv_GW 26Apr2015	307.818	410.425	22	$3s^2 4s^2 4p^6 4p^2 3d^{10}$
Br	Br_GW 20Mar2012	162.214	216.285	7	$4s^2 4p^5$
Sn	Sn_sv_GW 22Nov2013	276.583	368.778	22	$4s^2 5s^2 4p^6 5p^2 4d^{10}$
I	I_GW 12Mar2012	131.735	175.647	7	$5s^2 5p^5$
Pb	Pb_sv_GW 04Apr2014	237.894	317.193	22	$5s^2 6s^2 5p^6 6p^2 5d^{10}$

3 Computational Convergence Tests

Convergence tests were performed with (S-NEA)$_2$SnCl$_4$ structure based on the (S-NEA)$_2$PbBr$_4$ prototype. This choice was made because of the smaller atom sizes for both the cation and the anion; thus, the stress tensor calculation would change the cell size and we had a more consistent convergence test.

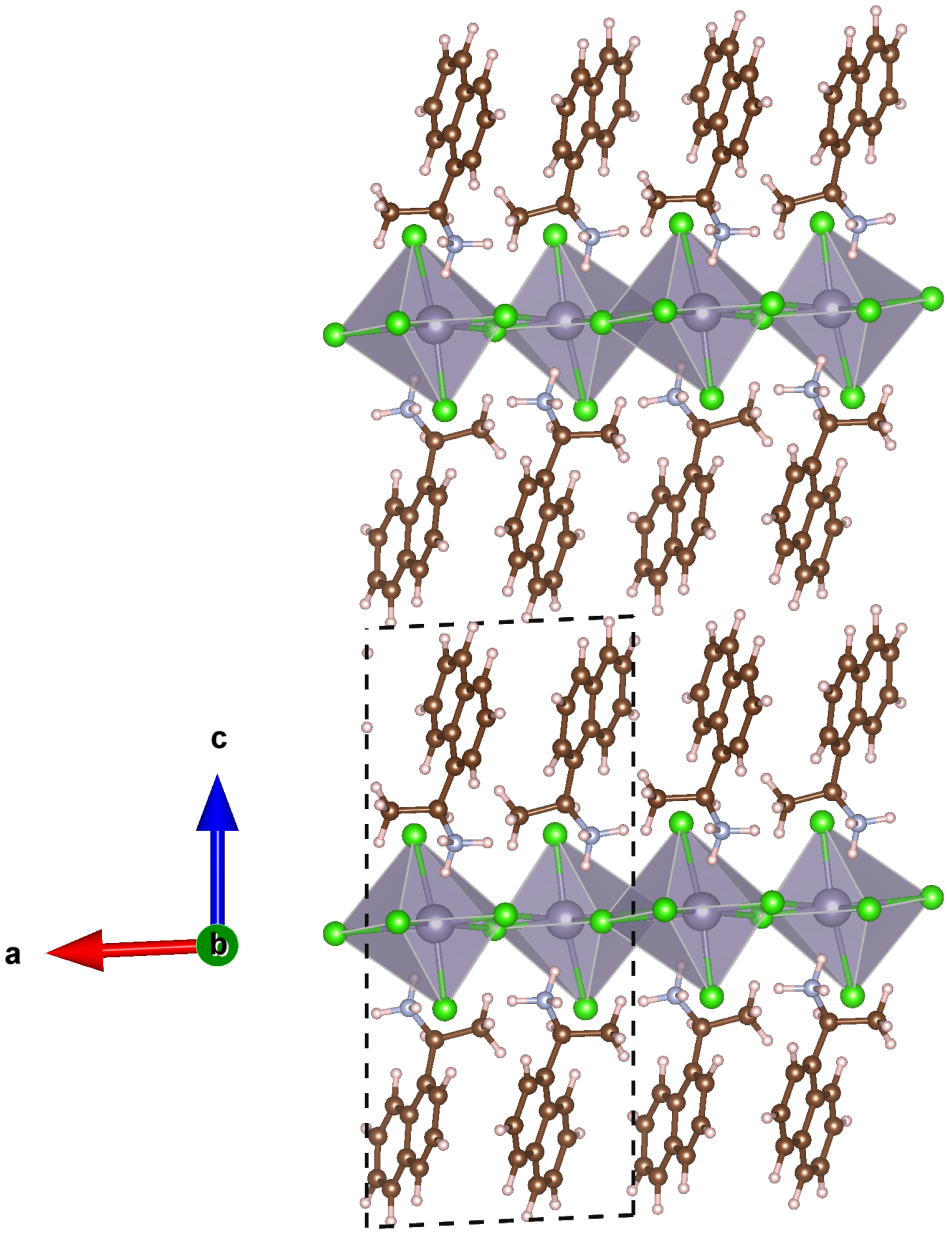

Figure S1: $(S\text{-}NEA)_2SnCl_4$ structure based on the prototype for convergence tests.

Table S2: Structural informations on Crystallographic Information Files with structure name, number of atoms (N_{at}), lattice parameters (a_0, b_0, c_0, α_0, β_0 and γ_0). Abbreviations: **NEA**: Naphthylethylammonium. Prefixes R- and S- are for right and left-hand, respectively, designated for enantiometers of chiral stereocenters.

Structure	N_{at}	a_0 (Å)	b_0 (Å)	c_0 (Å)	α_0 (°)	β_0 (°)	γ_0 (°)	Ref.
$(R\text{-}NEA)_2PbBr_4$	118	8.76	7.96	19.52	90.00	93.77	90.00	[1]
$(S\text{-}NEA)_2PbBr_4$	118	8.75	7.96	19.50	90.00	93.81	90.00	[1]

Table S3: **k**-points convergence test with ENCUT = 631.353 eV for (S-NEA)$_2$SnCl$_4$ perovskite structure with 118 atoms. Informations with automatic length ($R_{\mathbf{k}}$), generated **k**-mesh, number of **k**-points ($N_{\mathbf{k}}$), structural parameters (lattice parameters a_0, b_0, c_0 and volume V_0), energetic analysis energy per atom (E_{tot}) and gamma-point band gap (E_g^{Γ}). Relative values are indicated with Δ (e.g. $\Delta a_0 = a_0^i - a^{ref}$, $ref =$ largest number of **k**-points).

$R_{\mathbf{k}}$ (Å^{-3})	**k**-mesh	$N_{\mathbf{k}}$	a_0 (Å)	b_0 (Å)	c_0 (Å)	V_0 (Å^3)	E_{tot} (eV/atom)	E_g^{Γ} (eV)
10	$1\times1\times1$	1	8.59	7.66	19.01	1248.14	−6.09592	2.73
15	$2\times2\times1$	4	8.53	7.54	19.08	1224.72	−6.10062	2.55
20	$2\times3\times1$	4	8.51	7.54	19.06	1221.33	−6.10067	2.50
25	$3\times3\times1$	4	8.52	7.52	19.10	1221.17	−6.10076	2.53
30	$4\times4\times2$	18	8.52	7.54	19.06	1223.27	−6.10070	2.53
35	$4\times5\times2$	18	8.52	7.50	19.10	1219.31	−6.10075	2.50
40	$5\times5\times2$	18	8.52	7.52	19.10	1222.22	−6.10075	2.54
45	$5\times6\times2$	24	8.51	7.53	19.08	1221.34	−6.10072	2.51
$R_{\mathbf{k}}$ (Å^{-3})	**k**-mesh	$N_{\mathbf{k}}$	Δa_0 (Å)	Δb_0 (Å)	Δc_0 (Å)	ΔV_0 (Å^3)	ΔE_{tot} (eV/atom)	ΔE_g^{Γ} (eV)
10	$1\times1\times1$	1	0.08	0.13	−0.07	26.80	0.00480	0.22
15	$2\times2\times1$	4	0.02	0.01	0.00	3.38	0.00010	0.04
20	$2\times3\times1$	4	0.00	0.01	−0.02	−0.01	0.00005	−0.01
25	$3\times3\times1$	4	0.01	−0.01	0.02	−0.17	−0.00003	0.02
30	$4\times4\times2$	18	0.01	0.01	−0.02	1.93	0.00002	0.02
35	$4\times5\times2$	18	0.01	−0.03	0.02	−2.03	−0.00002	−0.01
40	$5\times5\times2$	18	0.01	−0.01	0.02	0.88	−0.00003	0.03
45	$5\times6\times2$	24	0.00	0.00	0.00	0.00	0.00000	0.00

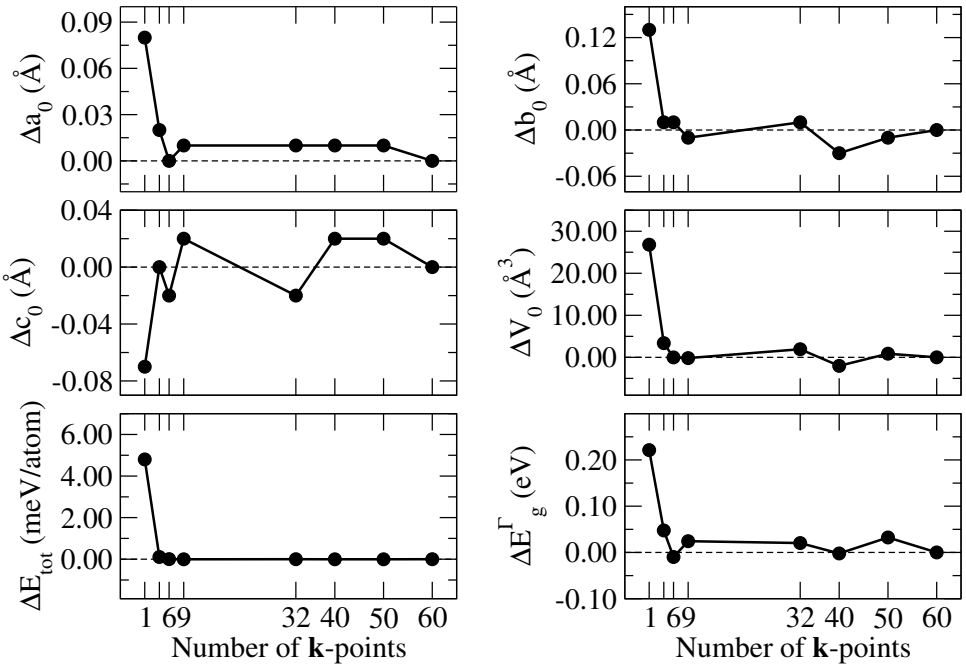

Figure S2: **k**-points convergence test for (S-NEA)$_2$SnCl$_4$ perovskite structure with physical properties relative values for lattice parameters (a_0, b_0 and c_0), volume (V_0), energy per atom (ΔE_{tot}) and gamma-point band gap (E_g^{Γ}) as a function of **k**-points number for the Brillouin Zone.

Table S4: Cutoff convergence test with $3 \times 3 \times 1$ **k**-mesh for $(\text{S-NEA})_2\text{SnCl}_4$ perovskite structure with 118 atoms. Informations with multiplier for PAW recommended $\texttt{ENMAX}_{max}$ value, cutoff energy ENCUT, structural parameters (lattice parameters a_0, b_0, c_0 and volume V_0) where ENCUT = x*$\texttt{ENMAX}_{max}$, energetic analysis energy per atom (E_{tot}) and gamma-point band gap (E_g^Γ). Relative values are indicated with Δ (e.g. $\Delta a_0 = a_0^i - a_0^{ref}$, $ref =$ highest cutoff).

x	ENCUT (eV)	a_0 (Å)	b_0 (Å)	c_0 (Å)	V_0 (Å^3)	E_{tot} (eV/atom)	E_g^Γ (eV)
1.00	420.902	7.92	7.35	18.18	1056.13	6.06706	1.99
1.25	526.128	8.36	7.48	18.88	1178.66	6.09684	2.38
1.50	631.353	8.52	7.52	19.10	1221.17	6.10076	2.53
1.75	736.578	8.56	7.54	19.15	1236.21	6.10177	2.58
2.00	841.804	8.61	7.55	19.18	1244.43	6.10223	2.62
2.25	947.029	8.61	7.54	19.22	1247.82	6.10255	2.63
2.50	1052.255	8.61	7.55	19.23	1249.95	6.10255	2.62
x	ENCUT (eV)	Δa_0 (Å)	Δb_0 (Å)	Δc_0 (Å)	ΔV_0 (Å^3)	ΔE_{tot} (eV/atom)	ΔE_g^Γ (eV)
1.00	420.902	−0.69	−0.20	−1.05	−193.82	0.03548	−0.63
1.25	526.128	−0.25	−0.07	−0.35	−71.29	0.00570	−0.24
1.50	631.353	−0.09	−0.03	−0.13	−28.78	0.00178	−0.09
1.75	736.578	−0.05	−0.01	−0.08	−13.74	0.00077	−0.03
2.00	841.804	0.00	0.00	−0.05	−5.52	0.00031	0.00
2.25	947.029	0.00	−0.01	−0.01	−2.13	0.00000	0.01
2.50	1052.255	0.00	0.00	0.00	0.00	0.00000	0.00

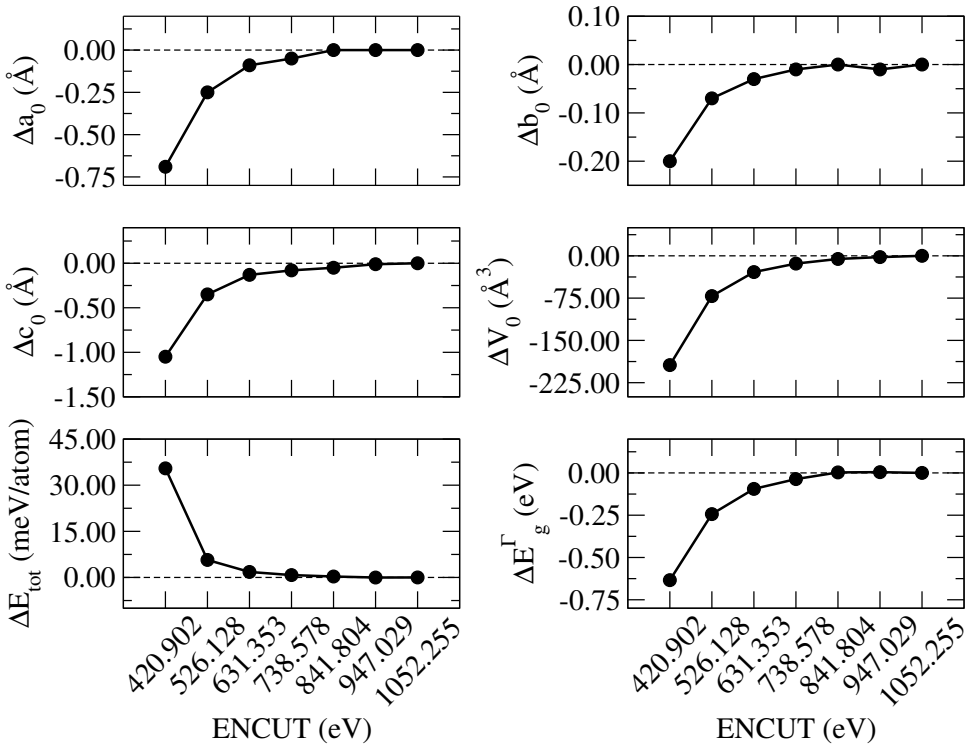

Figure S3: Cutoff energy convergence test for (S-NEA)$_2$SnCl$_4$ perovskite structure with physical properties relative values for lattice parameters (a_0, b_0 and c_0), volume (V_0), energy per atom (ΔE_{tot}) and gamma-point band gap (E_g^{Γ}) as a function of `ENCUT` input parameter based on a cutoff energy.

4 Structural and Energetic Properties

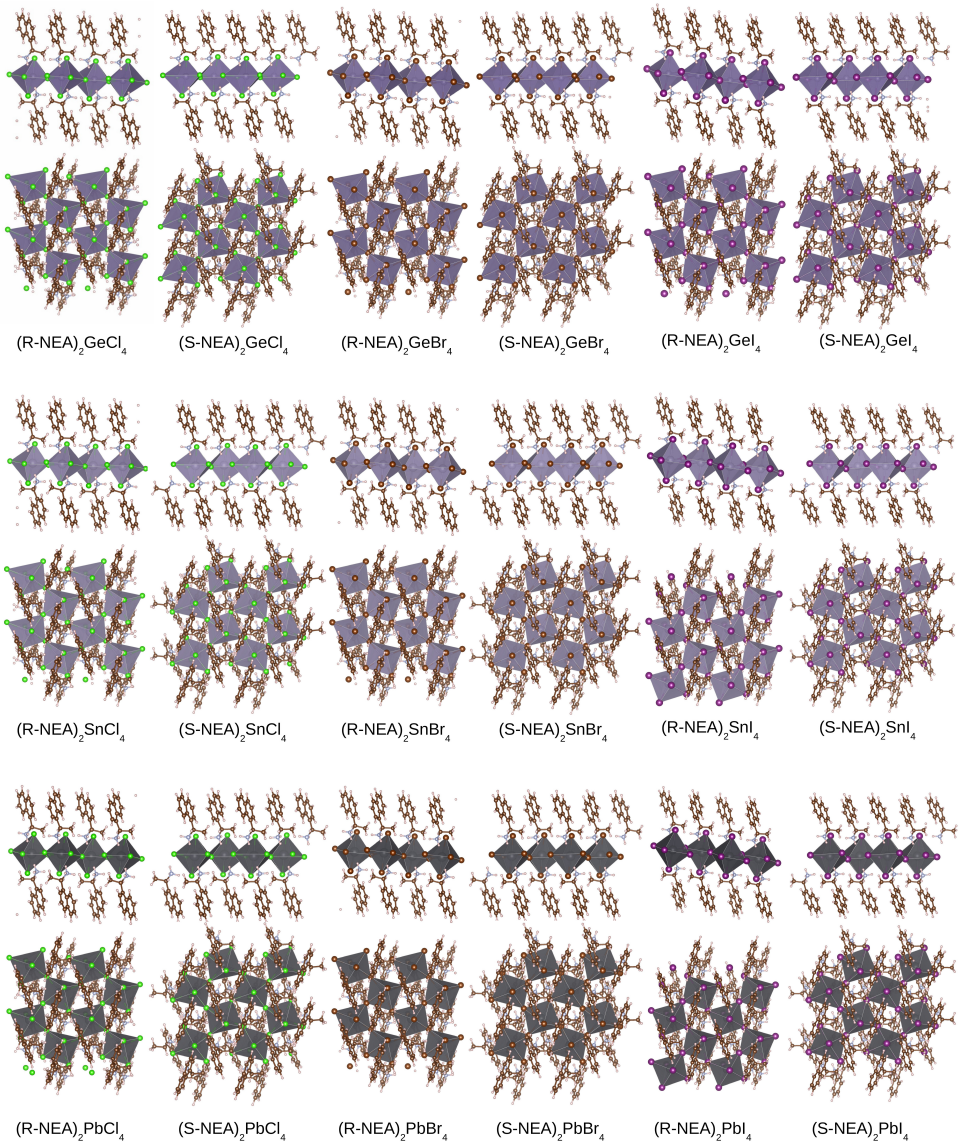

Figure S4: All chiral perovskite structures after atom changes from the literature perovskite [1] and structural optimization with PBE-GGA+D3(BJ) stress tensor.

Table S5: Structure name, lattice parameters (a_0, b_0, c_0, α_0, β_0, and γ_0), volume (V_0), average effective coordination number for B-site atoms and energy per atom for novel chiral perovskites structures with *Naphthylethylammonium* (NEA) cation and 118 atoms calculated with $3 \times 3 \times 1$ **k**-mesh and `ENCUT` = 841.804 eV.

Structure (bulk)	a_0 (Å)	b_0 (Å)	c_0 (Å)	α_0 (°)	β_0 (°)	γ_0 (°)	V_0 (Å^3)	ECN^B_{av} (NNN)	E_{tot} (eV/atom)	E^Γ_g (eV)
(R-NEA)$_2$GeCl$_4$	8.60	7.45	19.02	90.00	92.71	90.00	1218.51	3.17	−6.10261	2.73
(S-NEA)$_2$GeCl$_4$	8.61	7.45	19.01	90.00	92.67	90.00	1219.85	3.16	−6.10263	2.73
(R-NEA)$_2$GeBr$_4$	8.71	7.69	19.14	90.00	94.24	90.00	1280.73	3.62	−6.06855	2.53
(S-NEA)$_2$GeBr$_4$	8.70	7.71	19.15	90.00	94.20	90.00	1282.17	3.62	−6.06854	2.54
(R-NEA)$_2$GeI$_4$	8.89	8.00	19.31	90.00	96.40	90.00	1366.57	4.77	−6.03262	1.94
(S-NEA)$_2$GeI$_4$	8.92	8.01	19.24	90.00	96.74	90.00	1365.96	4.70	−6.03265	1.97
(R-NEA)$_2$SnCl$_4$	8.58	7.52	19.16	90.00	92.37	90.00	1237.51	3.69	−6.10225	2.54
(S-NEA)$_2$SnCl$_4$	8.57	7.53	19.15	90.00	92.30	90.00	1235.53	3.70	−6.10224	2.55
(R-NEA)$_2$SnBr$_4$	8.67	7.76	19.28	90.00	93.99	90.00	1295.51	5.23	−6.06860	2.09
(S-NEA)$_2$SnBr$_4$	8.65	7.77	19.27	90.00	94.05	90.00	1294.37	5.33	−6.06852	2.06
(R-NEA)$_2$SnI$_4$	8.96	8.09	19.52	90.00	96.21	90.00	1408.13	5.81	−6.03236	1.67
(S-NEA)$_2$SnI$_4$	8.97	8.08	19.41	90.00	96.64	90.00	1399.27	5.82	−6.03244	1.67
(R-NEA)$_2$PbCl$_4$	8.44	7.59	19.15	90.00	92.37	90.00	1227.66	4.98	−6.10466	2.90
(S-NEA)$_2$PbCl$_4$	8.46	7.58	19.15	90.00	92.38	90.00	1228.66	4.94	−6.10468	2.90
(R-NEA)$_2$PbBr$_4$	8.66	7.79	19.29	90.00	94.13	90.00	1300.95	5.51	−6.07101	2.73
(S-NEA)$_2$PbBr$_4$	8.65	7.80	19.36	90.00	93.86	90.00	1305.63	5.46	−6.07101	2.74
(R-NEA)$_2$PbI$_4$	9.02	8.12	19.51	90.00	96.60	90.00	1421.77	5.82	−6.03400	2.39
(S-NEA)$_2$PbI$_4$	9.02	8.11	19.48	90.00	96.71	90.00	1417.27	5.82	−6.03401	2.39

Table S6: Linear regression of equilibrium lattice parameters with halide atom radii for bulk models with R- or S- enantiomers and the respective bivalent metal involves determining the angular and linear coefficients for fitting the linear regression. The R^2 coefficient is used to assess the statistical measure of variance, and the relative variation (δ) from the larger to smaller halides radii is calculated by the formula $\delta = \frac{\text{larger}-\text{smaller}}{\text{smaller}} \times 100$.

a_0				
Enantiomer/Metal	Angular Coefficient	Linear Coefficient	R^2	Cl/I δ
R/Ge	0.809	7.957	0.999	3.372 %
S/Ge	0.873	7.905	0.990	3.600 %
R/Sn	1.076	7.703	0.980	4.429 %
S/Sn	1.138	7.638	0.972	4.667 %
R/Pb	1.618	7.154	0.999	6.872 %
S/Pb	1.569	7.204	0.996	6.619 %
b_0				
Enantiomer/Metal	Angular Coefficient	Linear Coefficient	R^2	Cl/I δ
R/Ge	1.524	6.250	1.000	7.383 %
S/Ge	1.547	6.238	0.999	7.517 %
R/Sn	1.583	6.271	1.000	7.580 %
S/Sn	1.524	6.330	1.000	7.304 %
R/Pb	1.479	6.414	0.999	6.983 %
S/Pb	1.472	6.416	1.000	6.992 %
c_0				
Enantiomer/Metal	Angular Coefficient	Linear Coefficient	R^2	Cl/I δ
R/Ge	0.806	18.383	1.000	1.525 %
S/Ge	0.625	18.533	0.976	1.210 %
R/Sn	1.009	18.351	0.996	1.879 %
S/Sn	0.719	18.587	0.999	1.358 %
R/Pb	1.003	18.354	0.999	1.880 %
S/Pb	0.894	18.471	0.968	1.723 %

Table S7: Linear regression of equilibrium lattice parameters with halide atom radii for bulk models with R- or S- enantiomers and the respective analyzed halide atom involves determining the angular and linear coefficients for fitting the linear regression. The R^2 coefficient is used to assess the statistical measure of variance, and the relative variation (δ) from the larger to smaller bivalent cation radii is calculated by the formula $\delta = \frac{\text{larger}-\text{smaller}}{\text{smaller}} \times 100$.

a_0				
Enantiomer/Metal	Angular Coefficient	Linear Coefficient	R^2	Ge/Pb δ
R/Cl	−0.477	9.214	0.811	−1.860 %
S/Cl	−0.464	9.203	0.888	−1.742 %
R/Br	−0.177	8.930	0.993	−0.574 %
S/Br	−0.185	8.929	0.953	−0.575 %
R/I	0.432	8.346	0.985	1.462 %
S/I	0.329	8.505	0.977	1.121 %
b_0				
Enantiomer/Metal	Angular Coefficient	Linear Coefficient	R^2	Ge/Pb δ
R/Cl	0.461	6.869	0.977	1.879 %
S/Cl	0.440	6.898	0.997	1.745 %
R/Br	0.346	7.258	1.000	1.300 %
S/Br	0.309	7.324	1.000	1.038 %
R/I	0.420	7.477	0.998	1.500 %
S/I	0.346	7.578	1.000	1.248 %
c_0				
Enantiomer/Metal	Angular Coefficient	Linear Coefficient	R^2	Ge/Pb δ
R/Cl	0.490	18.417	0.932	0.683 %
S/Cl	0.519	18.370	0.953	0.736 %
R/Br	0.548	18.463	0.969	0.784 %
S/Br	0.703	18.266	0.991	1.097 %
R/I	0.750	18.387	0.939	1.036 %
S/I	0.831	18.202	1.000	1.247 %

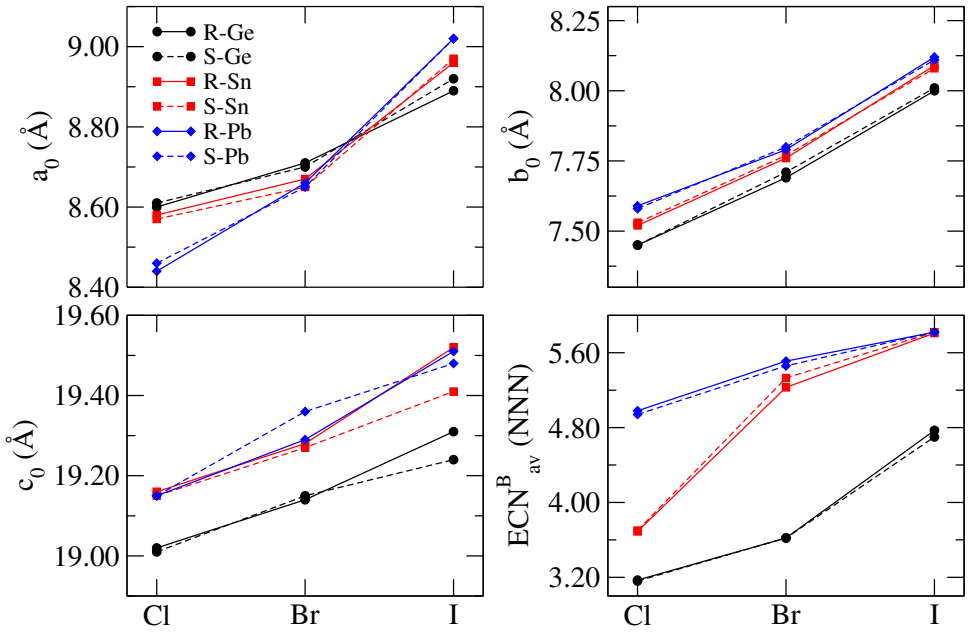

Figure S5: Equilibrium lattice parameters (a_0, b_0 and c_0) and effective coordination number for different cations and anions for bulk chiral perovskite with R- and S- Naphthylethylammonium (NEA) cation.

Table S8: Structure name, lattice parameters (a_0, b_0, c_0, α_0, β_0, and γ_0), and energy per atom for novel chiral perovskites slabs with *Naphthylethylammonium* (NEA) cation, 118 atoms and a 15 Å vacuum between layers calculated with $3 \times 3 \times 1$ **k**-mesh and `ENCUT` = 841.804 eV.

Structure (slab)	a_0 (Å)	b_0 (Å)	c_0 (Å)	α_0 (°)	β_0 (°)	γ_0 (°)	ECN^B_{av} (NNN)	E_{tot} (eV/atom)	E_g^Γ (eV)
(R-NEA)$_2$GeCl$_4$	8.64	7.39	33.76	90.00	90.00	90.00	3.13	−6.09795	2.82
(S-NEA)$_2$GeCl$_4$	8.63	7.39	33.75	90.00	90.00	90.00	3.15	−6.09795	2.80
(R-NEA)$_2$GeBr$_4$	8.70	7.69	33.90	90.00	90.00	90.00	3.61	−6.06329	2.62
(S-NEA)$_2$GeBr$_4$	8.70	7.70	33.89	90.00	90.00	90.00	3.63	−6.06328	2.62
(R-NEA)$_2$GeI$_4$	8.87	7.99	34.22	90.00	90.00	90.00	4.78	−6.02717	1.93
(S-NEA)$_2$GeI$_4$	8.87	7.98	34.25	90.00	90.00	90.00	4.78	−6.02718	1.93
(R-NEA)$_2$SnCl$_4$	8.61	7.47	33.86	90.00	90.00	90.00	3.72	−6.09737	2.59
(S-NEA)$_2$SnCl$_4$	8.61	7.43	33.85	90.00	90.00	90.00	3.79	−6.09745	2.55
(R-NEA)$_2$SnBr$_4$	8.69	7.65	33.96	90.00	90.00	90.00	5.19	−6.06347	2.09
(S-NEA)$_2$SnBr$_4$	8.68	7.70	33.93	90.00	90.00	90.00	5.23	−6.06342	2.12
(R-NEA)$_2$SnI$_4$	8.88	8.04	34.31	90.00	90.00	90.00	5.77	−6.02679	1.64
(S-NEA)$_2$SnI$_4$	8.93	8.05	34.28	90.00	90.00	90.00	5.78	−6.02700	1.64
(R-NEA)$_2$PbCl$_4$	8.50	7.49	33.87	90.00	90.00	90.00	4.95	−6.09983	3.05
(S-NEA)$_2$PbCl$_4$	8.50	7.46	33.86	90.00	90.00	90.00	4.89	−6.09988	3.05
(R-NEA)$_2$PbBr$_4$	8.66	7.76	33.99	90.00	90.00	90.00	5.47	−6.06577	2.79
(S-NEA)$_2$PbBr$_4$	8.65	7.72	34.02	90.00	90.00	90.00	5.46	−6.06585	2.77
(R-NEA)$_2$PbI$_4$	8.99	8.07	34.35	90.00	90.00	90.00	5.78	−6.02858	2.41
(S-NEA)$_2$PbI$_4$	9.00	8.08	34.28	90.00	90.00	90.00	5.79	−6.02860	2.41

Table S9: Linear regression of equilibrium lattice parameters with halide atom radii for slab models with R- or S- enantiomers and the respective bivalent metal involves determining the angular and linear coefficients for fitting the linear regression. The R^2 coefficient is used to assess the statistical measure of variance, and the relative variation (δ) from the larger to smaller halides radii is calculated by the formula $\delta = \frac{\text{larger}-\text{smaller}}{\text{smaller}} \times 100$.

a_0				
Enantiomer/Metal	Angular Coefficient	Linear Coefficient	R^2	Cl/I δ
R/Ge	0.650	8.113	0.985	2.662 %
S/Ge	0.676	8.085	0.990	2.780 %
R/Sn	0.760	7.997	0.991	3.135 %
S/Sn	0.908	7.868	0.976	3.716 %
R/Pb	1.375	7.397	0.995	5.764 %
S/Pb	1.407	7.366	0.991	5.882 %
b_0				
Enantiomer/Metal	Angular Coefficient	Linear Coefficient	R^2	Cl/I δ
R/Ge	1.651	6.105	0.995	8.119 %
S/Ge	1.619	6.136	0.992	7.983 %
R/Sn	1.601	6.183	0.994	7.630 %
S/Sn	1.719	6.077	1.000	8.344 %
R/Pb	1.602	6.235	0.998	7.743 %
S/Pb	1.722	6.100	1.000	8.310 %
c_0				
Enantiomer/Metal	Angular Coefficient	Linear Coefficient	R^2	Cl/I δ
R/Ge	1.294	32.718	0.992	1.392 %
S/Ge	1.410	32.610	0.988	1.481 %
R/Sn	1.277	32.818	0.977	1.329 %
S/Sn	1.225	32.844	0.968	1.270 %
R/Pb	1.358	32.767	0.983	1.417 %
S/Pb	1.171	32.929	0.999	1.240 %

Table S10: Linear regression of equilibrium lattice parameters with halide atom radii for slab models with R- or S- enantiomers and the respective analyzed halide atom involves determining the angular and linear coefficients for fitting the linear regression. The R^2 coefficient is used to assess the statistical measure of variance, and the relative variation (δ) from the larger to smaller bivalent cation radii is calculated by the formula $\delta = \frac{\text{larger}-\text{smaller}}{\text{smaller}} \times 100$.

a_0				
Enantiomer/Metal	Angular Coefficient	Linear Coefficient	R^2	Ge/Pb δ
R/Cl	−0.427	9.187	0.861	−1.620 %
S/Cl	−0.390	9.132	0.828	−1.506 %
R/Br	−0.123	8.858	0.879	−0.459 %
S/Br	−0.160	8.903	0.946	−0.574 %
R/I	0.353	8.414	0.788	1.352 %
S/I	0.424	8.335	0.966	1.465 %
b_0				
Enantiomer/Metal	Angular Coefficient	Linear Coefficient	R^2	Ge/Pb δ
R/Cl	0.354	6.950	0.993	1.353 %
S/Cl	0.234	7.095	0.991	0.947 %
R/Br	0.168	7.463	0.448	0.910 %
S/Br	0.057	7.625	0.739	0.259 %
R/I	0.272	7.650	0.997	1.001 %
S/I	0.346	7.548	1.000	1.253 %
c_0				
Enantiomer/Metal	Angular Coefficient	Linear Coefficient	R^2	Ge/Pb δ
R/Cl	0.399	33.266	0.975	0.325 %
S/Cl	0.399	33.256	0.975	0.326 %
R/Br	0.309	33.514	1.000	0.265 %
S/Br	0.407	33.371	0.907	0.384 %
R/I	0.449	33.659	1.000	0.380 %
S/I	0.111	34.113	0.953	0.088 %

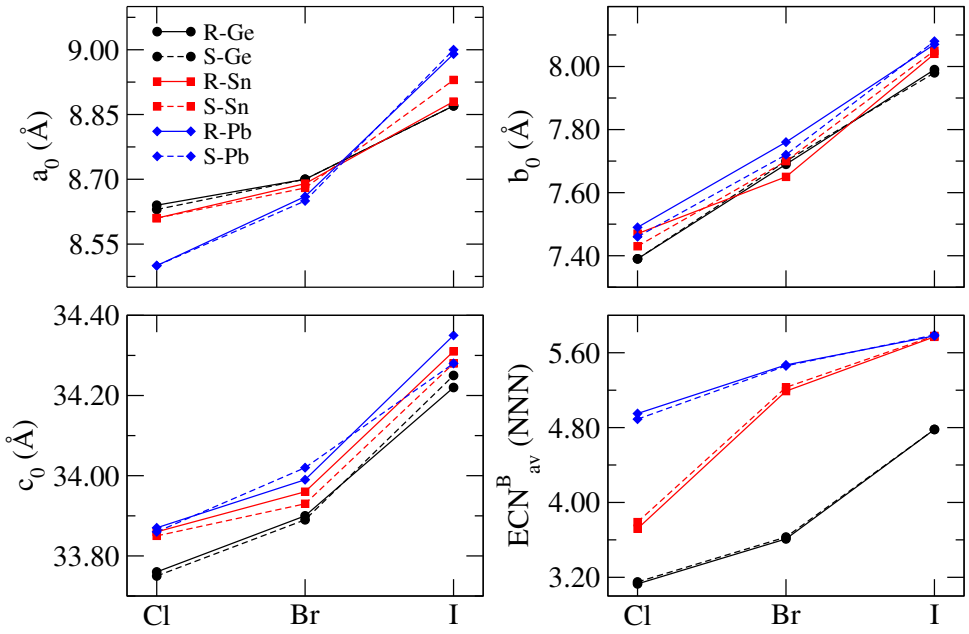

Figure S6: Equilibrium lattice parameters (a_0, b_0 and c_0) and effective coordination number for different cations and anions for slabs of chiral perovskite with R- and S-Naphthylethylammonium (NEA) cation.

Table S11: Differentiation of structural and energetic parameters between bulks and slabs of novel chiral perovskites with *Naphthylethylammonium* (NEA) cation with structure name, lattice parameters (Δa_0, Δb_0), energy per atom (ΔE_{tot}), and band gap energy (ΔE_g^{Γ}) (the difference is calculated as bulk minus slab values e.g. $\Delta a_0 = a_0^{bulk} - a_0^{slab}$). The structure contains 118 atoms calculated with $3 \times 3 \times 1$ **k**-mesh and ENCUT = 841.804 eV .

Structure	Δa_0 (Å)	Δb_0 (Å)	ΔECN^B_{av} (NNN)	ΔE_{tot} (eV/atom)	ΔE_g^{Γ} (eV)
(R-NEA)$_2$GeCl$_4$	−0.04	0.06	0.04	−0.00466	−0.09
(S-NEA)$_2$GeCl$_4$	−0.02	0.07	0.01	−0.00467	−0.06
(R-NEA)$_2$GeBr$_4$	0.00	0.01	0.01	−0.00526	−0.08
(S-NEA)$_2$GeBr$_4$	0.00	0.01	−0.01	−0.00526	−0.07
(R-NEA)$_2$GeI$_4$	0.01	0.01	−0.01	−0.00544	0.01
(S-NEA)$_2$GeI$_4$	0.05	0.02	−0.08	−0.00546	0.04
(R-NEA)$_2$SnCl$_4$	−0.03	0.05	−0.03	−0.00487	−0.05
(S-NEA)$_2$SnCl$_4$	−0.04	0.10	−0.09	−0.00478	0.00
(R-NEA)$_2$SnBr$_4$	−0.02	0.11	0.04	−0.00512	0.00
(S-NEA)$_2$SnBr$_4$	−0.03	0.07	0.10	−0.00510	−0.06
(R-NEA)$_2$SnI$_4$	0.08	0.05	0.04	−0.00557	0.02
(S-NEA)$_2$SnI$_4$	0.04	0.03	0.04	−0.00543	0.03
(R-NEA)$_2$PbCl$_4$	−0.06	0.10	0.03	−0.00483	−0.15
(S-NEA)$_2$PbCl$_4$	−0.05	0.12	0.05	−0.00480	−0.14
(R-NEA)$_2$PbBr$_4$	0.01	0.03	0.04	−0.00523	−0.06
(S-NEA)$_2$PbBr$_4$	0.00	0.08	0.00	−0.00516	−0.03
(R-NEA)$_2$PbI$_4$	0.03	0.05	0.04	−0.00541	−0.01
(S-NEA)$_2$PbI$_4$	0.02	0.03	0.03	−0.00541	−0.02

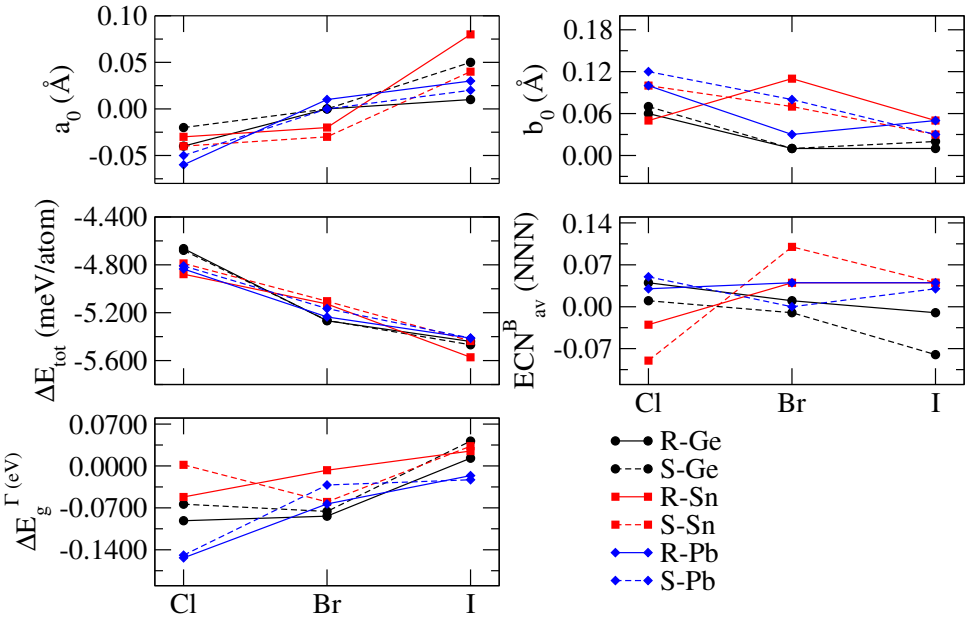

Figure S7: Difference between bulk and slab lattice properties a_0 and b_0, effective coordination number for B-site atom (ECN^B_{av}), total energy (E_{tot}) and gamma point band gap (E^{Γ}_g) of chiral perovskites comparing R- and S- *Naphthylethylammonium* (NEA) cation.

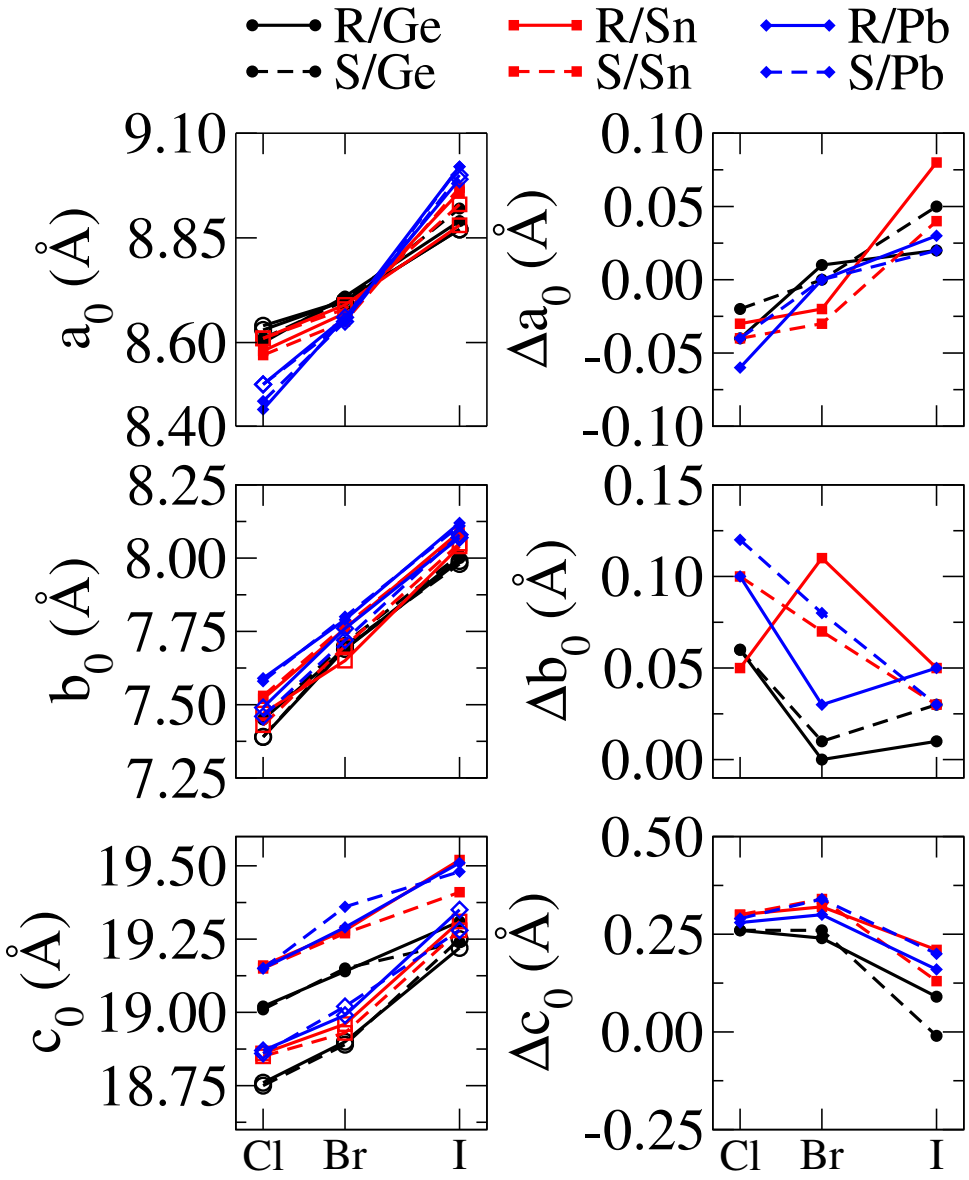

Figure S8: Equilibrium lattice parameters (a_0, b_0, and c_0) for chiral perovskites A_2BX_4 with A = R- and S-1–(1–naphthyl)ethylammonium (NEA) cation. Full symbols represent bulk structures values and empty symbols are for slabs. Δ represents differences between bulk and slab. The c_0 values for slabs were obtained by reducing their measurements by 15 Å to exclude the vacuum region and obtain a more accurate comparison with a projection on z-axis on bulk values.

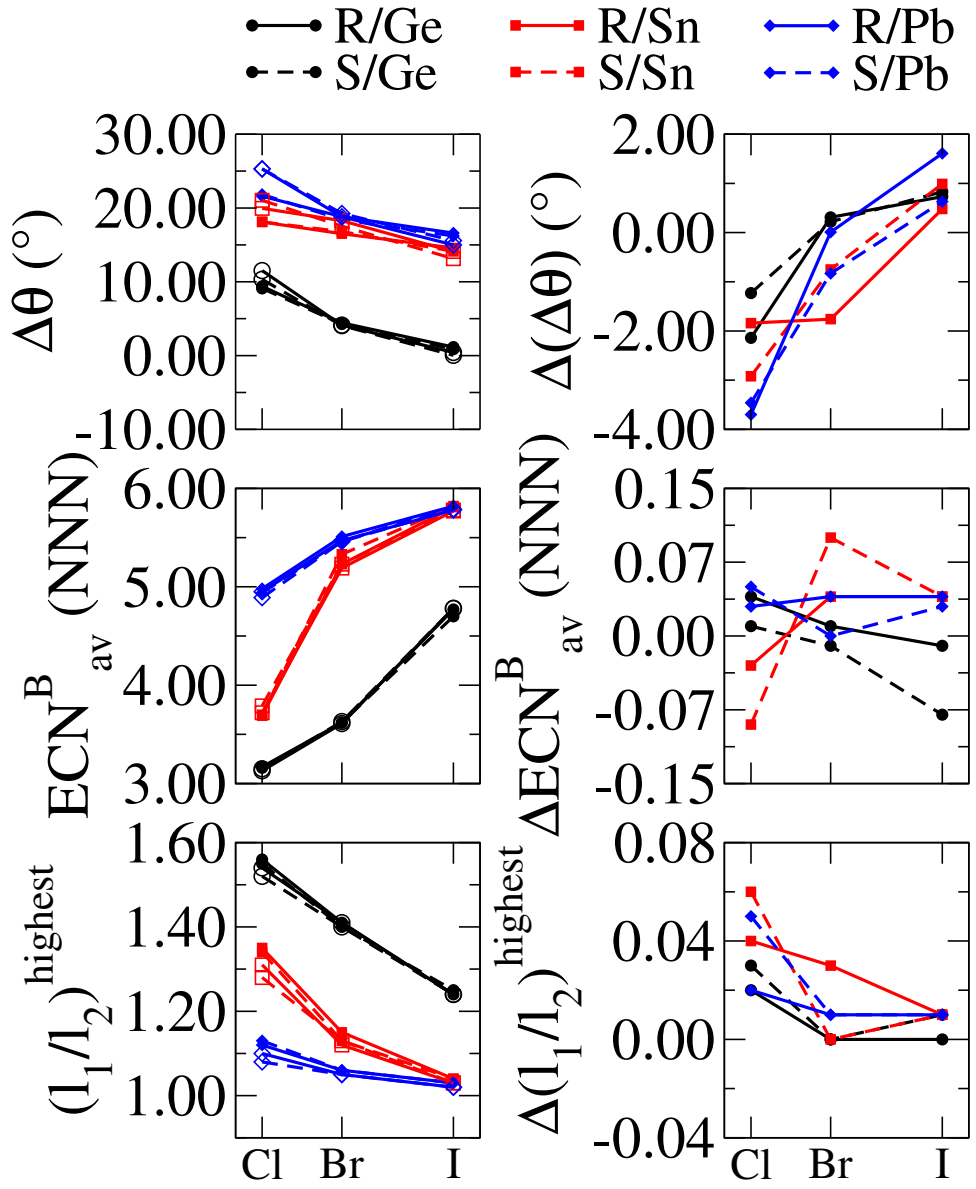

Figure S9: Local structure parameters for chiral perovskites A_2BX_4 with A = R- and S-1–(1–naphthyl)ethylammonium (NEA) cation. $\Delta\theta$ octahedron distortion, average effective coordination number of metal atoms (ECN^{B}_{av}), and the highest value for opposite bond lengths ratio (l_1/l_2). Full symbols represents bulk structures and empty symbols are for slabs. Δ represents the differences between bulk and slab.

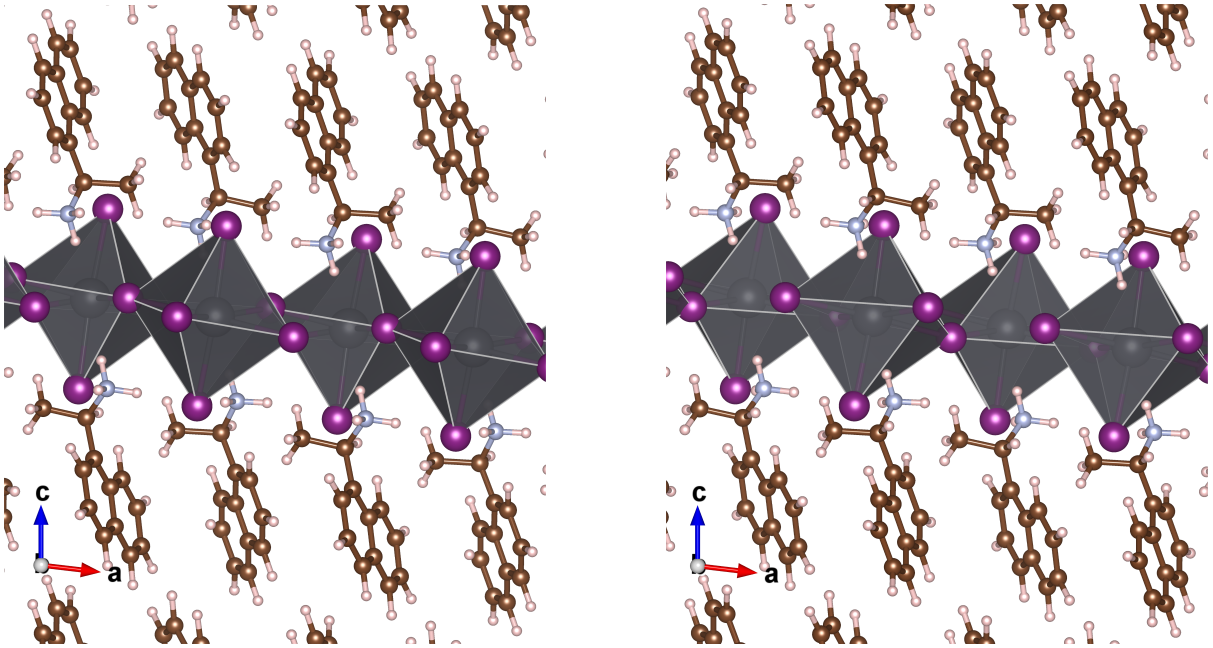

(a) $(R\text{-}NEA)_2PbI_4$ (b) $(S\text{-}NEA)_2PbI_4$

Figure S10: Visual comparison of R- and S- structures using Visualization for Electronic and Structural Analysis (VESTA)[2] software.

Table S12: Comparison of opposite distances in the octahedron between B and X on bulk perovskites with *Naphthylethylammonium* (NEA) cation where l_1 is a bond lenght and l_2 its opposite bond lenght and l_1/l_2 being the ratio between bond lenght and its opposite. All calculations were performed with $3 \times 3 \times 1$ **k**-mesh and ENCUT = 841.804 eV .

Structure (bulk)	l_1 (Å)	l_2 (Å)	l_1/l_2	Structure (bulk)	l_1 (Å)	l_2 (Å)	l_1/l_2
(R-NEA)$_2$GeCl$_4$	2.92	2.56	1.14	(S-NEA)$_2$GeCl$_4$	2.93	2.56	1.14
	3.22	2.44	1.31		3.22	2.43	1.32
	3.72	2.37	1.56		3.69	2.37	1.55
(R-NEA)$_2$GeBr$_4$	2.99	2.75	1.08	(S-NEA)$_2$GeBr$_4$	2.99	2.74	1.09
	3.27	2.60	1.25		3.26	2.60	1.25
	3.59	2.54	1.41		3.58	2.55	1.40
(R-NEA)$_2$GeI$_4$	3.04	2.96	1.02	(S-NEA)$_2$GeI$_4$	3.04	2.96	1.02
	3.26	2.84	1.14		3.28	2.84	1.15
	3.50	2.80	1.24		3.53	2.80	1.25
(R-NEA)$_2$SnCl$_4$	3.01	2.73	1.10	(S-NEA)$_2$SnCl$_4$	3.01	2.74	1.10
	3.14	2.69	1.17		3.13	2.69	1.16
	3.50	2.60	1.35		3.48	2.60	1.34
(R-NEA)$_2$SnBr$_4$	3.02	2.89	1.04	(S-NEA)$_2$SnBr$_4$	3.01	2.88	1.05
	3.08	2.92	1.05		3.06	2.93	1.04
	3.28	2.85	1.15		3.24	2.87	1.13
(R-NEA)$_2$SnI$_4$	3.17	3.10	1.02	(S-NEA)$_2$SnI$_4$	3.18	3.11	1.02
	3.18	3.15	1.01		3.18	3.15	1.01
	3.26	3.12	1.04		3.26	3.13	1.04
(R-NEA)$_2$PbCl$_4$	2.94	2.80	1.05	(S-NEA)$_2$PbCl$_4$	2.94	2.80	1.05
	2.95	2.91	1.01		2.96	2.91	1.02
	3.16	2.83	1.12		3.18	2.82	1.13
(R-NEA)$_2$PbBr$_4$	3.04	2.95	1.03	(S-NEA)$_2$PbBr$_4$	3.04	2.96	1.03
	3.04	3.04	1.00		3.05	3.04	1.00
	3.17	2.99	1.06		3.17	2.99	1.06
(R-NEA)$_2$PbI$_4$	3.21	3.21	1.00	(S-NEA)$_2$PbI$_4$	3.21	3.21	1.00
	3.21	3.16	1.02		3.22	3.17	1.02
	3.28	3.18	1.03		3.27	3.19	1.03

Table S13: Comparison of opposite distances in the octahedron between B and X on slabs of perovskites with *Naphthylethylammonium* (NEA) cation where l_1 is a bond lenght and l_2 its opposite bond lenght and l_1/l_2 being the ratio between bond lenght and its opposite. All calculations were performed with $3 \times 3 \times 1$ **k**-mesh and ENCUT = 841.804 eV .

Structure (slab)	l_1 (Å)	l_2 (Å)	l_1/l_2	Structure (slab)	l_1 (Å)	l_2 (Å)	l_1/l_2
(R-NEA)$_2$GeCl$_4$	2.93	2.54	1.15	(S-NEA)$_2$GeCl$_4$	2.92	2.54	1.14
	3.23	2.43	1.32		3.21	2.43	1.32
	3.65	2.37	1.54		3.62	2.37	1.52
(R-NEA)$_2$GeBr$_4$	3.00	2.74	1.09	(S-NEA)$_2$GeBr$_4$	2.99	2.74	1.09
	3.26	2.60	1.25		3.25	2.60	1.25
	3.60	2.55	1.41		3.59	2.55	1.40
(R-NEA)$_2$GeI$_4$	3.05	2.95	1.03	(S-NEA)$_2$GeI$_4$	3.05	2.96	1.03
	3.25	2.84	1.14		3.26	2.84	1.14
	3.49	2.81	1.24		3.49	2.81	1.24
(R-NEA)$_2$SnCl$_4$	2.98	2.72	1.09	(S-NEA)$_2$SnCl$_4$	2.99	2.71	1.10
	3.08	2.69	1.14		3.06	2.71	1.12
	3.43	2.61	1.31		3.37	2.63	1.28
(R-NEA)$_2$SnBr$_4$	3.01	2.88	1.04	(S-NEA)$_2$SnBr$_4$	3.02	2.88	1.04
	3.04	2.91	1.04		3.04	2.91	1.04
	3.22	2.86	1.12		3.24	2.85	1.13
(R-NEA)$_2$SnI$_4$	3.15	3.13	1.00	(S-NEA)$_2$SnI$_4$	3.16	3.12	1.01
	3.17	3.10	1.02		3.17	3.11	1.01
	3.22	3.11	1.03		3.22	3.11	1.03
(R-NEA)$_2$PbCl$_4$	2.93	2.89	1.01	(S-NEA)$_2$PbCl$_4$	2.92	2.90	1.00
	2.92	2.80	1.04		2.94	2.80	1.05
	3.13	2.82	1.10		3.08	2.85	1.08
(R-NEA)$_2$PbBr$_4$	3.03	3.02	1.00	(S-NEA)$_2$PbBr$_4$	3.02	3.02	1.00
	3.03	2.95	1.02		3.04	2.95	1.03
	3.14	2.98	1.05		3.14	2.99	1.05
(R-NEA)$_2$PbI$_4$	3.19	3.19	1.00	(S-NEA)$_2$PbI$_4$	3.19	3.19	1.00
	3.22	3.16	1.01		3.22	3.16	1.01
	3.24	3.17	1.02		3.24	3.17	1.02

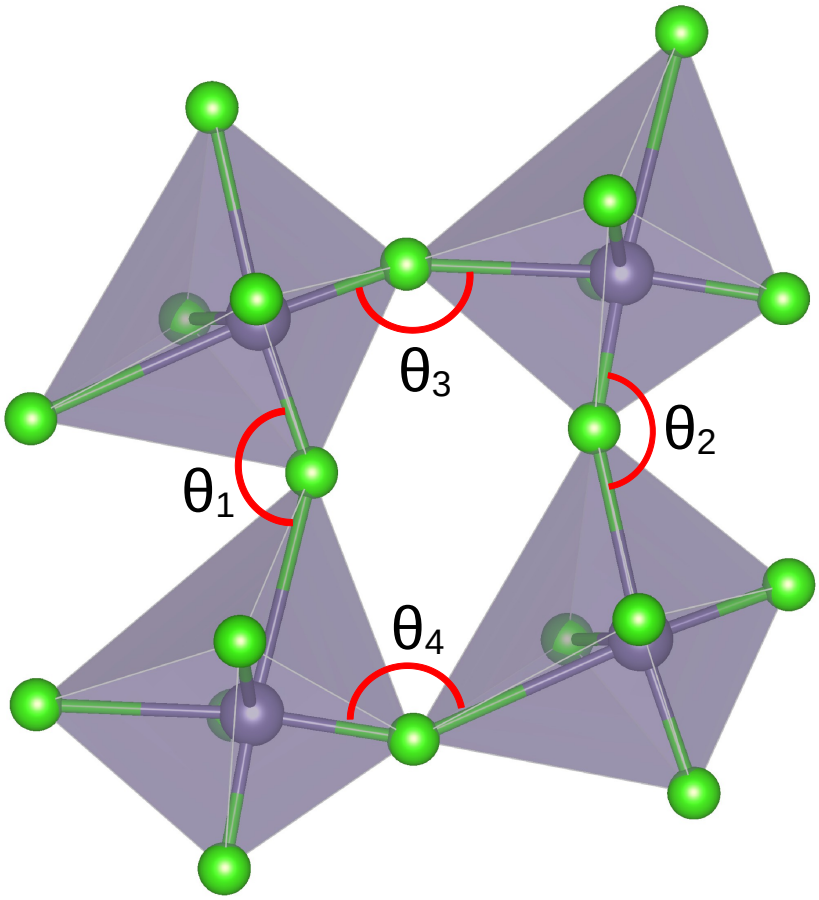

Figure S11: Octahedron distortion analysis performed through θ.

Table S14: Structural distortion between inorganic octahedrons for bulk systems of NEA-based chiral perovskites. $\Delta\theta$ is calculated based on the formula $\Delta\theta = \frac{|\theta_1-\theta_2|+|\theta_3-\theta_4|}{2}$.

System (bulk)	θ_1 (°)	θ_2 (°)	θ_3 (°)	θ_4 (°)	$\Delta\theta$ (°)
(R-NEA)$_2$GeCl$_4$	156.02	146.64	156.02	146.64	9.38
(S-NEA)$_2$GeCl$_4$	157.10	147.99	157.10	147.99	9.10
(R-NEA)$_2$GeBr$_4$	152.73	148.30	152.73	148.30	4.43
(S-NEA)$_2$GeBr$_4$	153.07	148.79	153.07	148.79	4.28
(R-NEA)$_2$GeI$_4$	149.32	148.16	149.32	148.16	1.16
(S-NEA)$_2$GeI$_4$	148.84	147.97	148.84	147.97	0.87
(R-NEA)$_2$SnCl$_4$	156.89	138.77	156.89	138.77	18.11
(S-NEA)$_2$SnCl$_4$	156.98	138.86	156.98	138.86	18.12
(R-NEA)$_2$SnBr$_4$	156.83	140.30	156.83	140.30	16.52
(S-NEA)$_2$SnBr$_4$	157.76	140.96	157.76	140.96	16.80
(R-NEA)$_2$SnI$_4$	151.96	137.38	151.96	137.38	14.58
(S-NEA)$_2$SnI$_4$	151.34	137.22	151.34	137.22	14.12
(R-NEA)$_2$PbCl$_4$	159.56	137.97	159.56	137.97	21.59
(S-NEA)$_2$PbCl$_4$	159.71	137.87	159.71	137.87	21.84
(R-NEA)$_2$PbBr$_4$	155.47	136.66	155.47	136.66	18.82
(S-NEA)$_2$PbBr$_4$	154.80	136.37	154.80	136.37	18.42
(R-NEA)$_2$PbI$_4$	150.26	133.66	150.26	133.66	16.60
(S-NEA)$_2$PbI$_4$	149.86	133.65	149.86	133.65	16.21

Table S15: Structural distortion between inorganic octahedrons for slab systems of NEA-based chiral perovskites. $\Delta\theta$ is calculated based on the formula $\Delta\theta = \frac{|\theta_1-\theta_2|+|\theta_3-\theta_4|}{2}$.

System (slab)	θ_1 (°)	θ_2 (°)	θ_3 (°)	θ_4 (°)	$\Delta\theta$ (°)
(R-NEA_2)$GeCl_4$	159.37	147.86	159.37	147.86	11.52
(S-NEA_2)$GeCl_4$	159.89	149.56	159.89	149.56	10.33
(R-NEA)$_2GeBr_4$	152.42	148.30	152.42	148.30	4.12
(S-NEA)$_2GeBr_4$	152.84	148.77	152.84	148.77	4.06
(R-NEA)$_2GeI_4$	148.97	148.55	148.97	148.55	0.43
(S-NEA)$_2GeI_4$	148.56	148.53	148.56	148.53	0.04
(R-NEA)$_2SnCl_4$	157.78	137.83	157.78	137.83	19.95
(S-NEA)$_2SnCl_4$	159.54	138.43	159.41	138.44	21.04
(R-NEA)$_2SnBr_4$	156.95	139.36	156.89	137.94	18.28
(S-NEA)$_2SnBr_4$	157.31	139.35	156.46	139.32	17.55
(R-NEA)$_2SnI_4$	151.06	136.96	151.06	136.96	14.10
(S-NEA)$_2SnI_4$	150.35	137.16	150.21	137.13	13.13
(R-NEA)$_2PbCl_4$	161.86	136.57	161.86	136.57	25.29
(S-NEA)$_2PbCl_4$	162.27	136.70	161.91	136.88	25.30
(R-NEA)$_2PbBr_4$	154.42	135.61	154.42	135.61	18.81
(S-NEA)$_2PbBr_4$	154.45	134.98	154.16	135.12	19.25
(R-NEA)$_2PbI_4$	148.44	133.46	148.44	133.46	14.99
(S-NEA)$_2PbI_4$	148.59	133.41	149.11	133.13	15.58

Table S16: Structural distortion between inorganic octahedrons for bulk and slab systems of NEA-based chiral perovskites. $\Delta\theta$ is calculated based on the formula $\Delta\theta = \frac{|\theta_1-\theta_2|+|\theta_3-\theta_4|}{2}$.

System	$\Delta\theta$ (bulk) (°)	$\Delta\theta$ (slab) (°)
(R-NEA$_2$)GeCl$_4$	9.38	11.52
(S-NEA$_2$)GeCl$_4$	9.10	10.33
(R-NEA)$_2$GeBr$_4$	4.43	4.12
(S-NEA)$_2$GeBr$_4$	4.28	4.06
(R-NEA)$_2$GeI$_4$	1.16	0.43
(S-NEA)$_2$GeI$_4$	0.87	0.04
(R-NEA)$_2$SnCl$_4$	18.11	19.95
(S-NEA)$_2$SnCl$_4$	18.12	21.04
(R-NEA)$_2$SnBr$_4$	16.52	18.28
(S-NEA)$_2$SnBr$_4$	16.80	17.55
(R-NEA)$_2$SnI$_4$	14.58	14.10
(S-NEA)$_2$SnI$_4$	14.12	13.13
(R-NEA)$_2$PbCl$_4$	21.59	25.29
(S-NEA)$_2$PbCl$_4$	21.84	25.30
(R-NEA)$_2$PbBr$_4$	18.82	18.81
(S-NEA)$_2$PbBr$_4$	18.42	19.25
(R-NEA)$_2$PbI$_4$	16.60	14.99
(S-NEA)$_2$PbI$_4$	16.21	15.58

Table S17: Free atom energies calculated with a 15 Å×15.5 Å×16 Å sized orthorhombic vacuum box.

Atom	$E_{\text{isolated atom}}$ (eV)	E_{HOMO} (eV)	E_{LUMO} (eV)	Unpaired electrons (e)
Ge	−0.800278	-4.3283	-4.1800	2
Sn	−0.713017	-4.0343	-3.9389	2
Pb	−0.642885	-3.8204	-3.7536	2
Cl	−0.348993	-8.0692	-7.6554	1
Br	−0.268894	-7.7373	-7.1381	1
I	−0.212483	-6.6357	-6.4735	1
C	−1.377021	-6.0625	-5.5494	2
N	−3.127995	-8.2701	-4.1086	3
H	−1.115599	-7.5801	-0.1085	1

Table S18: Energetic analysis for NEA-based bulk chiral perovskites with cohesive energy per atom calculated with $E_{coh}^{part} = \frac{1}{N_{part}}(E_{tot}^{part} - \sum_{i=1}^{N_{part}} E_i^{atom})$, where $part = org, inorg$, N is the total number of atoms for both frozen organic and inorganic perovskite framework, and binding energy (E_b) calculated with $E_b = E_{tot} - E_{org}^{frozen} - E_{inorg}^{frozen}$.

System (bulk)	E_{coh} ($\mathrm{eV\,atom^{-1}}$)	$E_{\mathrm{coh}}^{\mathrm{org}}$ ($\mathrm{eV\,atom^{-1}}$)	$E_{\mathrm{coh}}^{\mathrm{inorg}}$ ($\mathrm{eV\,atom^{-1}}$)	E_b ($\mathrm{eV\,atom^{-1}}$)
(R-NEA)$_2$GeCl$_4$	−4.869777	−4.907863	−2.149425	−0.195680
(S-NEA)$_2$GeCl$_4$	−4.869797	−4.907948	−2.147790	−0.195761
(R-NEA)$_2$GeBr$_4$	−4.841150	−4.907123	−1.959674	−0.183811
(S-NEA)$_2$GeBr$_4$	−4.841139	−4.907123	−1.961735	−0.183626
(R-NEA)$_2$GeI$_4$	−4.809035	−4.905783	−1.798915	−0.166547
(S-NEA)$_2$GeI$_4$	−4.809066	−4.905724	−1.796049	−0.166874
(R-NEA)$_2$SnCl$_4$	−4.870893	−4.907473	−2.196379	−0.193174
(S-NEA)$_2$SnCl$_4$	−4.870882	−4.907486	−2.195584	−0.193218
(R-NEA)$_2$SnBr$_4$	−4.842676	−4.906775	−2.039410	−0.178898
(S-NEA)$_2$SnBr$_4$	−4.842596	−4.906775	−2.042697	−0.178540
(R-NEA)$_2$SnI$_4$	−4.810263	−4.904870	−1.849144	−0.164353
(S-NEA)$_2$SnI$_4$	−4.810335	−4.904908	−1.847499	−0.164529
(R-NEA)$_2$PbCl$_4$	−4.874498	−4.907281	−2.099519	−0.205163
(S-NEA)$_2$PbCl$_4$	−4.874518	−4.907283	−2.099164	−0.205211
(R-NEA)$_2$PbBr$_4$	−4.846273	−4.906548	−1.953517	−0.189982
(S-NEA)$_2$PbBr$_4$	−4.846276	−4.906394	−1.952586	−0.190205
(R-NEA)$_2$PbI$_4$	−4.813084	−4.904677	−1.787451	−0.172579
(S-NEA)$_2$PbI$_4$	−4.813101	−4.904759	−1.787330	−0.172531

Table S19: Energetic analysis for NEA-based slabs of chiral perovskites with cohesive energy per atom calculated with $E_{coh}^{part} = \frac{1}{N_{part}}(E_{tot}^{part} - \sum_{i=1}^{N_{part}} E_i^{atom})$, where $part = org, inorg$, N is the total number of atoms for both frozen organic and inorganic perovskite framework, and binding energy (E_b) calculated with $E_b = E_{tot} - E_{org}^{frozen} - E_{inorg}^{frozen}$.

System (slab)	E_{coh} ($\mathrm{eV\,atom^{-1}}$)	$E_{\mathrm{coh}}^{\mathrm{org}}$ ($\mathrm{eV\,atom^{-1}}$)	$E_{\mathrm{coh}}^{\mathrm{inorg}}$ ($\mathrm{eV\,atom^{-1}}$)	E_b ($\mathrm{eV\,atom^{-1}}$)
(R-NEA)$_2$GeCl$_4$	−4.865112	−4.903038	−2.152856	−0.195140
(S-NEA)$_2$GeCl$_4$	−4.865118	−4.903085	−2.156292	−0.194812
(R-NEA)$_2$GeBr$_4$	−4.835884	−4.901386	−1.959263	−0.183830
(S-NEA)$_2$GeBr$_4$	−4.835875	−4.901410	−1.961377	−0.183620
(R-NEA)$_2$GeI$_4$	−4.803595	−4.899687	−1.798510	−0.166720
(S-NEA)$_2$GeI$_4$	−4.803598	−4.899595	−1.798208	−0.166832
(R-NEA)$_2$SnCl$_4$	−4.866015	−4.901992	−2.210378	−0.192126
(S-NEA)$_2$SnCl$_4$	−4.866094	−4.902294	−2.211521	−0.191832
(R-NEA)$_2$SnBr$_4$	−4.837549	−4.901202	−2.050649	−0.177919
(S-NEA)$_2$SnBr$_4$	−4.837492	−4.901087	−2.046815	−0.178292
(R-NEA)$_2$SnI$_4$	−4.804691	−4.899117	−1.857629	−0.163327
(S-NEA)$_2$SnI$_4$	−4.804900	−4.899084	−1.856932	−0.163625
(R-NEA)$_2$PbCl$_4$	−4.869663	−4.901983	−2.110695	−0.204230
(S-NEA)$_2$PbCl$_4$	−4.869709	−4.902068	−2.107767	−0.204446
(R-NEA)$_2$PbBr$_4$	−4.841038	−4.900863	−1.959936	−0.189407
(S-NEA)$_2$PbBr$_4$	−4.841111	−4.900893	−1.958495	−0.189573
(R-NEA)$_2$PbI$_4$	−4.807672	−4.898947	−1.793489	−0.171899
(S-NEA)$_2$PbI$_4$	−4.807690	−4.898725	−1.792838	−0.172176

5 Density Derived Electrostatic and Chemical

Table S20: Density Derived Electrostatic and Chemical (DDEC) analysis for bulk R- and S-NEA perovskites.

System (bulk)	Q^{A} (e)	Q^{B} (e)	Q^{X} (e)
(R-NEA)$_2$GeCl$_4$	0.627497	0.669552	−0.481136
(S-NEA)$_2$GeCl$_4$	0.628544	0.667666	−0.481189
(R-NEA)$_2$GeBr$_4$	0.603847	0.570556	−0.444562
(S-NEA)$_2$GeBr$_4$	0.602543	0.569734	−0.443704
(R-NEA)$_2$GeI$_4$	0.571520	0.455739	−0.399695
(S-NEA)$_2$GeI$_4$	0.575878	0.457443	−0.402300
(R-NEA)$_2$SnCl$_4$	0.624552	0.783385	−0.508123
(S-NEA)$_2$SnCl$_4$	0.622962	0.784228	−0.507538
(R-NEA)$_2$SnBr$_4$	0.600740	0.703588	−0.476266
(S-NEA)$_2$SnBr$_4$	0.598661	0.704456	−0.475445
(R-NEA)$_2$SnI$_4$	0.575506	0.571740	−0.430688
(S-NEA)$_2$SnI$_4$	0.578626	0.574824	−0.433019
(R-NEA)$_2$PbCl$_4$	0.620994	0.948098	−0.547522
(S-NEA)$_2$PbCl$_4$	0.620493	0.946522	−0.546877
(R-NEA)$_2$PbBr$_4$	0.602680	0.812609	−0.504492
(S-NEA)$_2$PbBr$_4$	0.601058	0.814108	−0.504056
(R-NEA)$_2$PbI$_4$	0.580829	0.666365	−0.457006
(S-NEA)$_2$PbI$_4$	0.580533	0.665721	−0.456698

Table S21: DDEC analysis for slab R- and S- NEA perovskites.

System (slab)	Q^{A} (e)	Q^{B} (e)	Q^{X} (e)
(R-NEA)$_2$GeCl$_4$	0.625181	0.661746	−0.478027
(S-NEA)$_2$GeCl$_4$	0.625488	0.664398	−0.478843
(R-NEA)$_2$GeBr$_4$	0.602611	0.570782	−0.444001
(S-NEA)$_2$GeBr$_4$	0.602075	0.570018	−0.443542
(R-NEA)$_2$GeI$_4$	0.570741	0.458294	−0.399945
(S-NEA)$_2$GeI$_4$	0.572394	0.460356	−0.401285
(R-NEA)$_2$SnCl$_4$	0.615390	0.782566	−0.503338
(S-NEA)$_2$SnCl$_4$	0.615285	0.791504	−0.505518
(R-NEA)$_2$SnBr$_4$	0.595669	0.702579	−0.473479
(S-NEA)$_2$SnBr$_4$	0.594820	0.700659	−0.472574
(R-NEA)$_2$SnI$_4$	0.569429	0.570648	−0.427377
(S-NEA)$_2$SnI$_4$	0.571813	0.573424	−0.429262
(R-NEA)$_2$PbCl$_4$	0.614297	0.942356	−0.542737
(S-NEA)$_2$PbCl$_4$	0.614045	0.945246	−0.543334
(R-NEA)$_2$PbBr$_4$	0.594613	0.807680	−0.499226
(S-NEA)$_2$PbBr$_4$	0.597598	0.810973	−0.501542
(R-NEA)$_2$PbI$_4$	0.577042	0.668322	−0.455601
(S-NEA)$_2$PbI$_4$	0.577450	0.668635	−0.455883

6 Density of States

6.1 Bulk

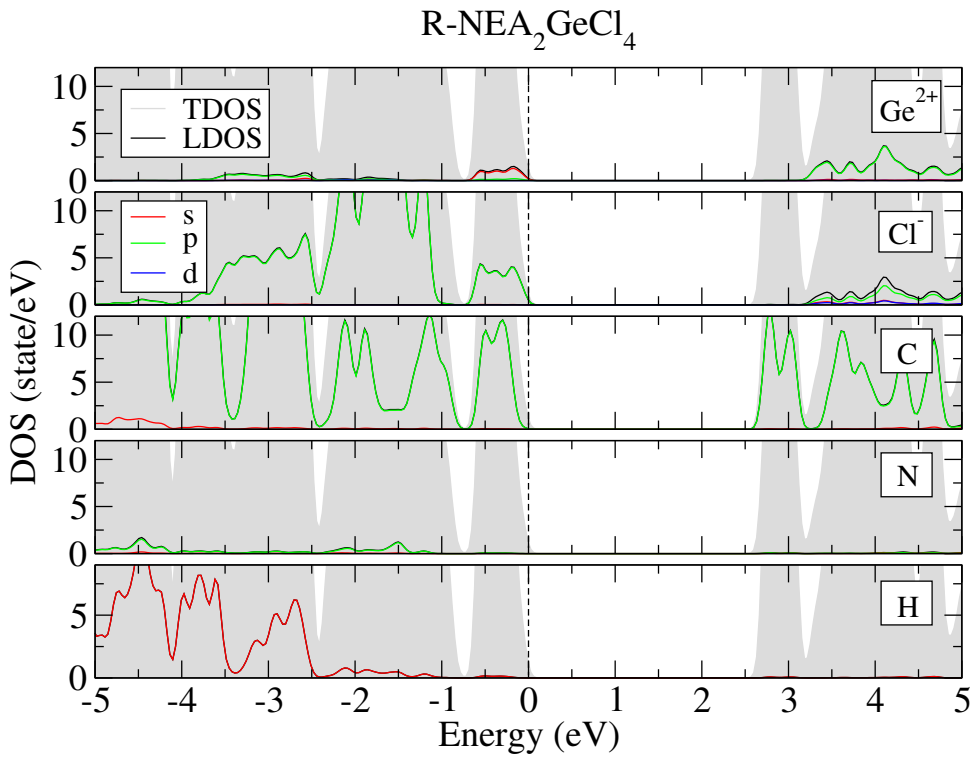

Figure S12: Density of states for $(R\text{-}NEA)_2GeCl_4$ bulk with PBE+D3 functional.

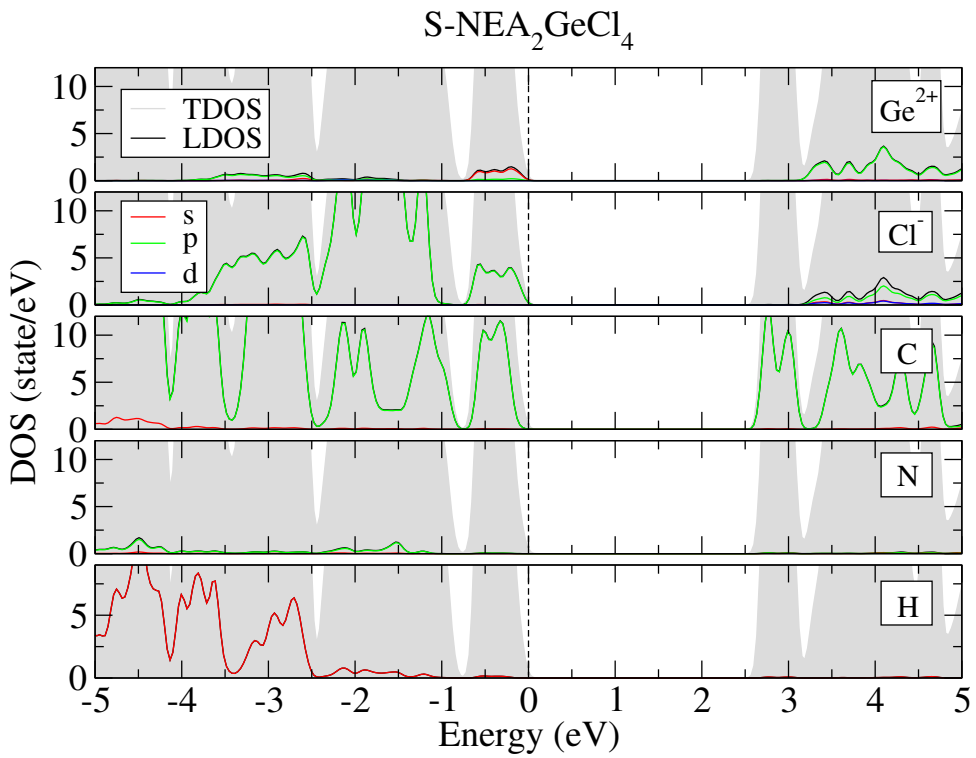

Figure S13: Density of states for $(S\text{-}NEA)_2GeCl_4$ bulk with PBE+D3 functional.

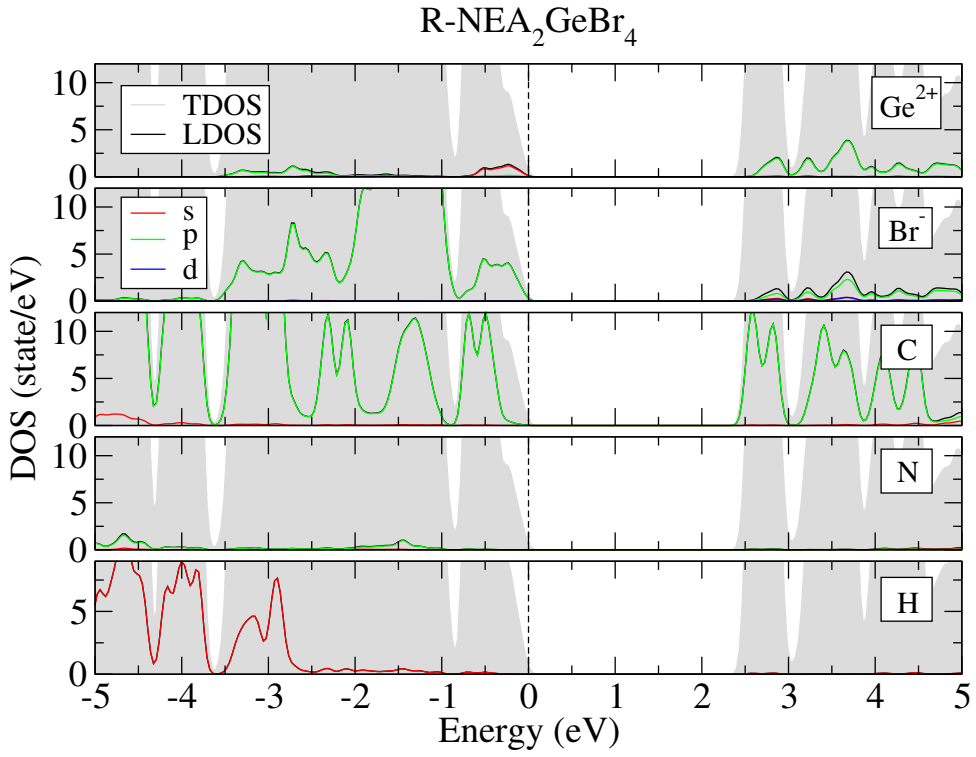

Figure S14: Density of states for $(R\text{-}NEA)_2GeBr_4$ bulk with PBE+D3 functional.

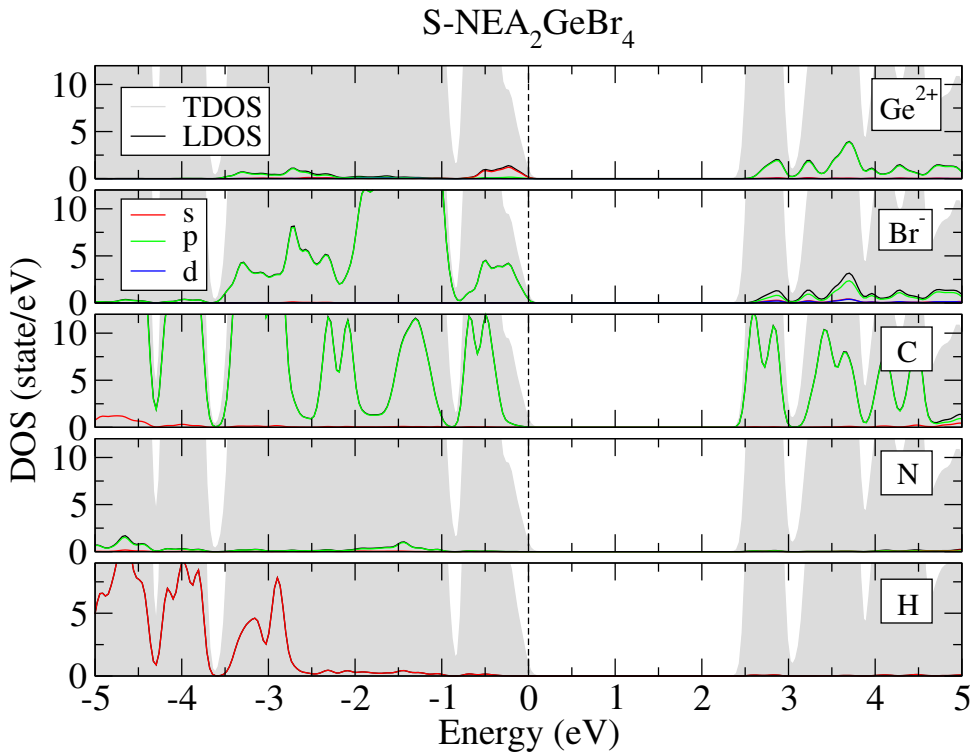

Figure S15: Density of states for $(S\text{-}NEA)_2GeBr_4$ bulk with PBE+D3 functional.

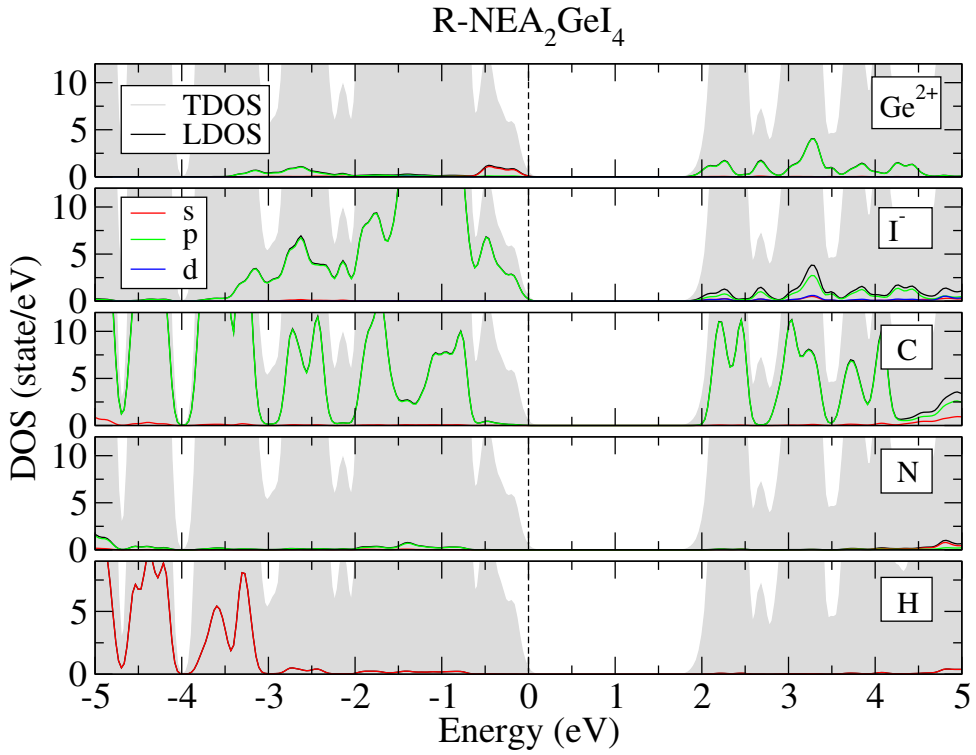

Figure S16: Density of states for $(R\text{-}NEA)_2GeI_4$ bulk with PBE+D3 functional.

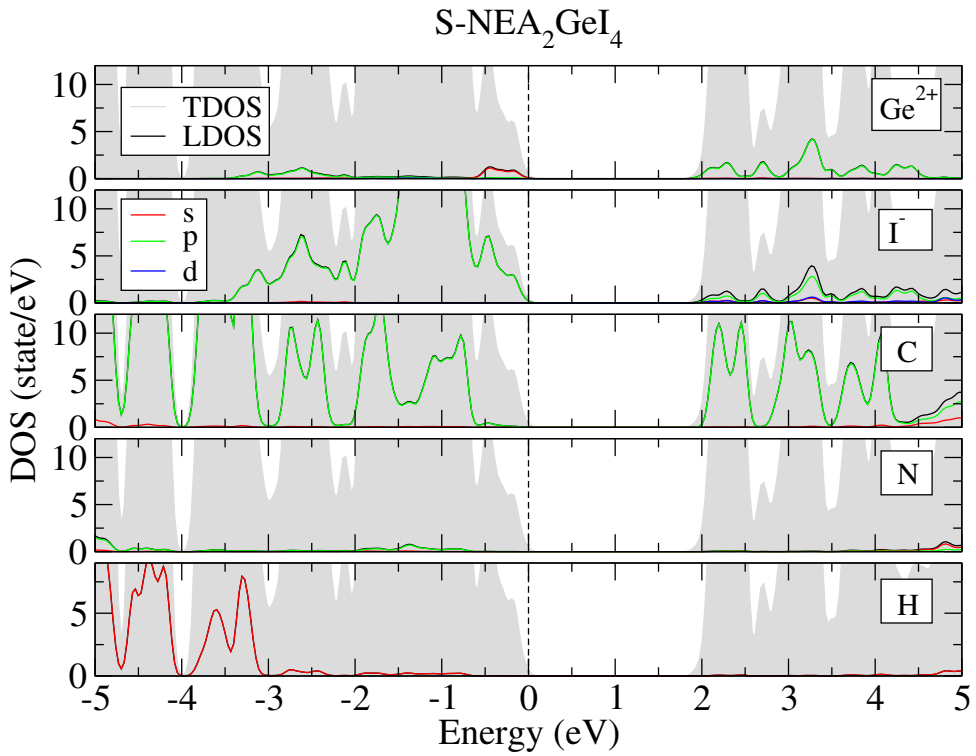

Figure S17: Density of states for $(S\text{-}NEA)_2GeI_4$ bulk with PBE+D3 functional.

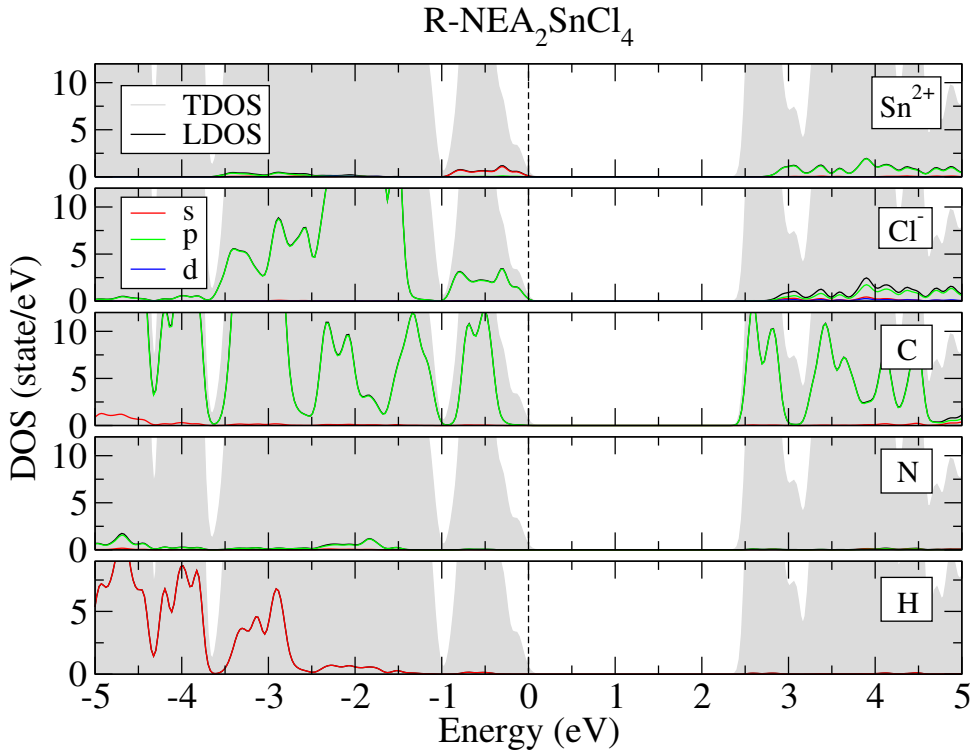

Figure S18: Density of states for $(R\text{-}NEA)_2SnCl_4$ bulk with PBE+D3 functional.

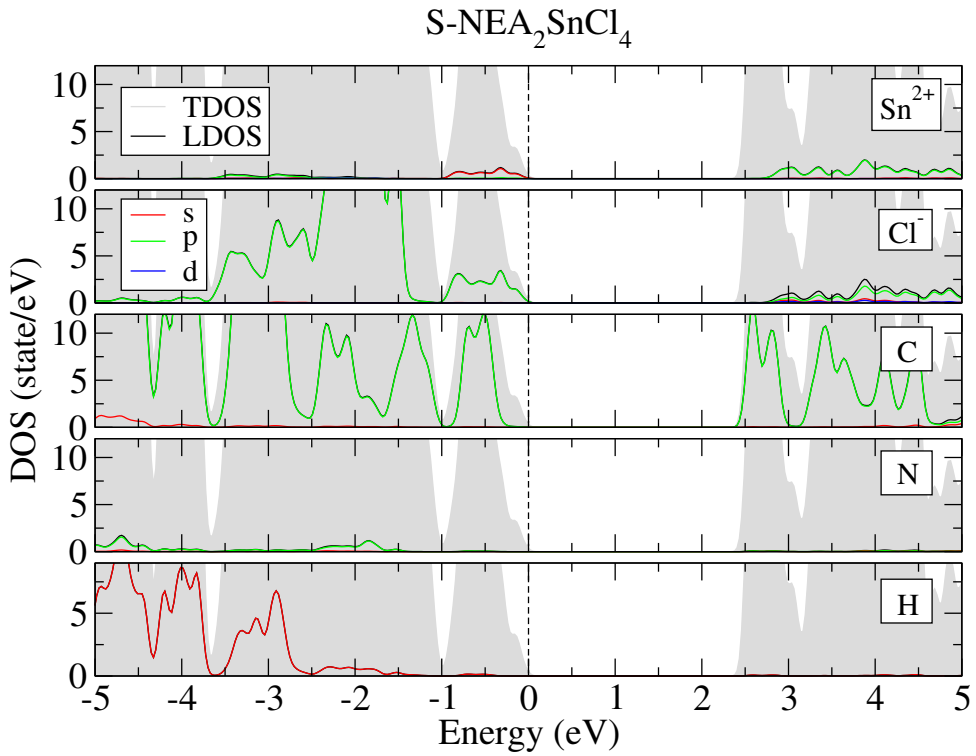

Figure S19: Density of states for $(S\text{-}NEA)_2SnCl_4$ bulk with PBE+D3 functional.

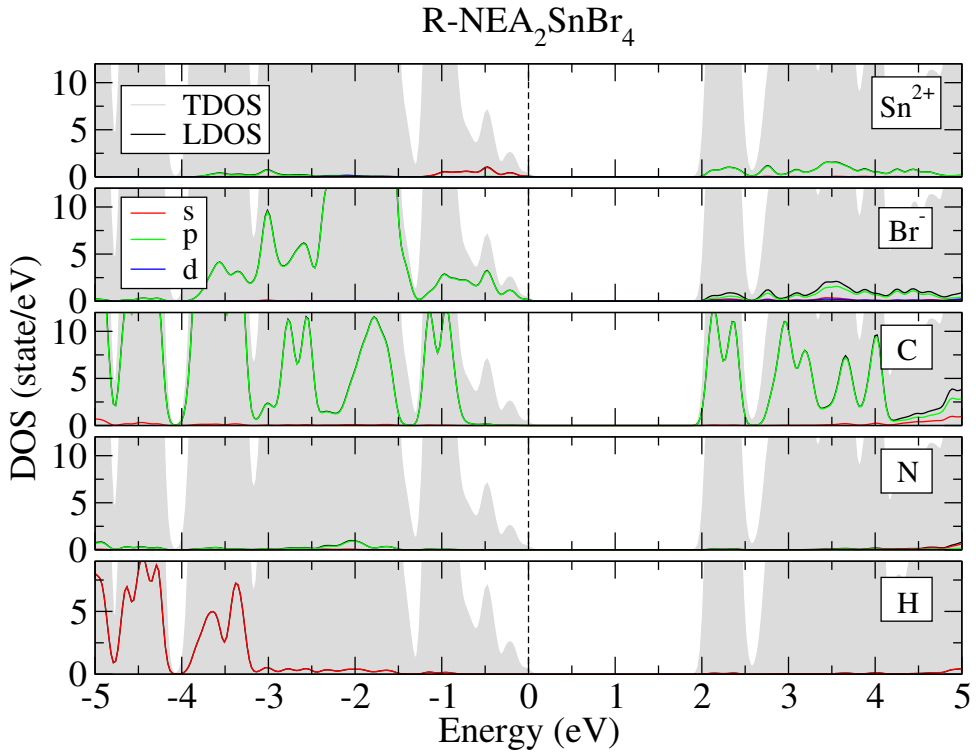

Figure S20: Density of states for $(R\text{-}NEA)_2SnBr_4$ bulk with PBE+D3 functional.

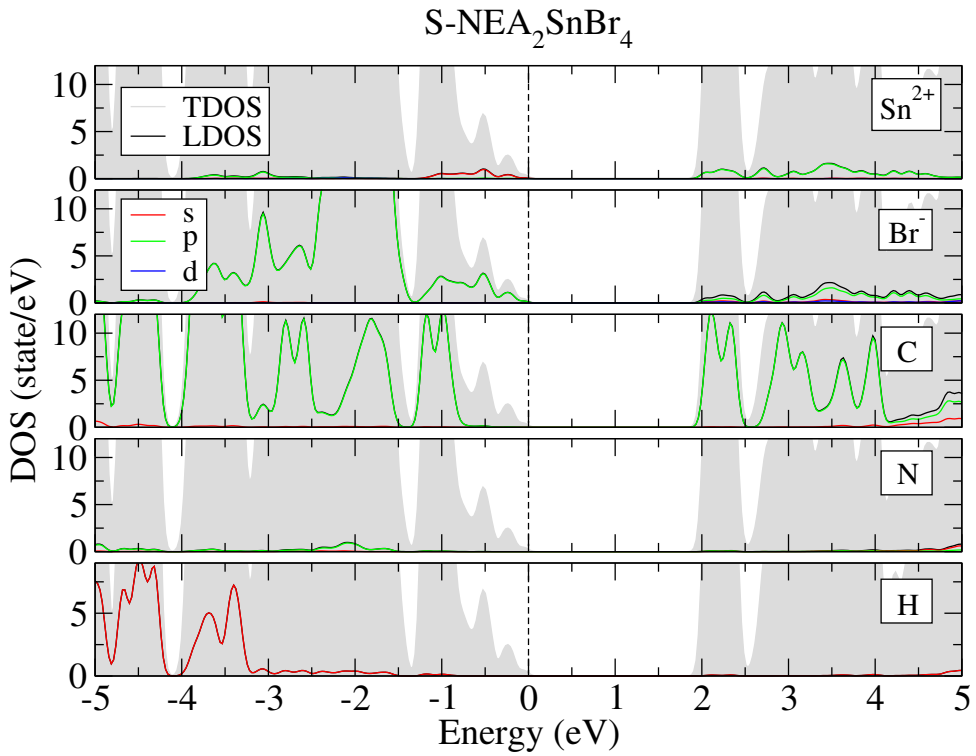

Figure S21: Density of states for $(S\text{-}NEA)_2SnBr_4$ bulk with PBE+D3 functional.

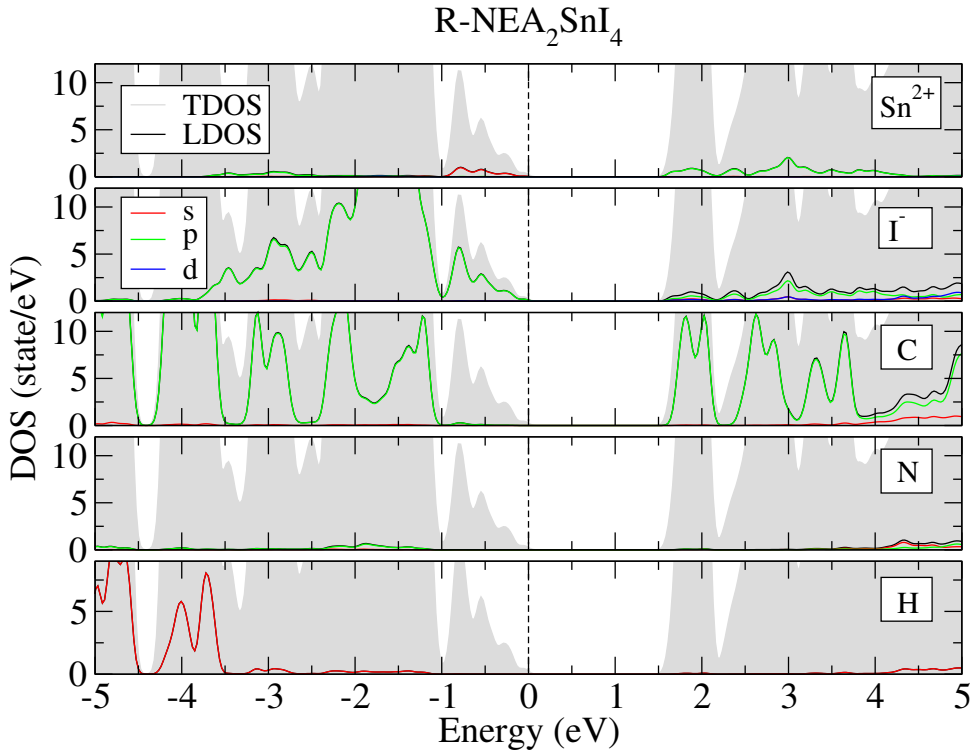

Figure S22: Density of states for $(R\text{-}NEA)_2SnI_4$ bulk with PBE+D3 functional.

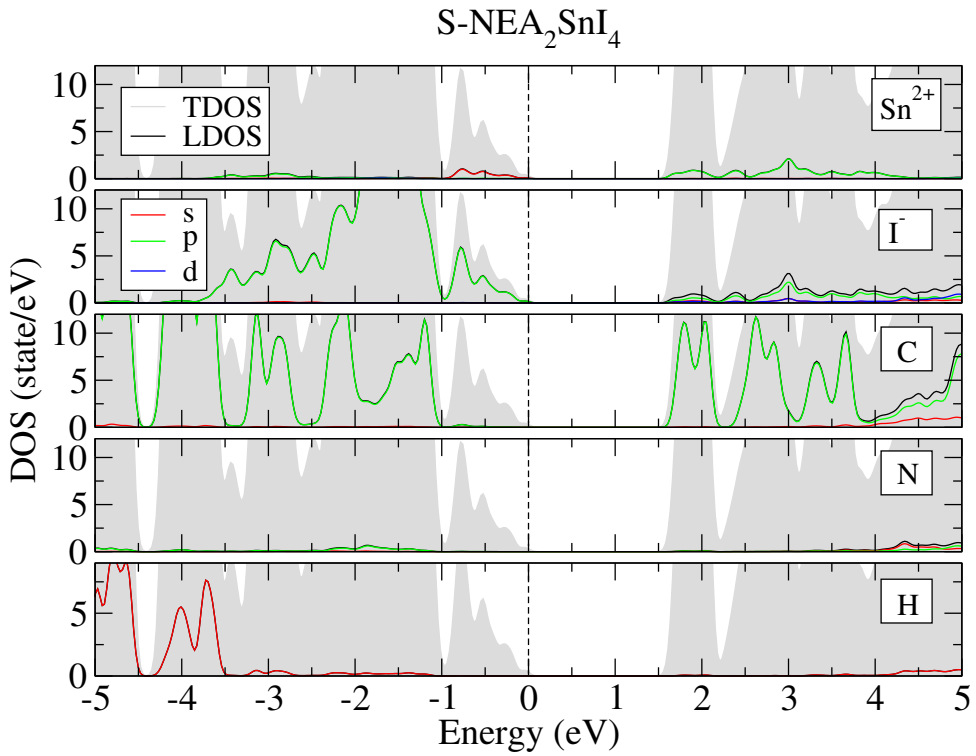

Figure S23: Density of states for $(S\text{-}NEA)_2SnI_4$ bulk with PBE+D3 functional.

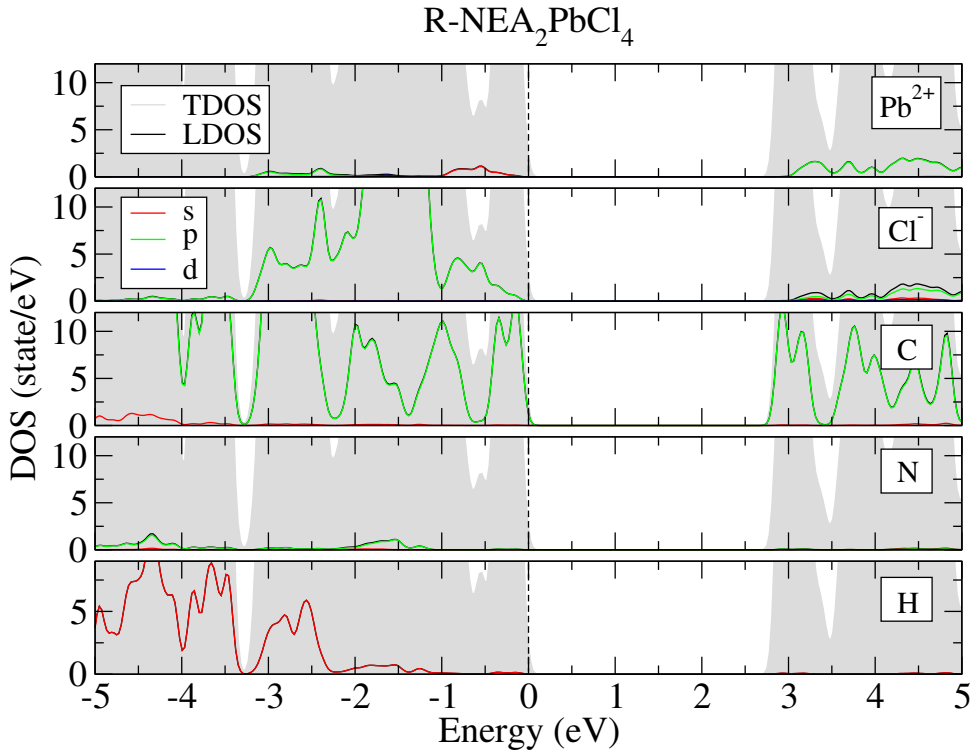

Figure S24: Density of states for $(R\text{-}NEA)_2PbCl_4$ bulk with PBE+D3 functional.

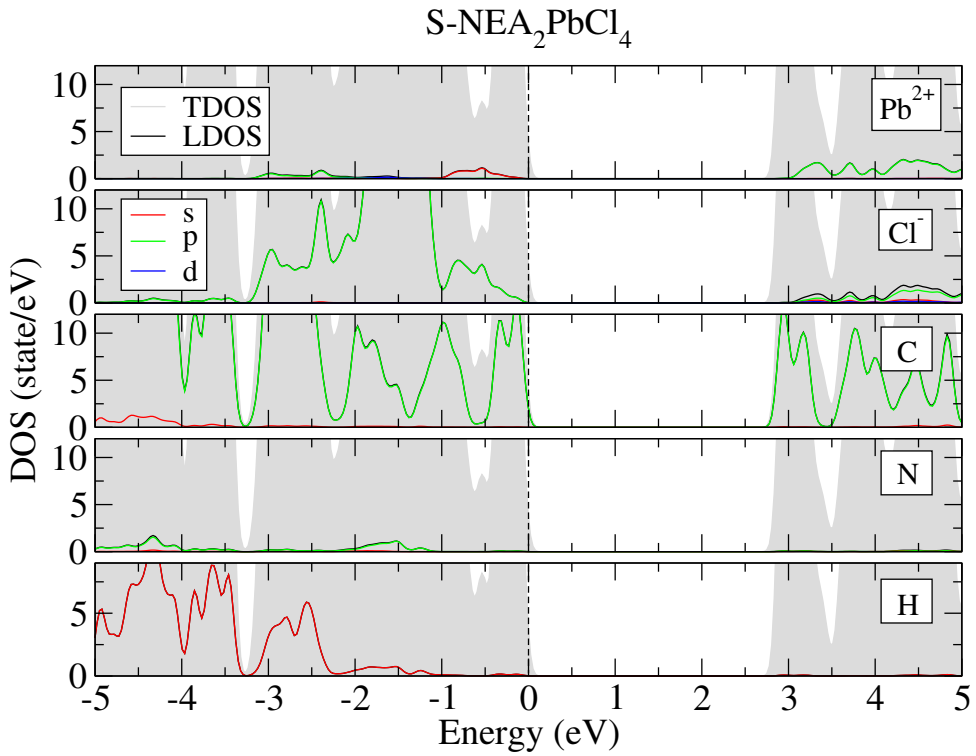

Figure S25: Density of states for $(S\text{-}NEA)_2PbCl_4$ bulk with PBE+D3 functional.

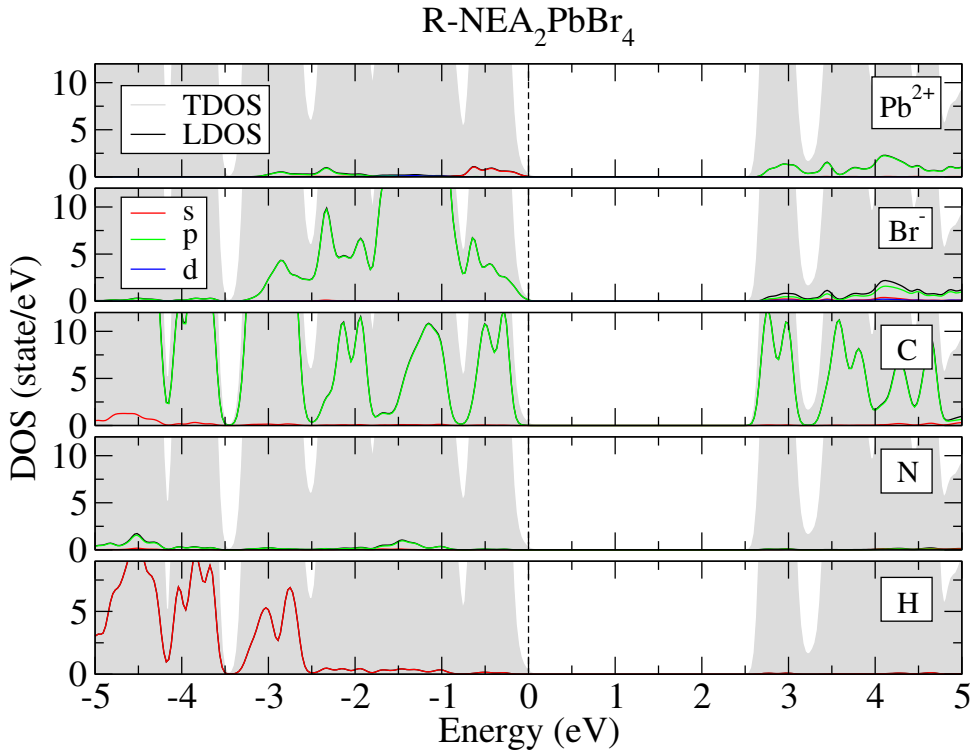

Figure S26: Density of states for $(R\text{-}NEA)_2PbBr_4$ bulk with PBE+D3 functional.

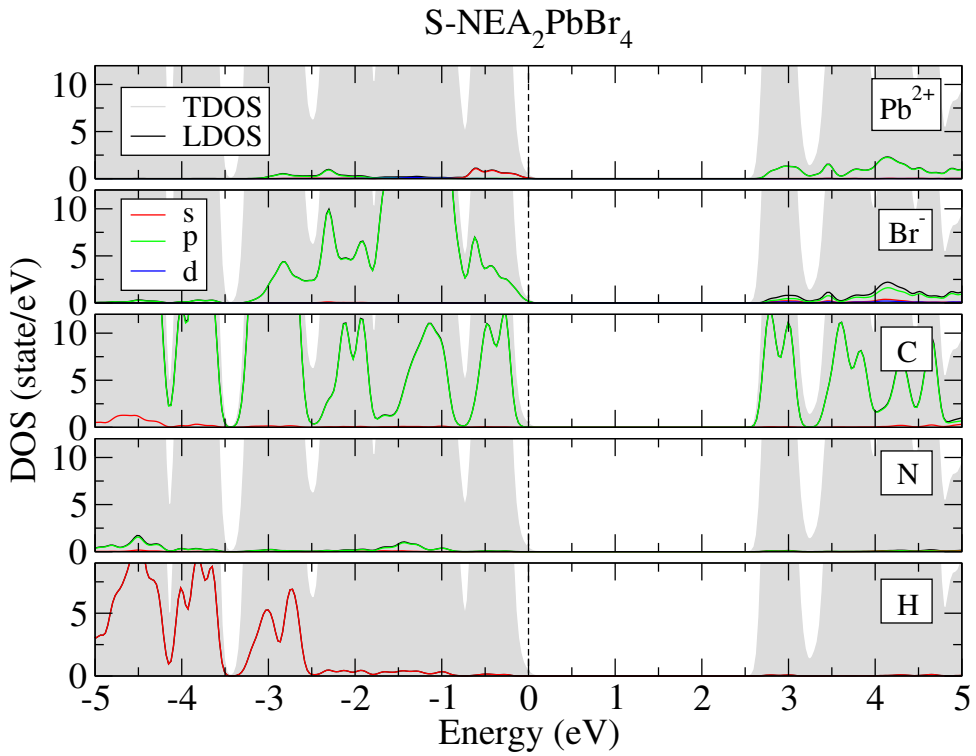

Figure S27: Density of states for $(S\text{-}NEA)_2PbBr_4$ bulk with PBE+D3 functional.

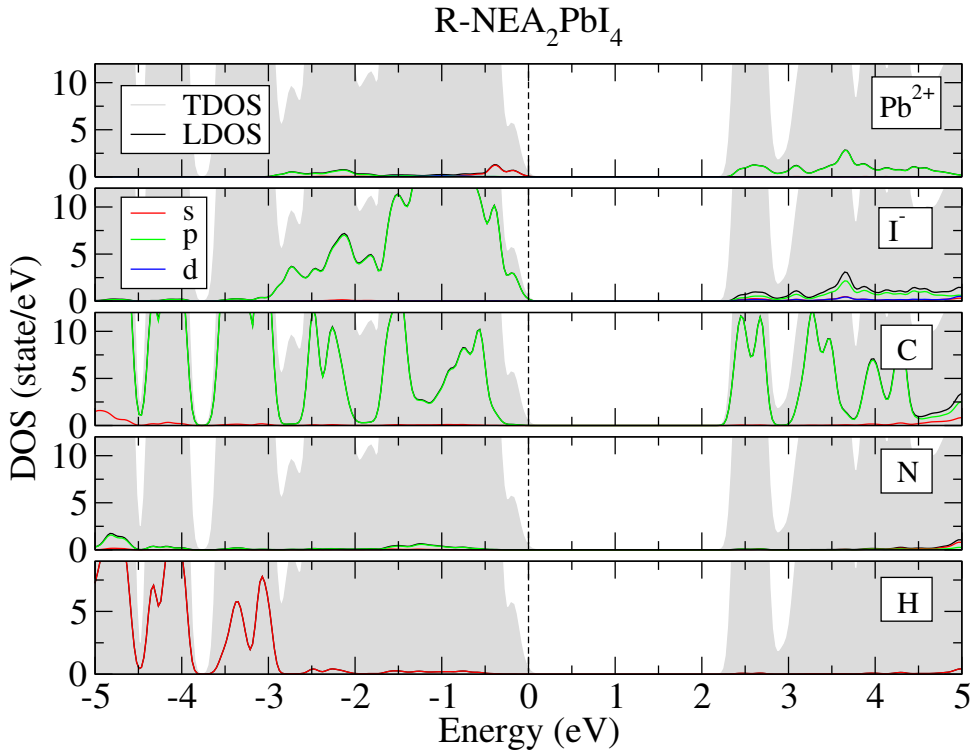

Figure S28: Density of states for $(R\text{-}NEA)_2PbI_4$ bulk with PBE+D3 functional.

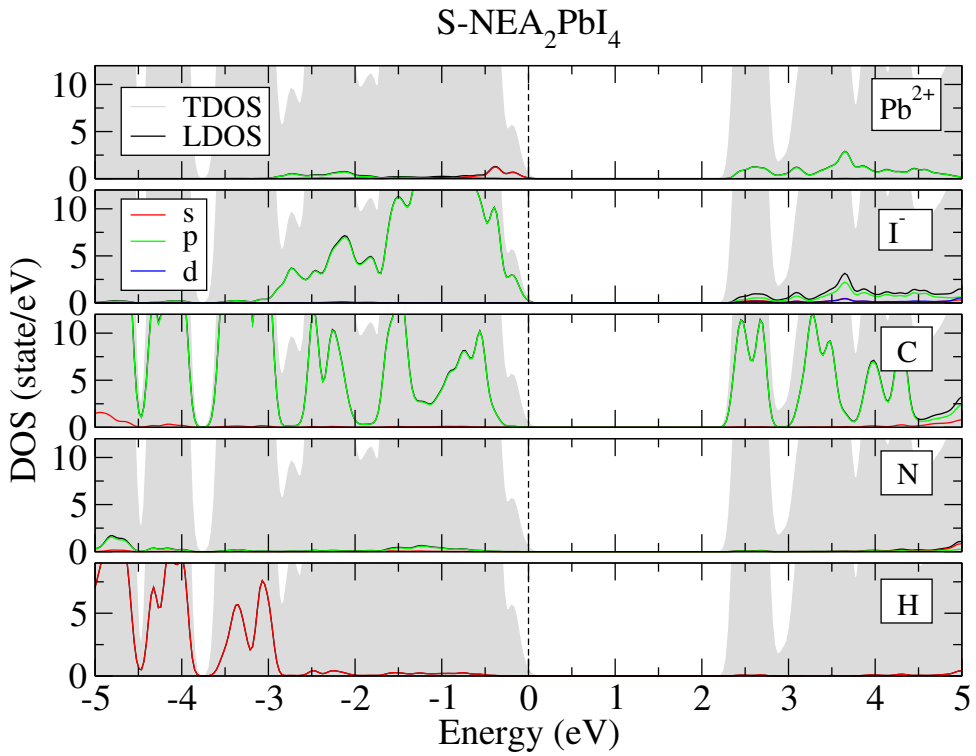

Figure S29: Density of states for $(S\text{-}NEA)_2PbI_4$ bulk with PBE+D3 functional.

6.2 Slab

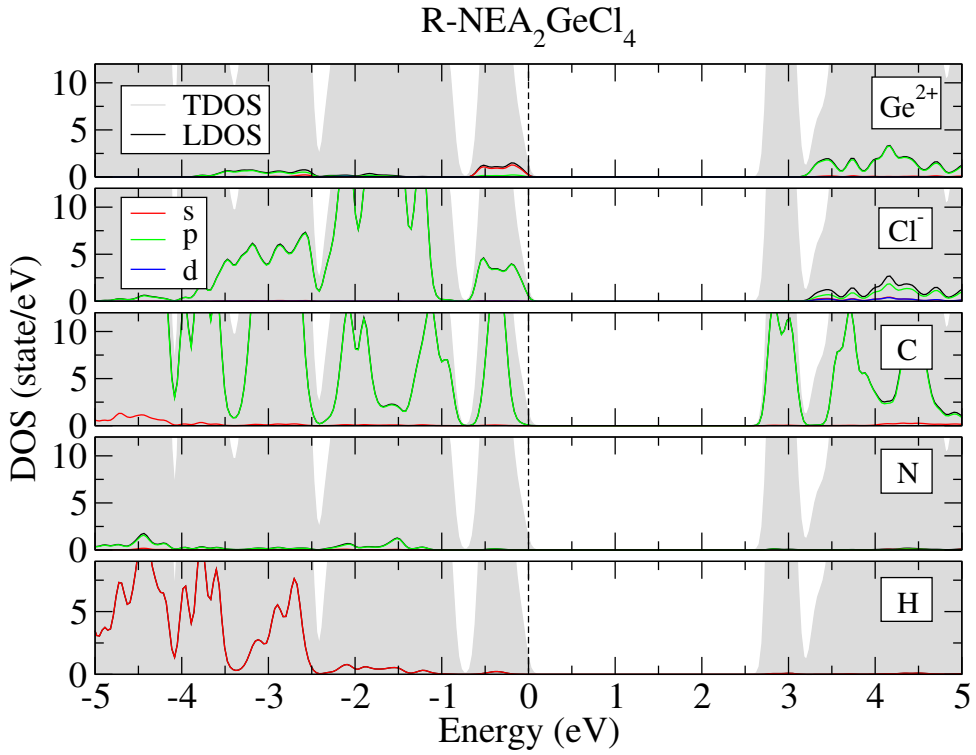

Figure S30: Density of states for $(R\text{-}NEA)_2GeCl_4$ slab with PBE+D3 functional.

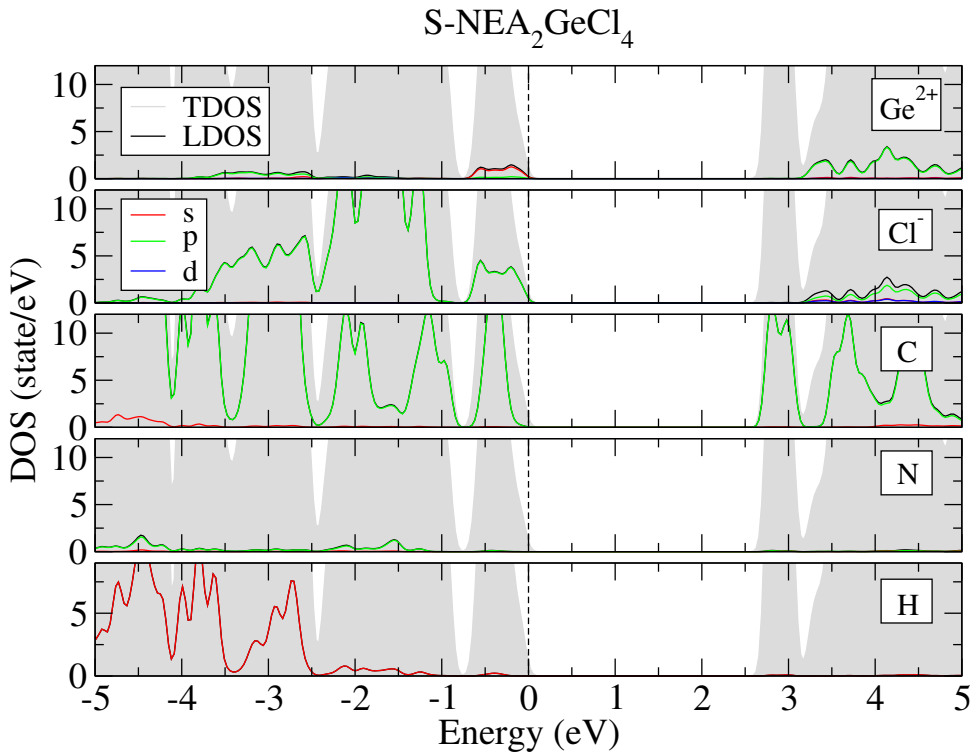

Figure S31: Density of states for $(S\text{-}NEA)_2GeCl_4$ slab with PBE+D3 functional.

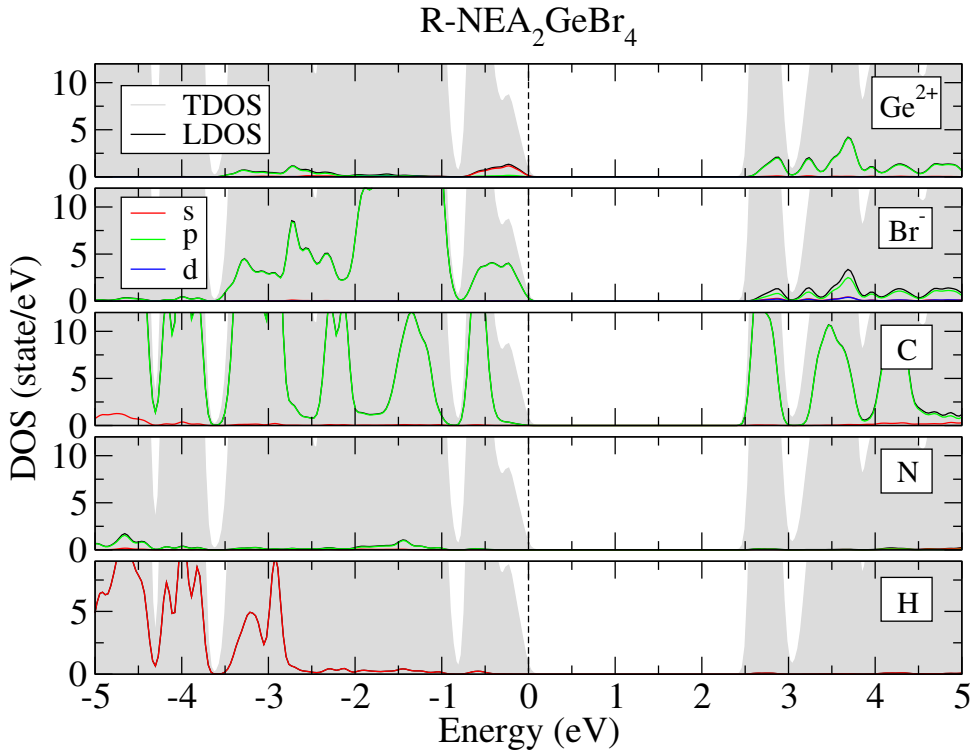

Figure S32: Density of states for $(R\text{-}NEA)_2GeBr_4$ slab with PBE+D3 functional.

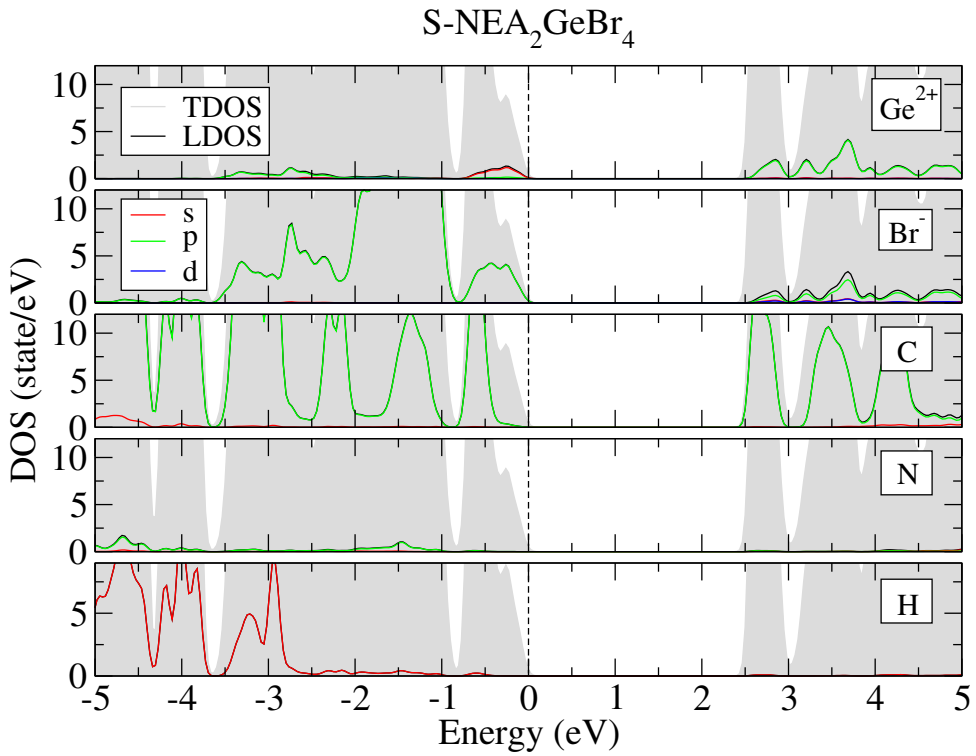

Figure S33: Density of states for $(S\text{-}NEA)_2GeBr_4$ slab with PBE+D3 functional.

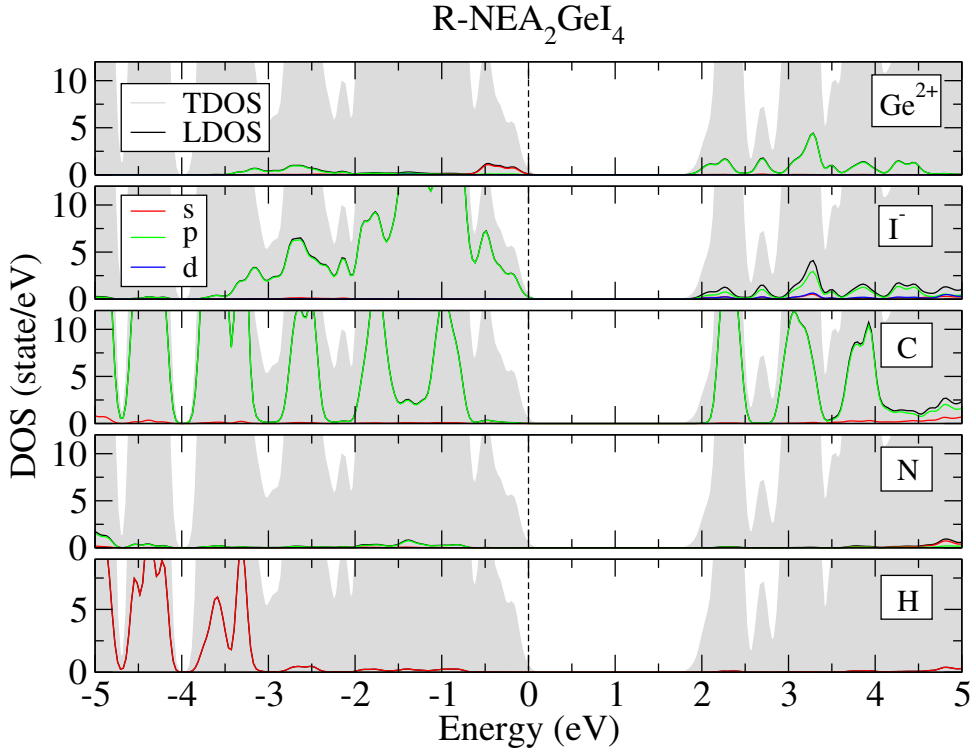

Figure S34: Density of states for $(R\text{-}NEA)_2GeI_4$ slab with PBE+D3 functional.

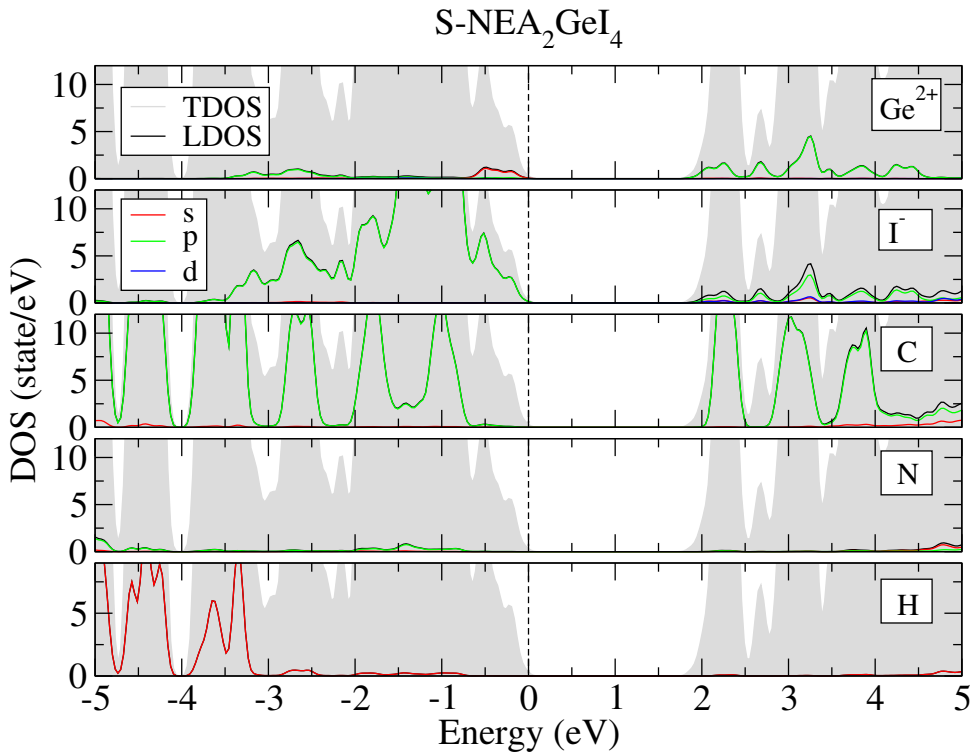

Figure S35: Density of states for $(S\text{-}NEA)_2GeI_4$ slab with PBE+D3 functional.

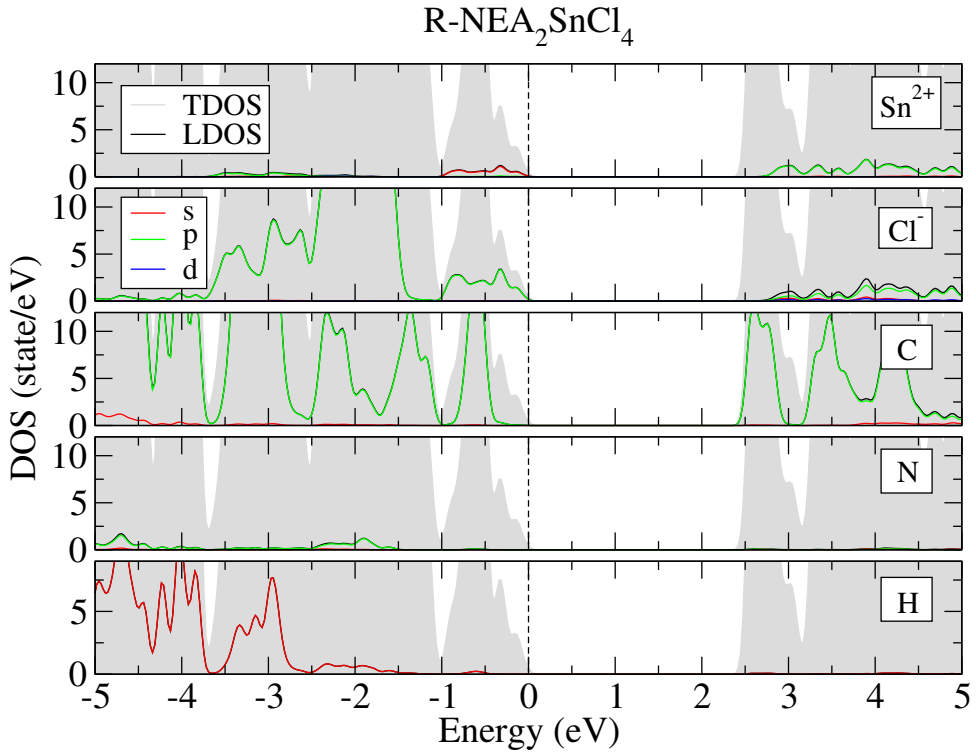

Figure S36: Density of states for $(R\text{-}NEA)_2SnCl_4$ slab with PBE+D3 functional.

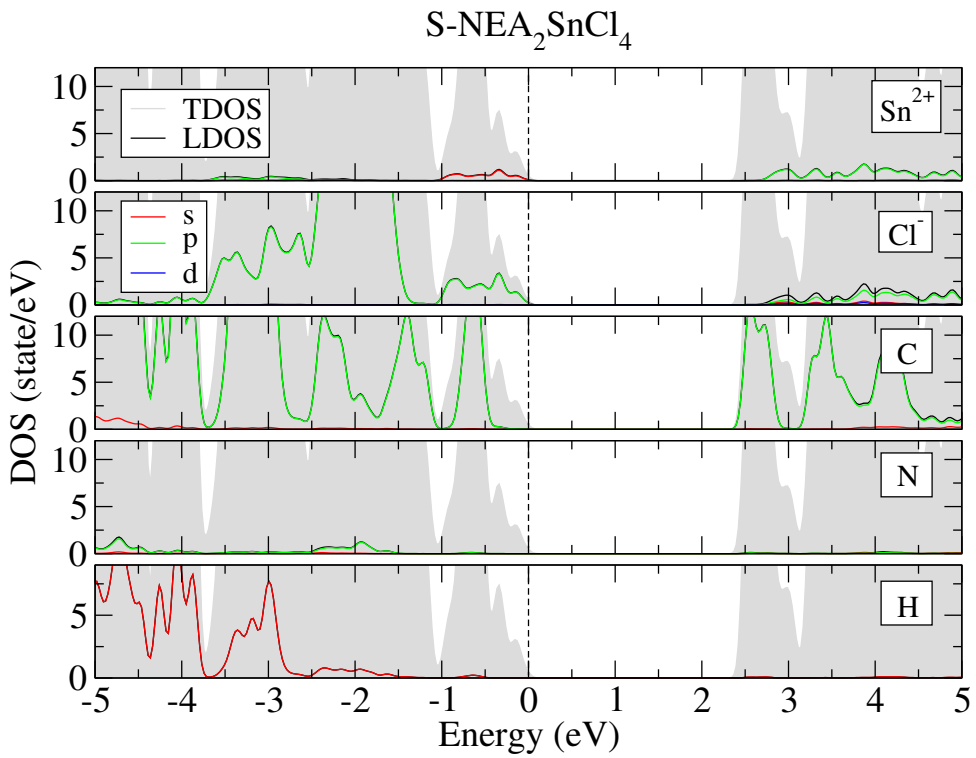

Figure S37: Density of states for $(S\text{-}NEA)_2SnCl_4$ slab with PBE+D3 functional.

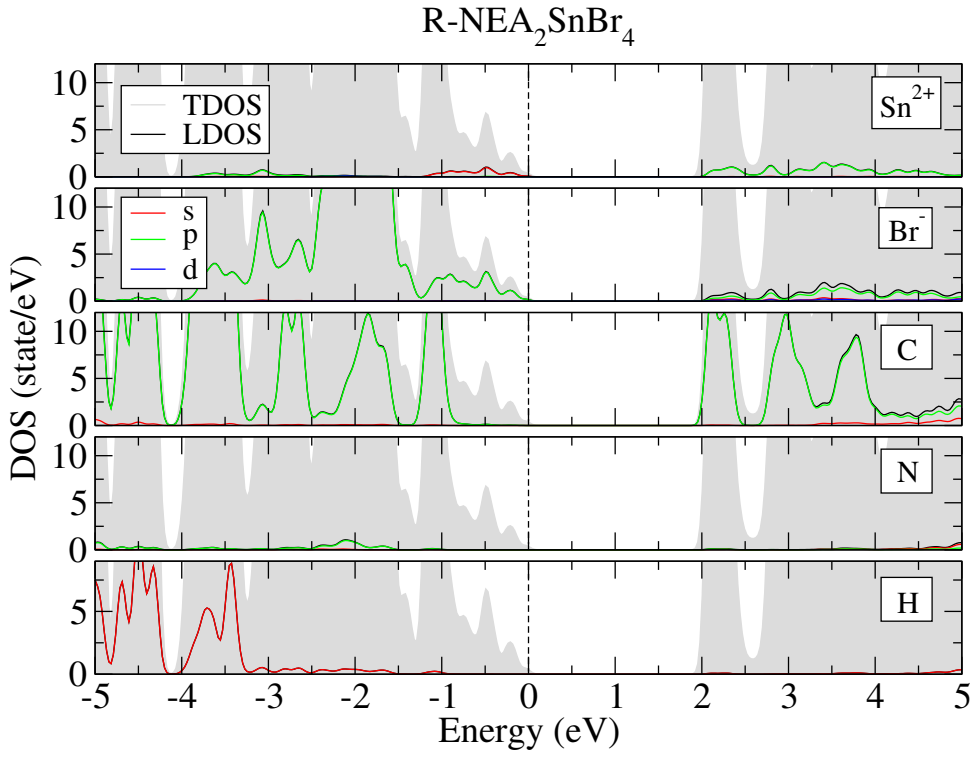

Figure S38: Density of states for $(R\text{-}NEA)_2SnBr_4$ slab with PBE+D3 functional.

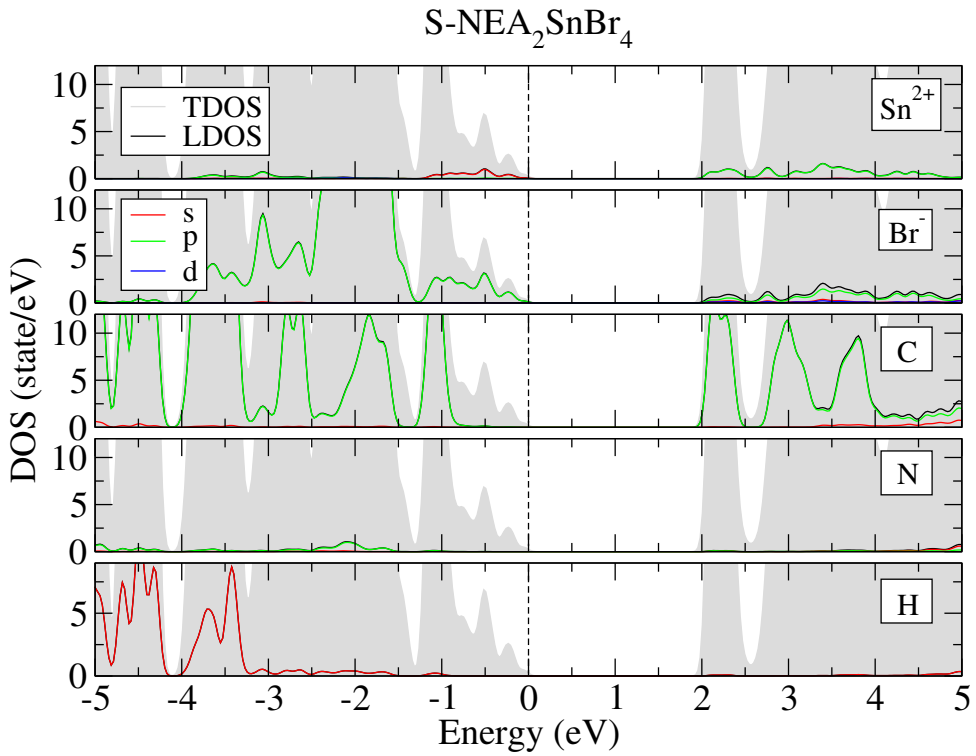

Figure S39: Density of states for $(S\text{-}NEA)_2SnBr_4$ slab with PBE+D3 functional.

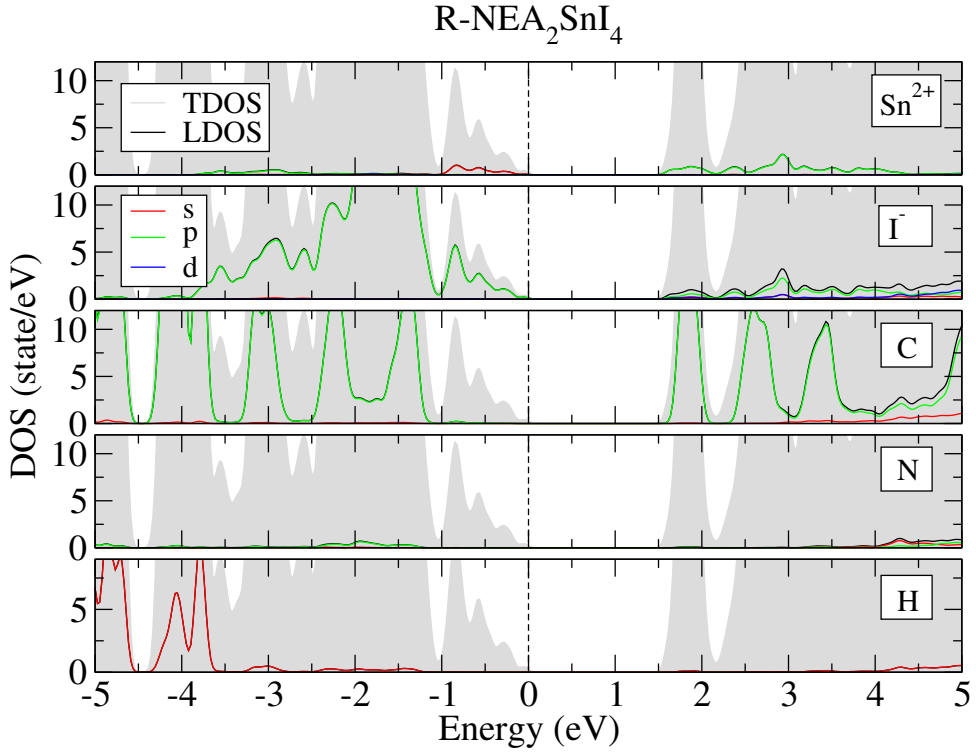

Figure S40: Density of states for $(R\text{-}NEA)_2SnI_4$ slab with PBE+D3 functional.

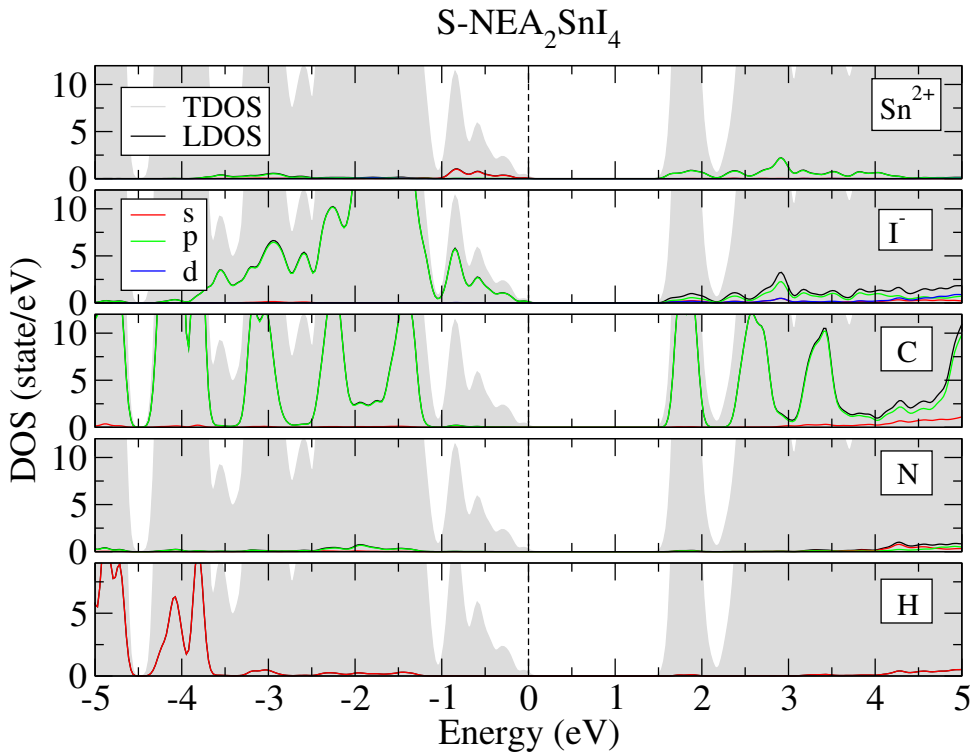

Figure S41: Density of states for $(S\text{-}NEA)_2SnI_4$ slab with PBE+D3 functional.

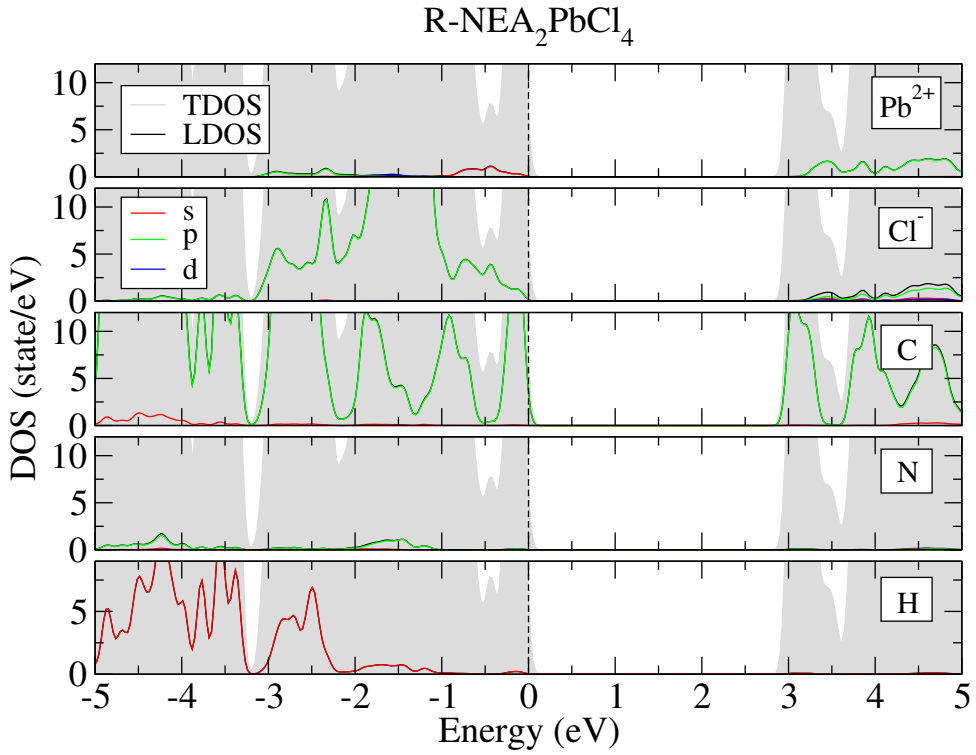

Figure S42: Density of states for $(R\text{-}NEA)_2PbCl_4$ slab with PBE+D3 functional.

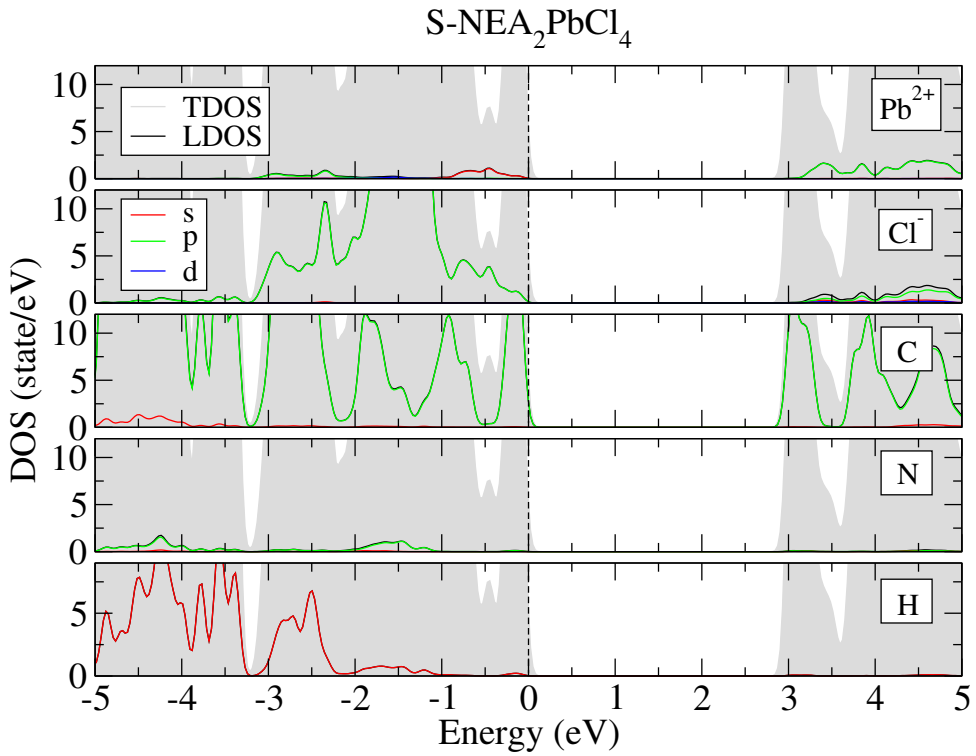

Figure S43: Density of states for $(S\text{-}NEA)_2PbCl_4$ slab with PBE+D3 functional.

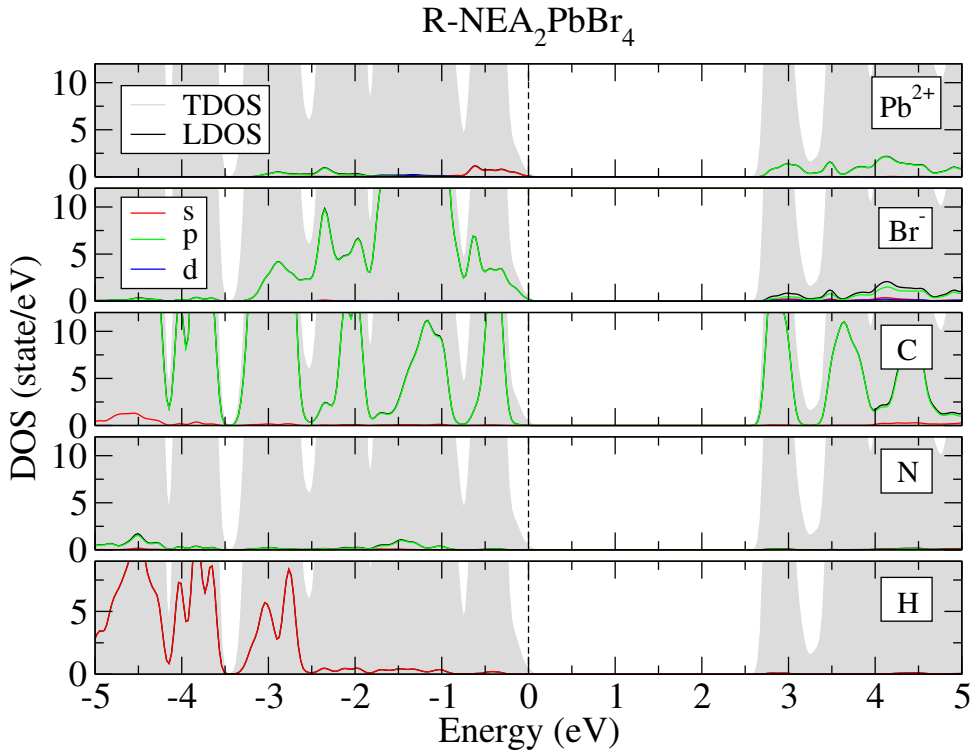

Figure S44: Density of states for $(R\text{-}NEA)_2PbBr_4$ slab with PBE+D3 functional.

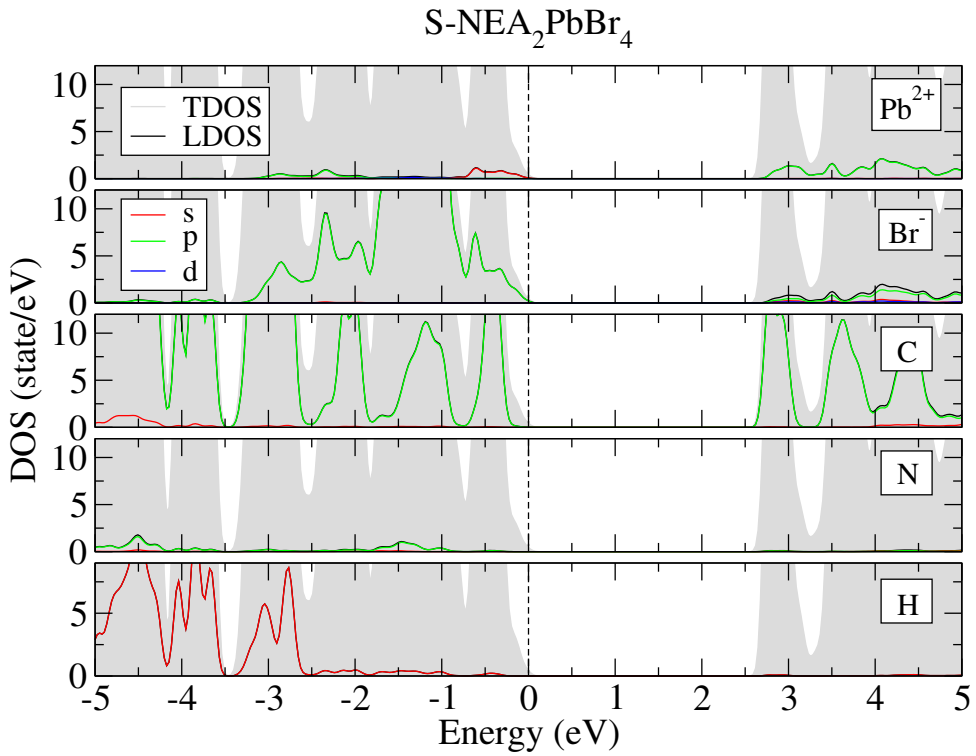

Figure S45: Density of states for $(S\text{-}NEA)_2PbBr_4$ slab with PBE+D3 functional.

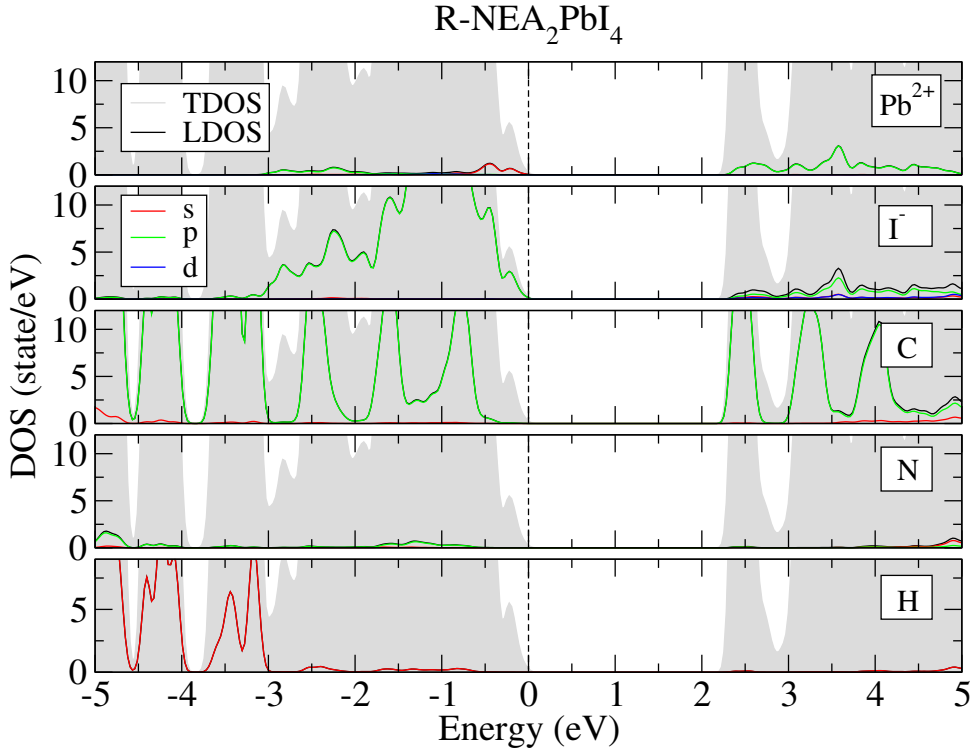

Figure S46: Density of states for $(R\text{-}NEA)_2PbI_4$ slab with PBE+D3 functional.

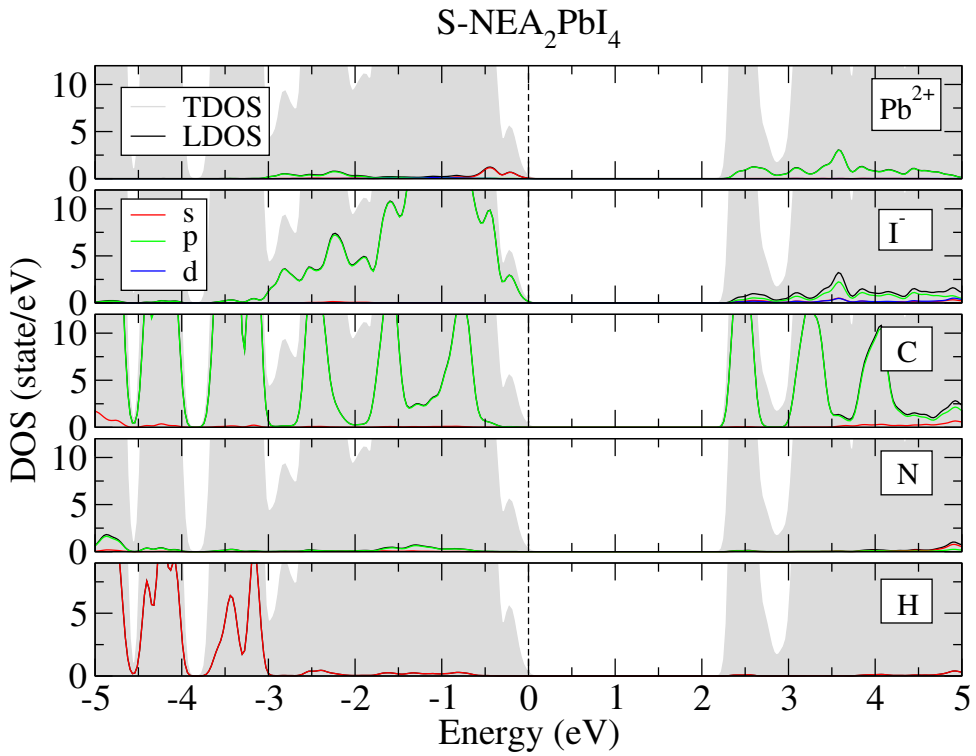

Figure S47: Density of states for $(S\text{-}NEA)_2PbI_4$ slab with PBE+D3 functional.

7 Band Structure

7.1 Bulk

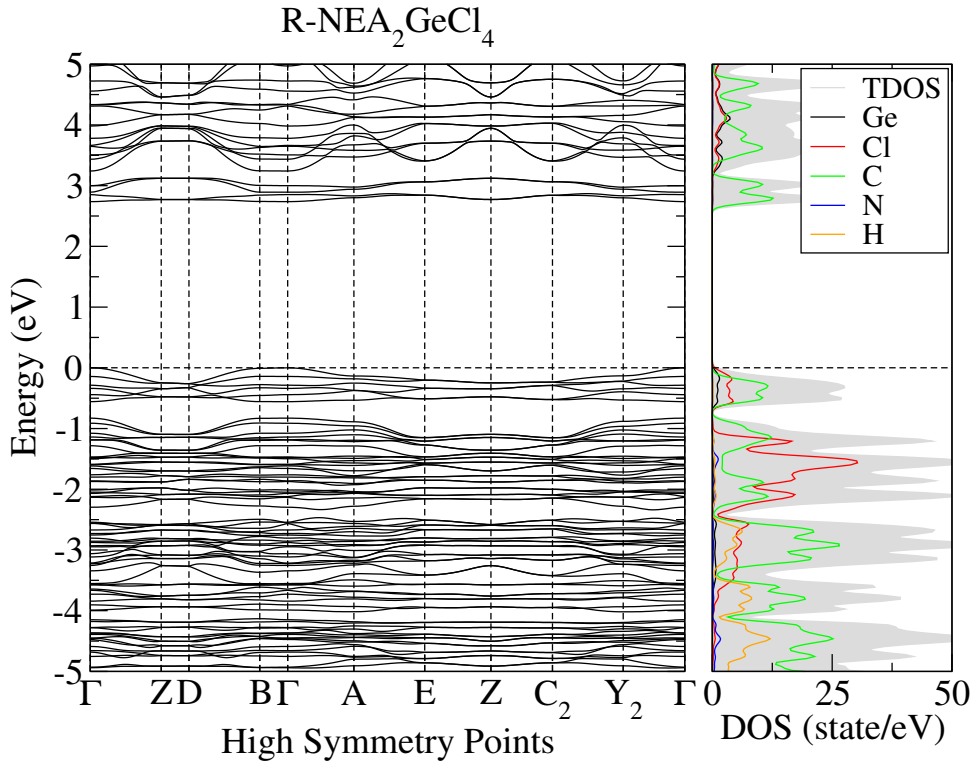

Figure S48: Band structure for $(R\text{-}NEA)_2GeCl_4$ bulk with PBE+D3 functional.

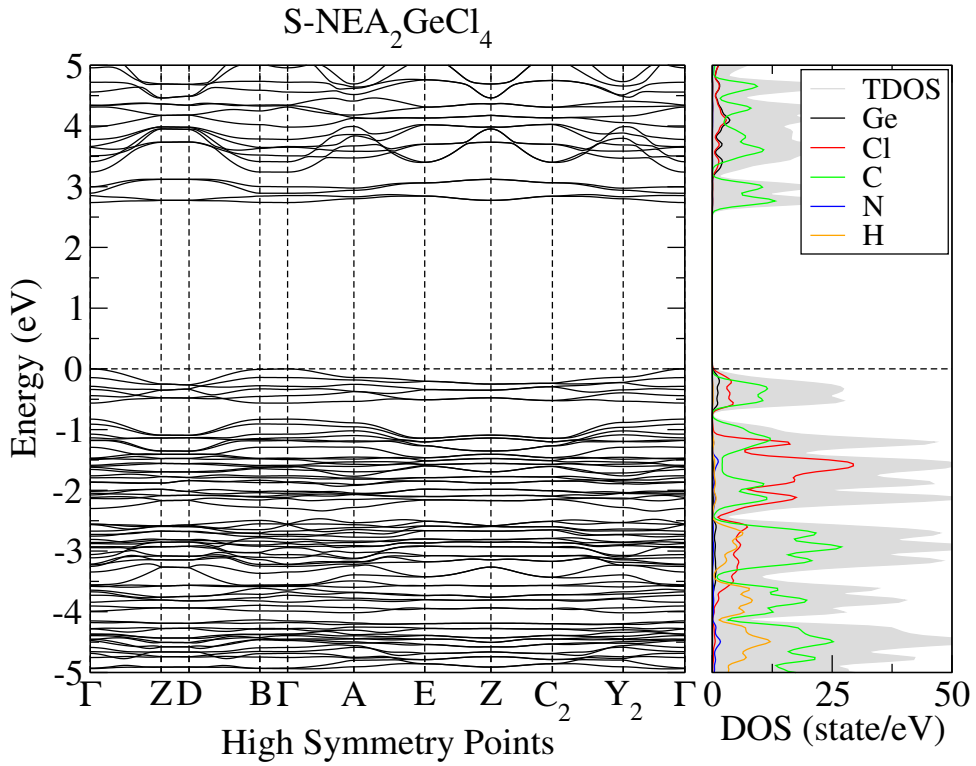

Figure S49: Band structure for $(S\text{-}NEA)_2GeCl_4$ bulk with PBE+D3 functional.

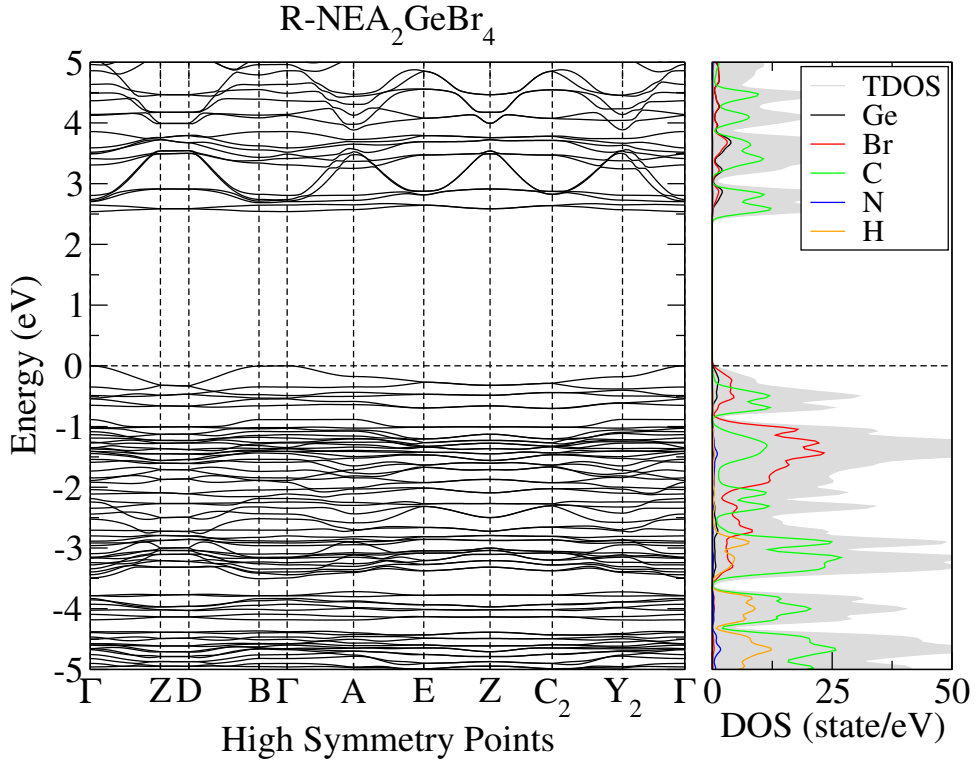

Figure S50: Band structure for $(R\text{-}NEA)_2GeBr_4$ bulk with PBE+D3 functional.

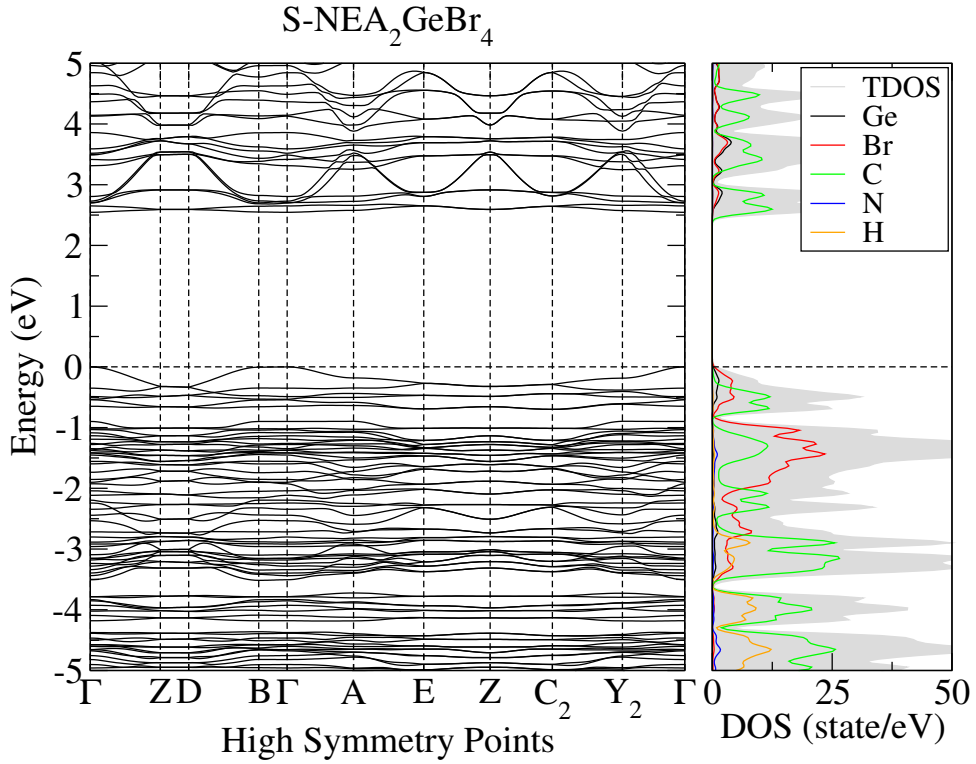

Figure S51: Band structure for $(S\text{-}NEA)_2GeBr_4$ bulk with PBE+D3 functional.

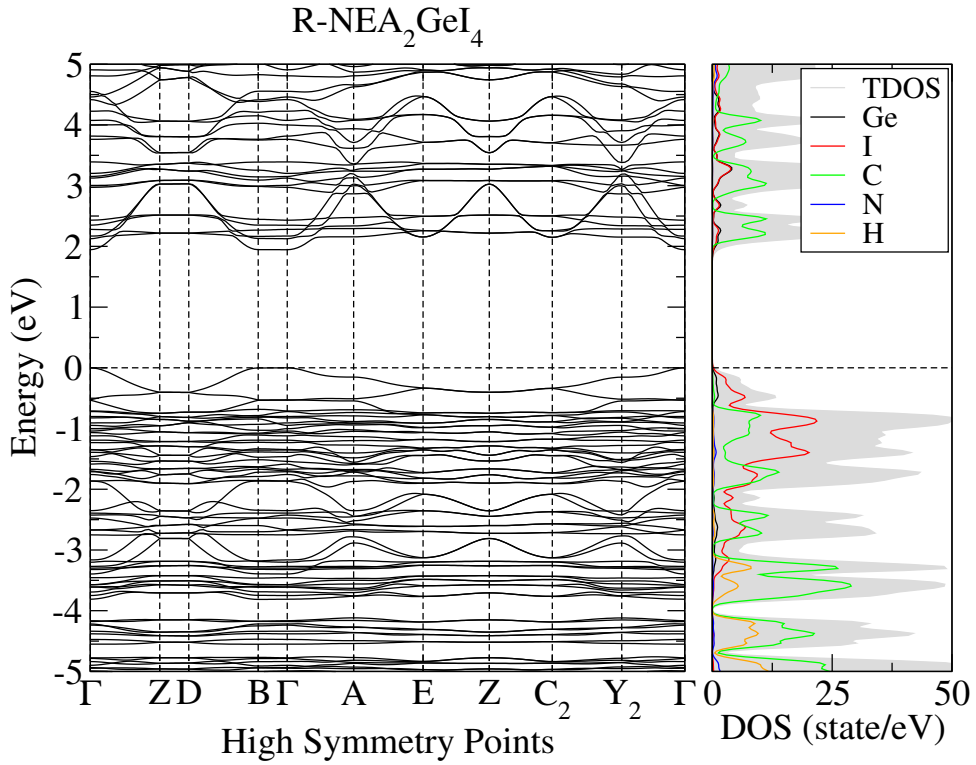

Figure S52: Band structure for $(R\text{-}NEA)_2GeI_4$ bulk with PBE+D3 functional.

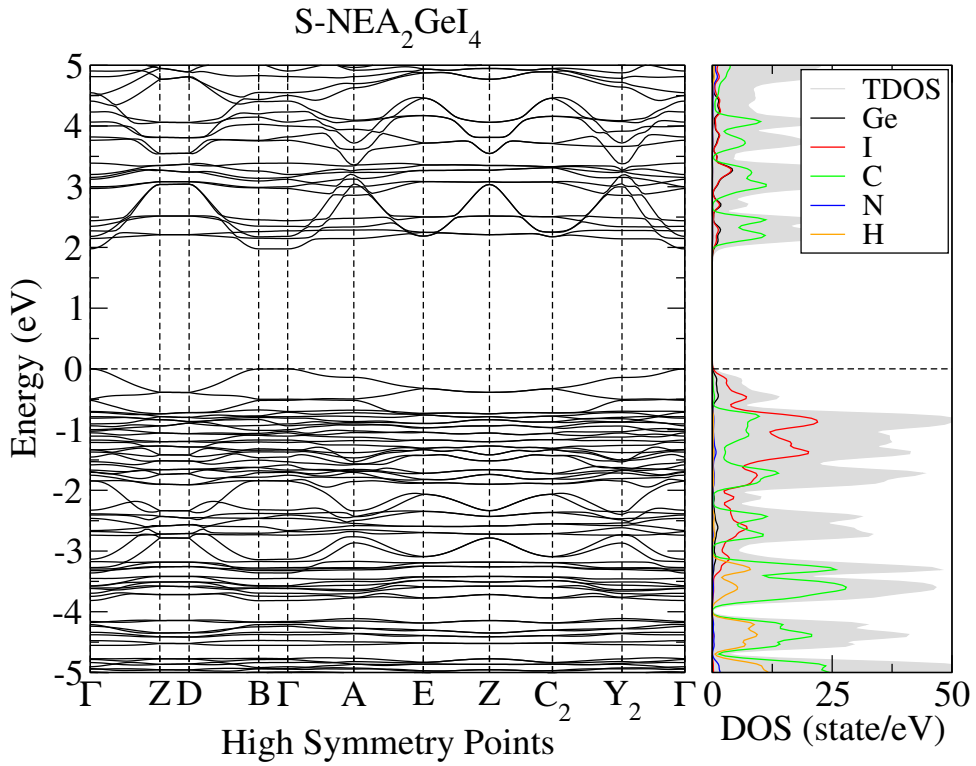

Figure S53: Band structure for $(S\text{-}NEA)_2GeI_4$ bulk with PBE+D3 functional.

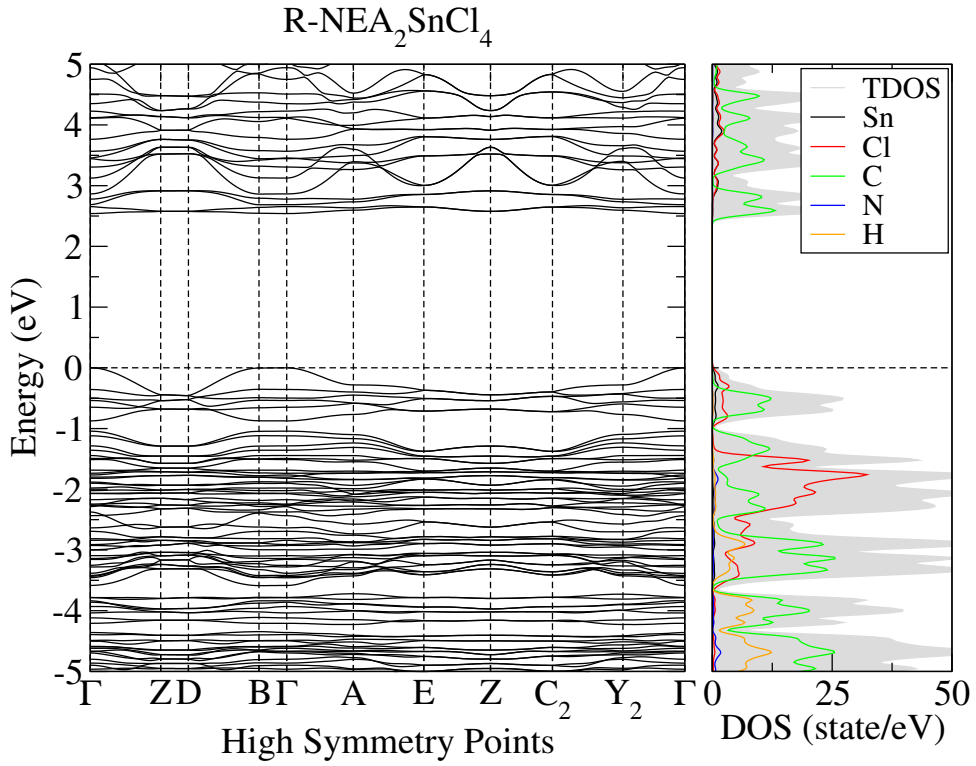

Figure S54: Band structure for $(R\text{-}NEA)_2SnCl_4$ bulk with PBE+D3 functional.

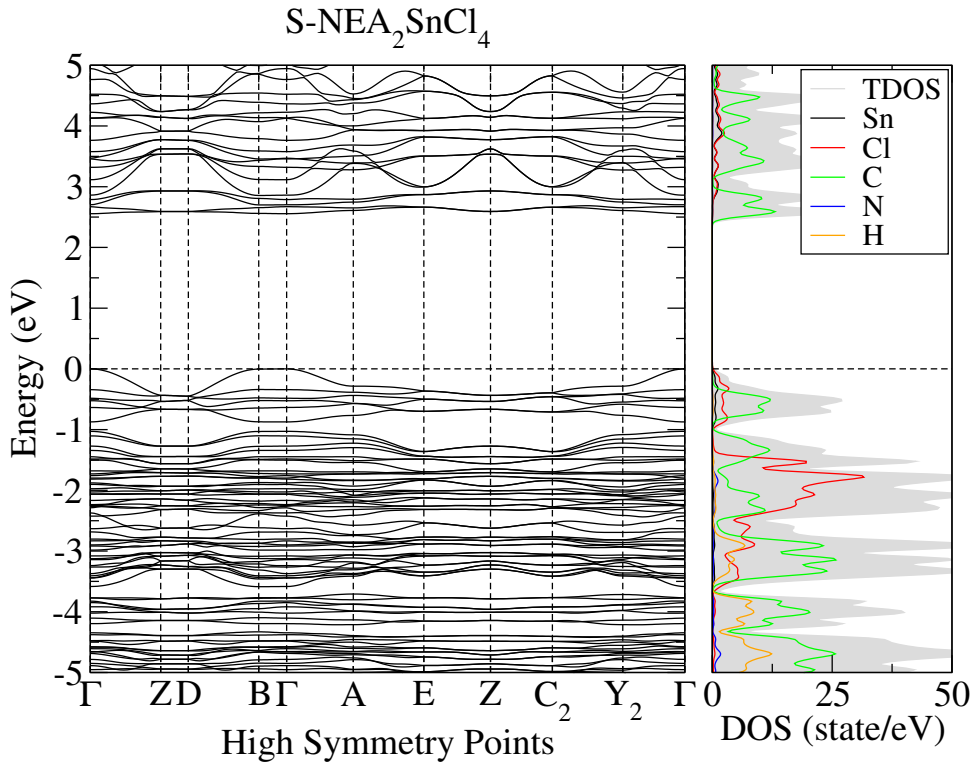

Figure S55: Band structure for $(S\text{-}NEA)_2SnCl_4$ bulk with PBE+D3 functional.

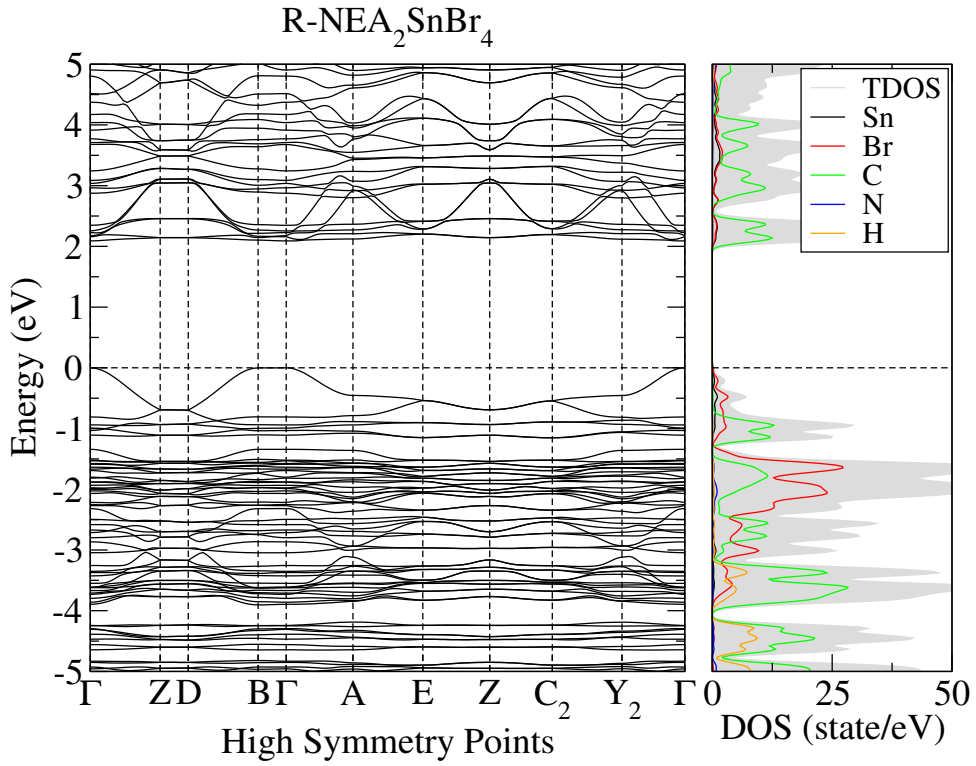

Figure S56: Band structure for $(R\text{-}NEA)_2SnBr_4$ bulk with PBE+D3 functional.

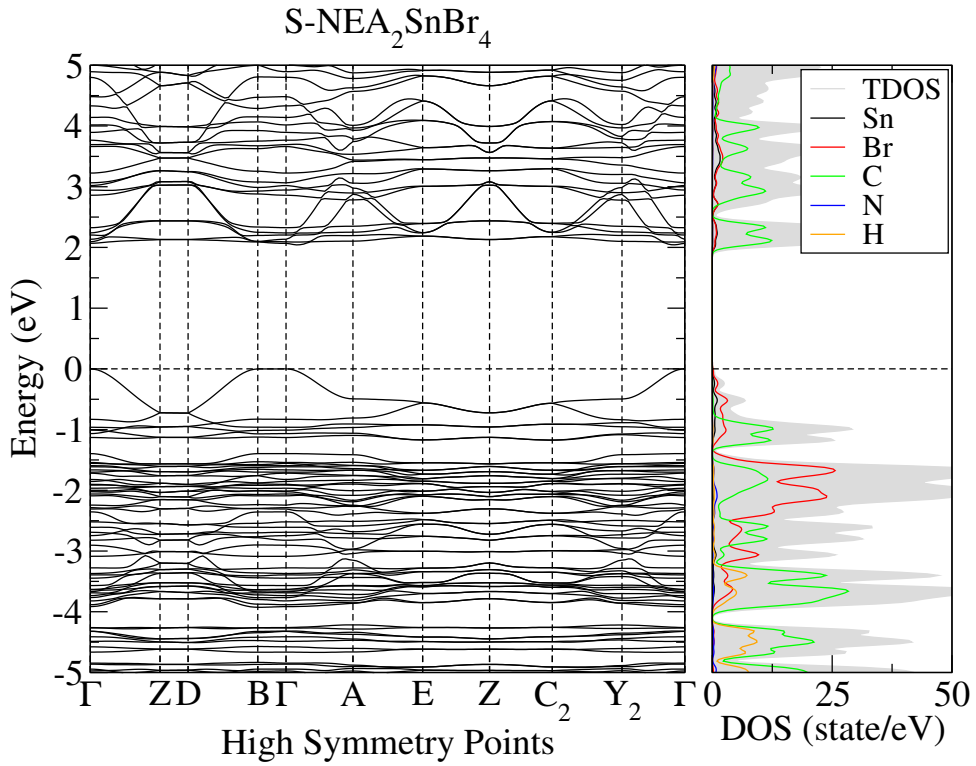

Figure S57: Band structure for $(S\text{-}NEA)_2SnBr_4$ bulk with PBE+D3 functional.

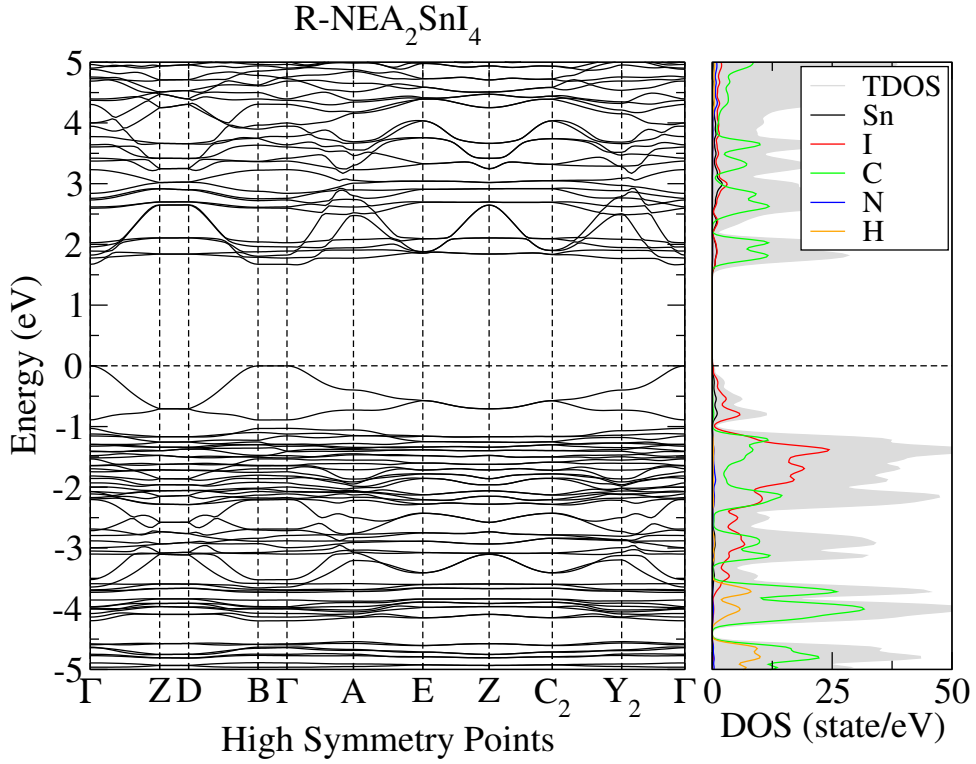

Figure S58: Band structure for $(R\text{-}NEA)_2SnI_4$ bulk with PBE+D3 functional.

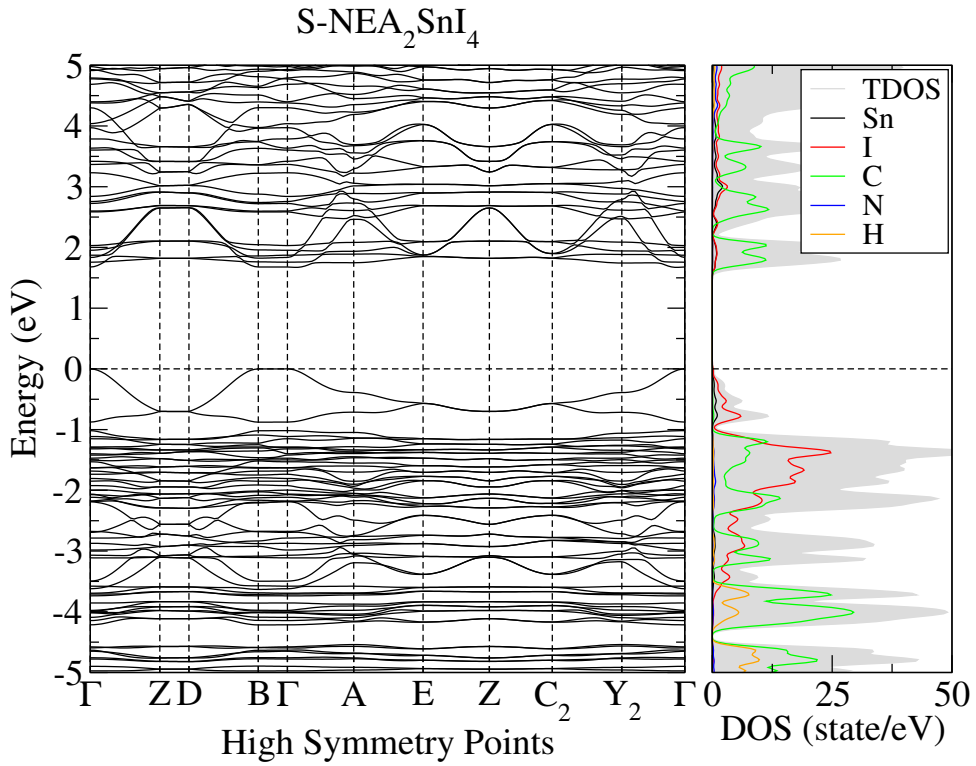

Figure S59: Band structure for $(S\text{-}NEA)_2SnI_4$ bulk with PBE+D3 functional.

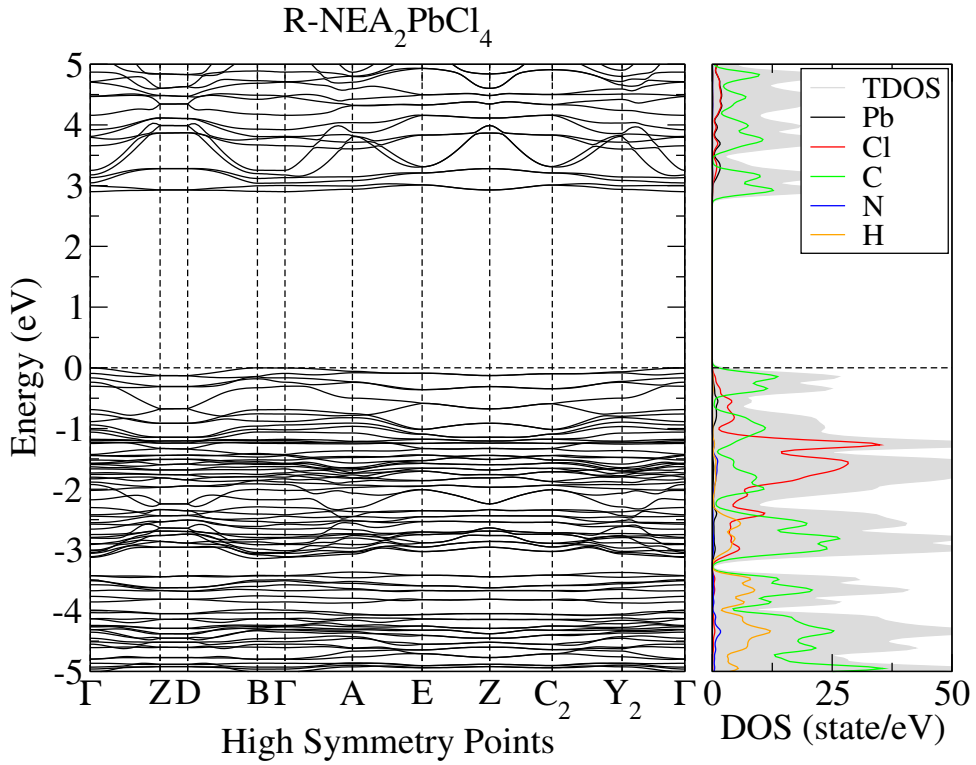

Figure S60: Band structure for $(R\text{-}NEA)_2PbCl_4$ bulk with PBE+D3 functional.

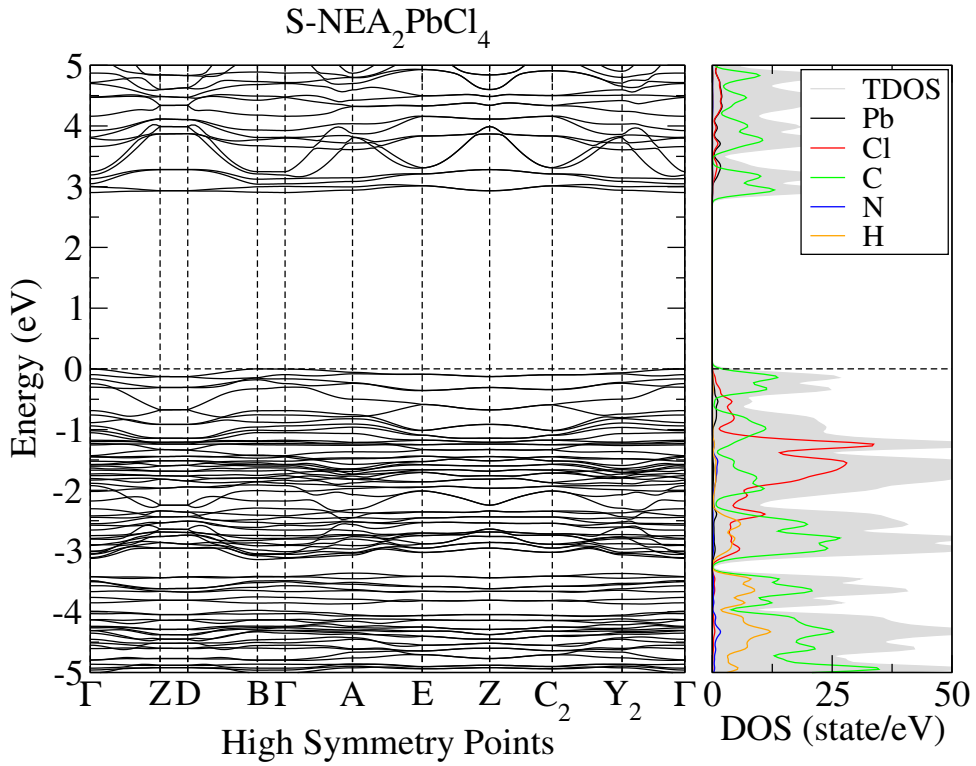

Figure S61: Band structure for $(S\text{-}NEA)_2PbCl_4$ bulk with PBE+D3 functional.

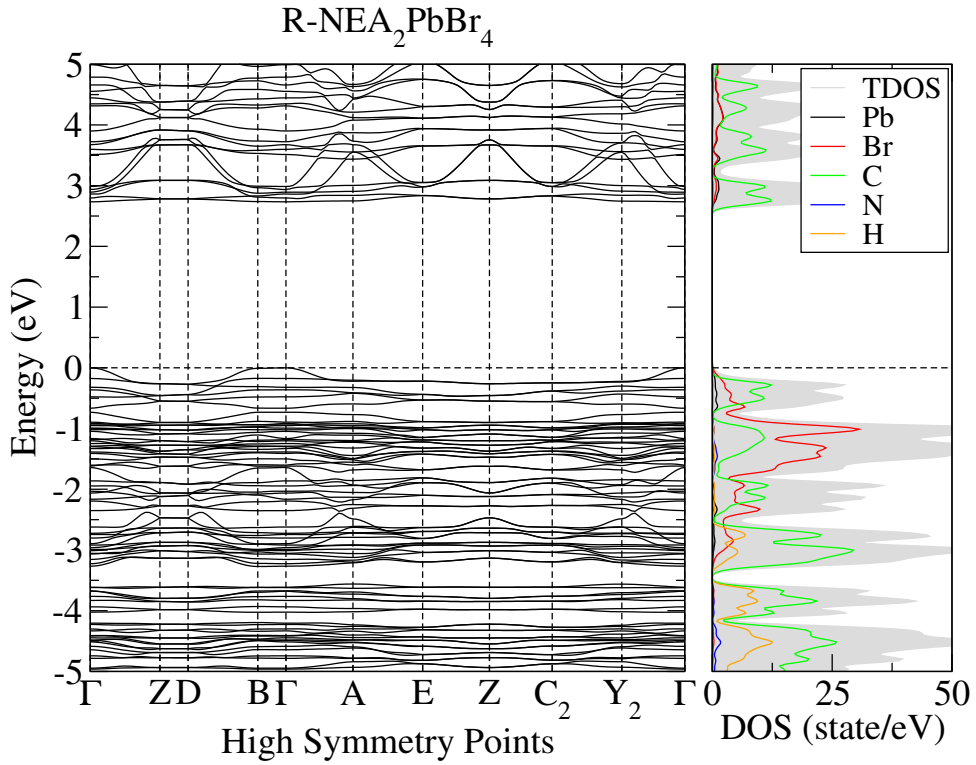

Figure S62: Band structure for $(R\text{-}NEA)_2PbBr_4$ bulk with PBE+D3 functional.

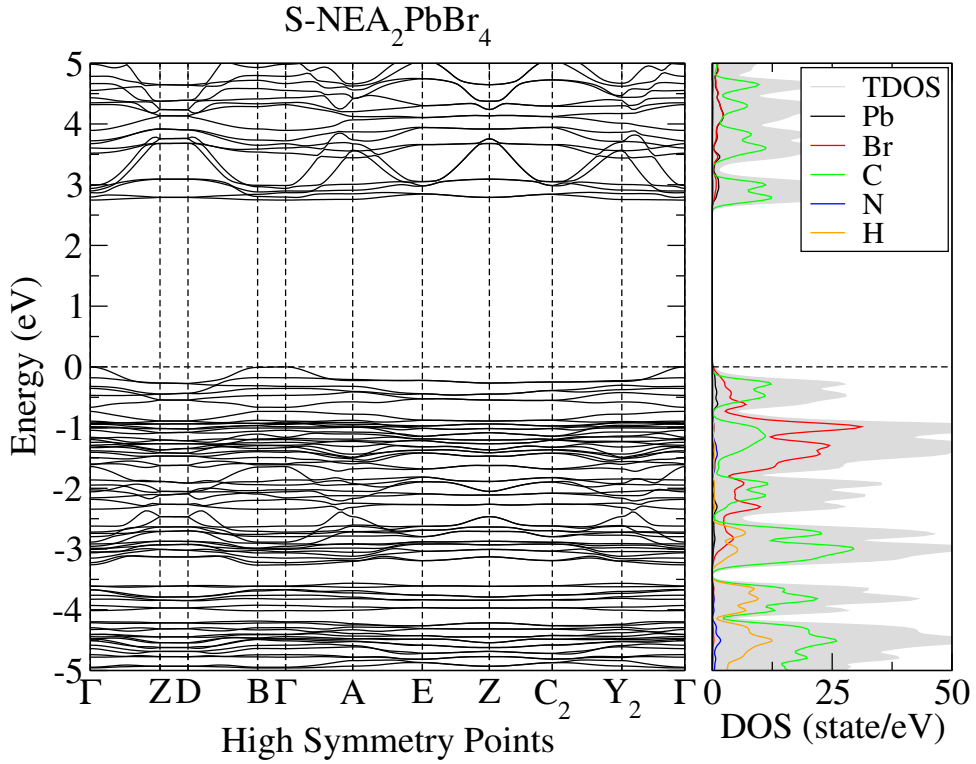

Figure S63: Band structure for $(S\text{-}NEA)_2PbBr_4$ bulk with PBE+D3 functional.

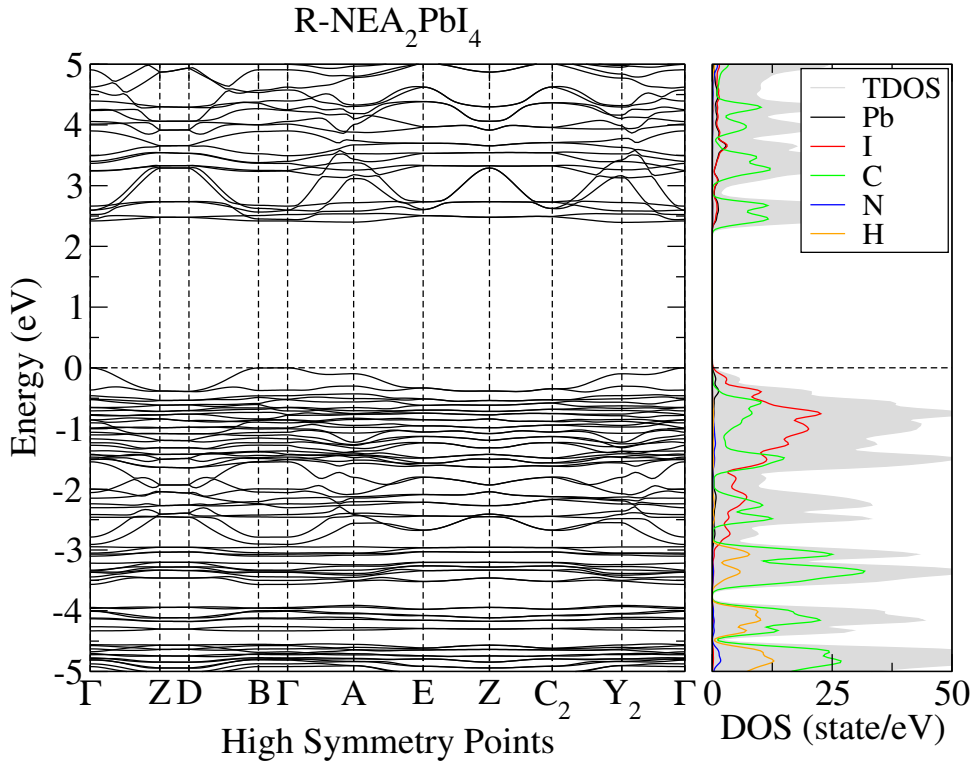

Figure S64: Band structure for $(R\text{-}NEA)_2PbI_4$ bulk with PBE+D3 functional.

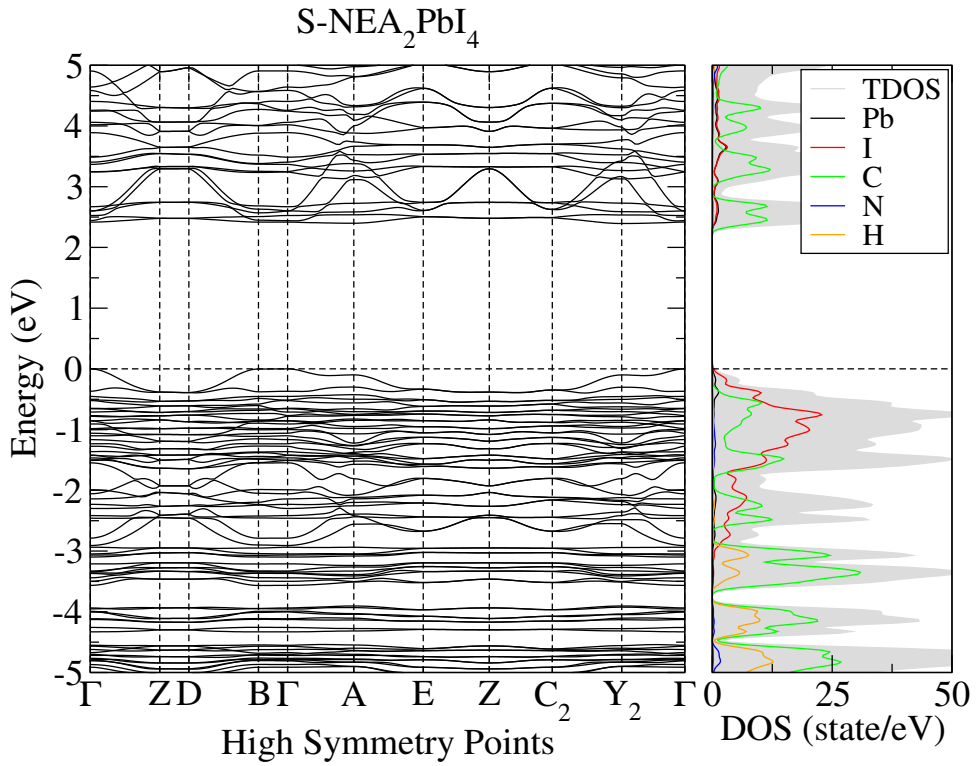

Figure S65: Band structure for $(S\text{-}NEA)_2PbI_4$ bulk with PBE+D3 functional.

7.2 Slab

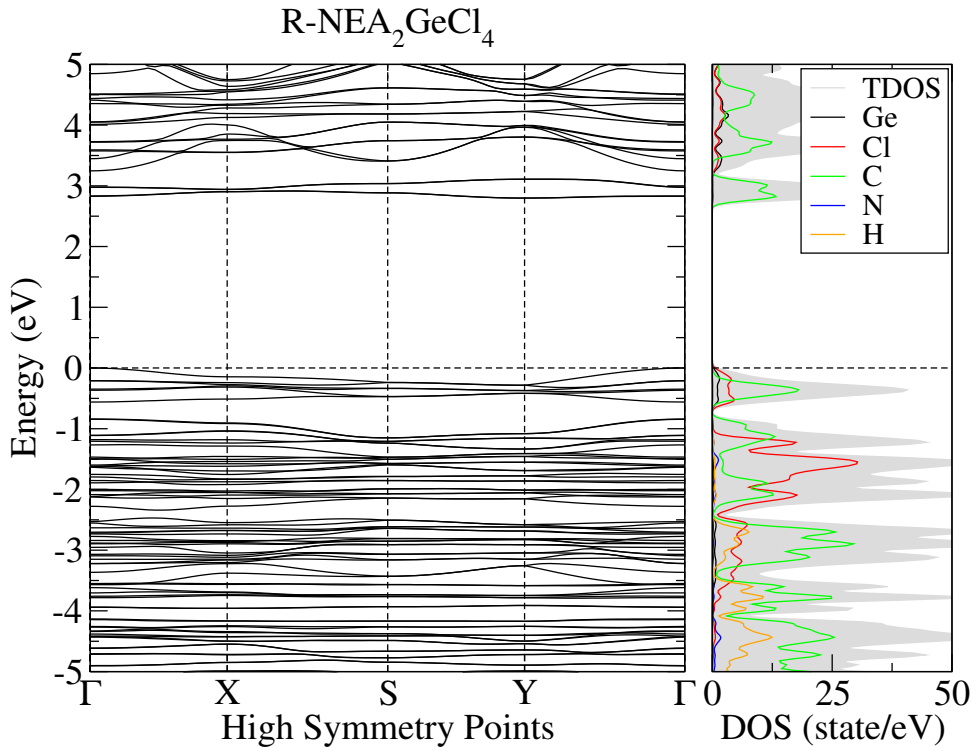

Figure S66: Band structure for $(R\text{-}NEA)_2GeCl_4$ slab with PBE+D3 functional.

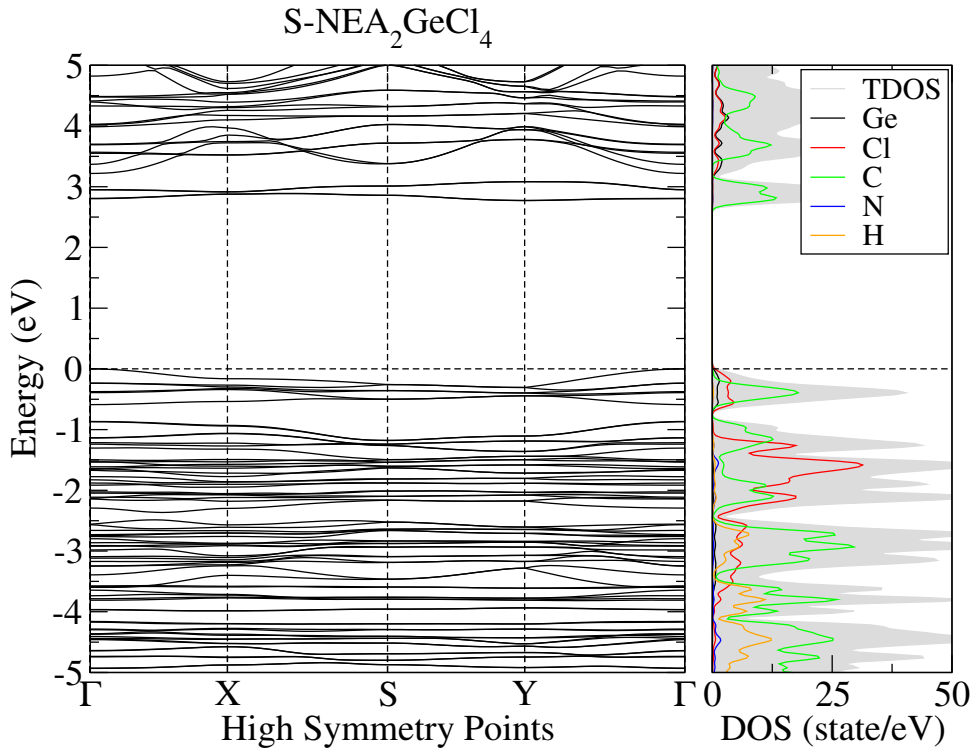

Figure S67: Band structure for $(S\text{-}NEA)_2GeCl_4$ slab with PBE+D3 functional.

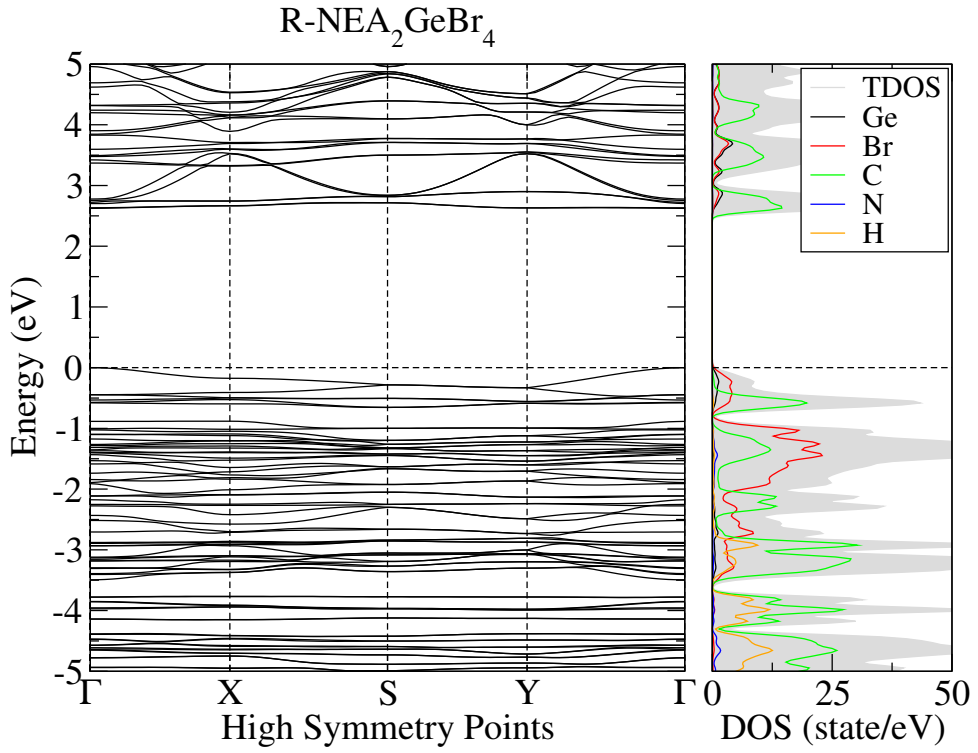

Figure S68: Band structure for $(R\text{-}NEA)_2GeBr_4$ slab with PBE+D3 functional.

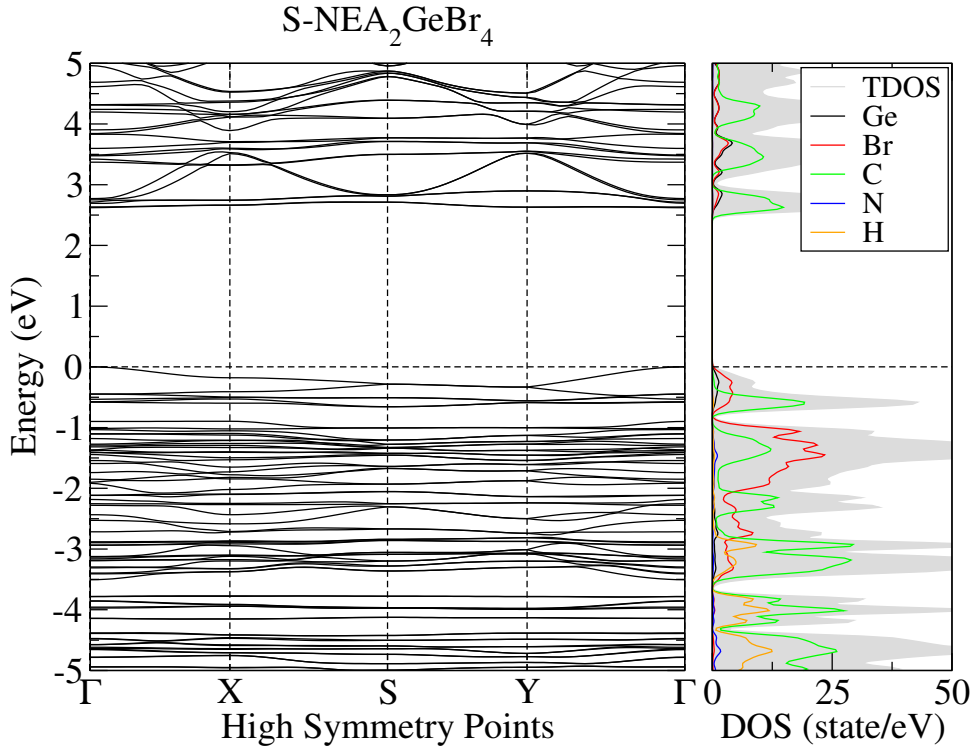

Figure S69: Band structure for $(S\text{-}NEA)_2GeBr_4$ slab with PBE+D3 functional.

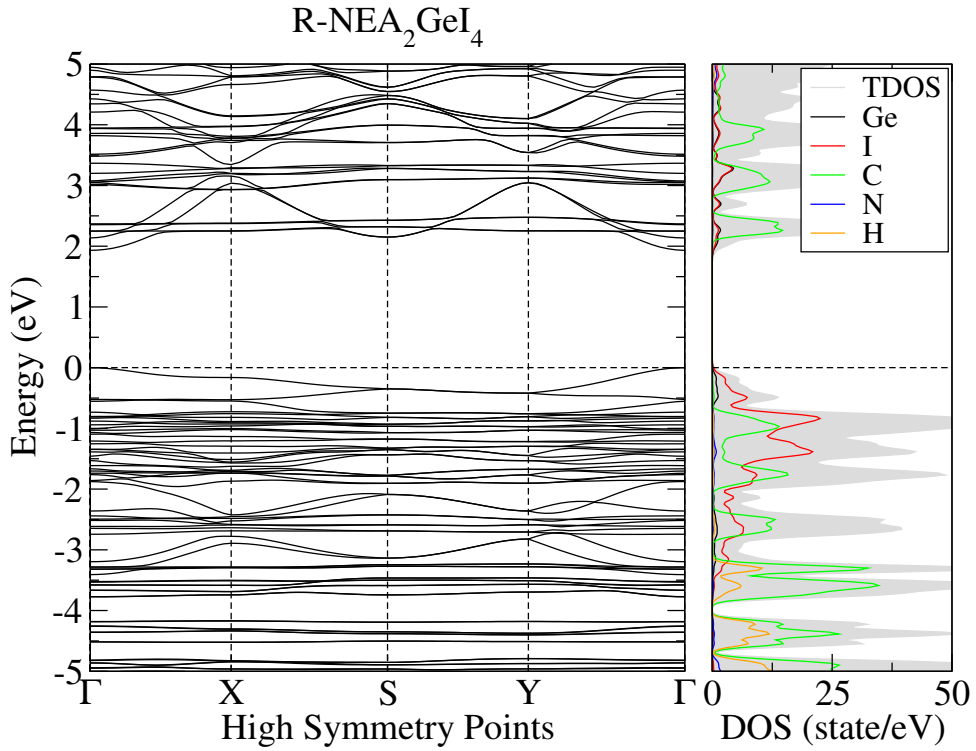

Figure S70: Band structure for $(R\text{-}NEA)_2GeI_4$ slab with PBE+D3 functional.

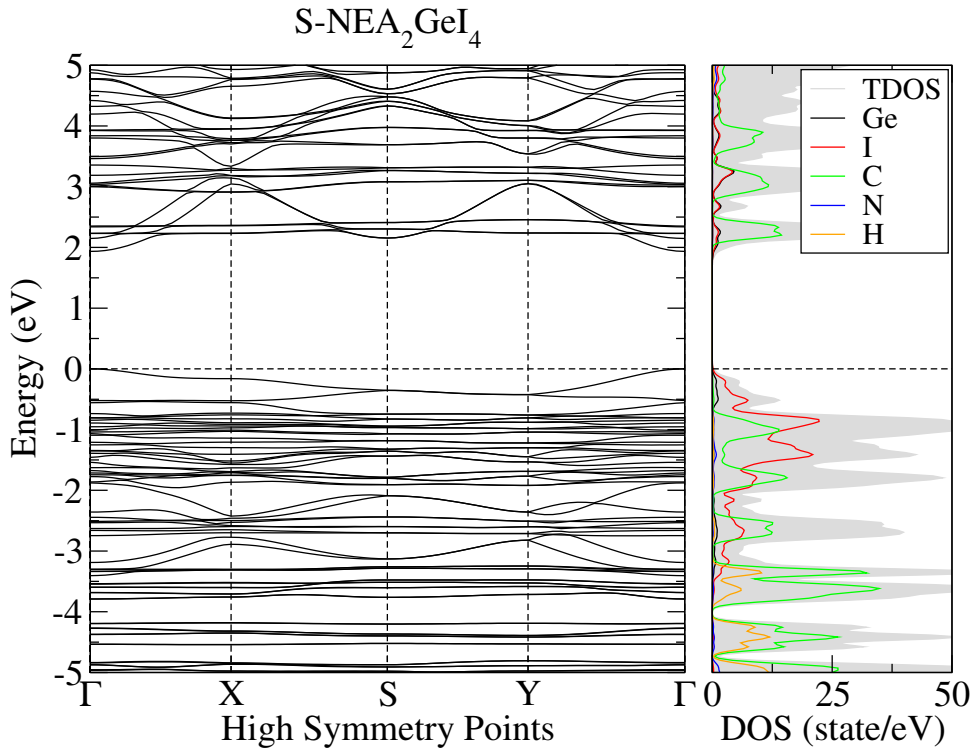

Figure S71: Band structure for $(S\text{-}NEA)_2GeI_4$ slab with PBE+D3 functional.

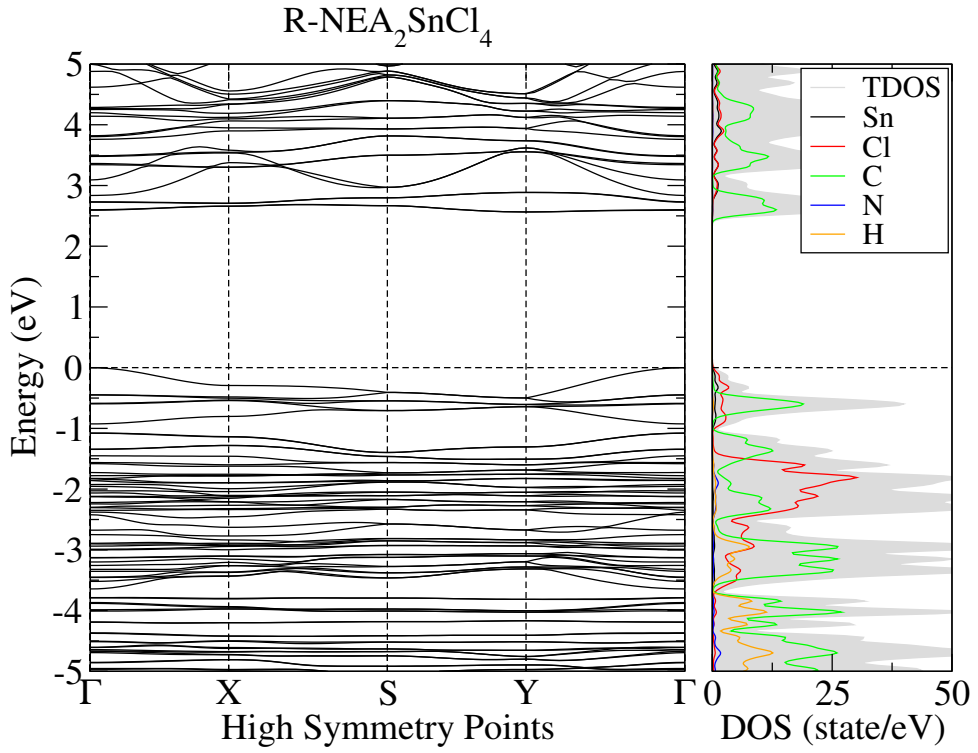

Figure S72: Band structure for $(R\text{-}NEA)_2SnCl_4$ slab with PBE+D3 functional.

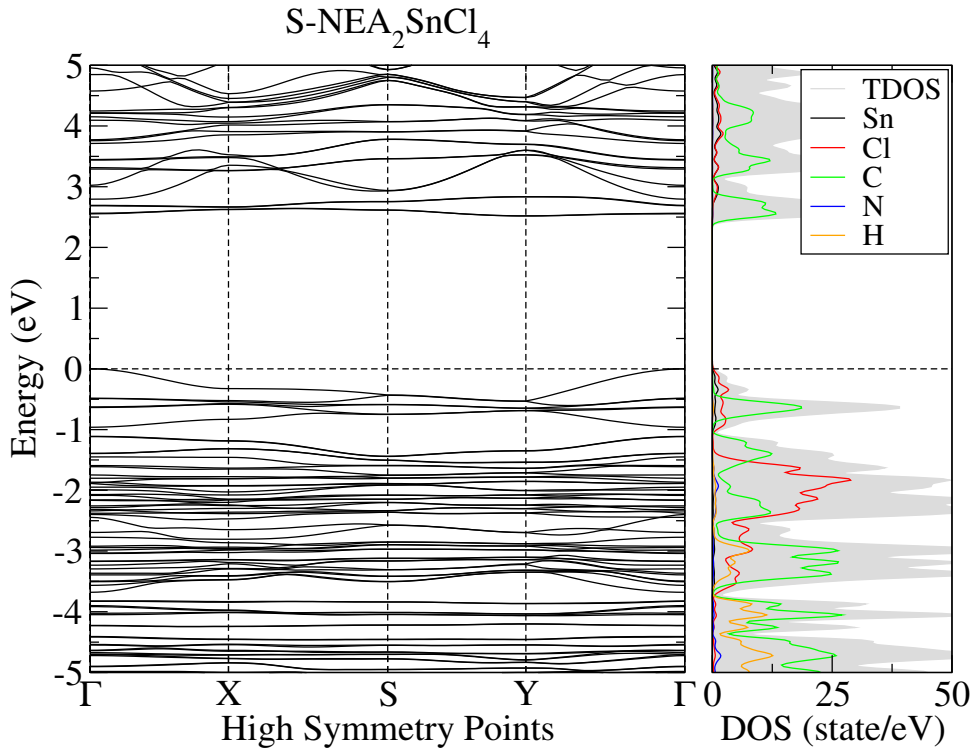

Figure S73: Band structure for $(S\text{-}NEA)_2SnCl_4$ slab with PBE+D3 functional.

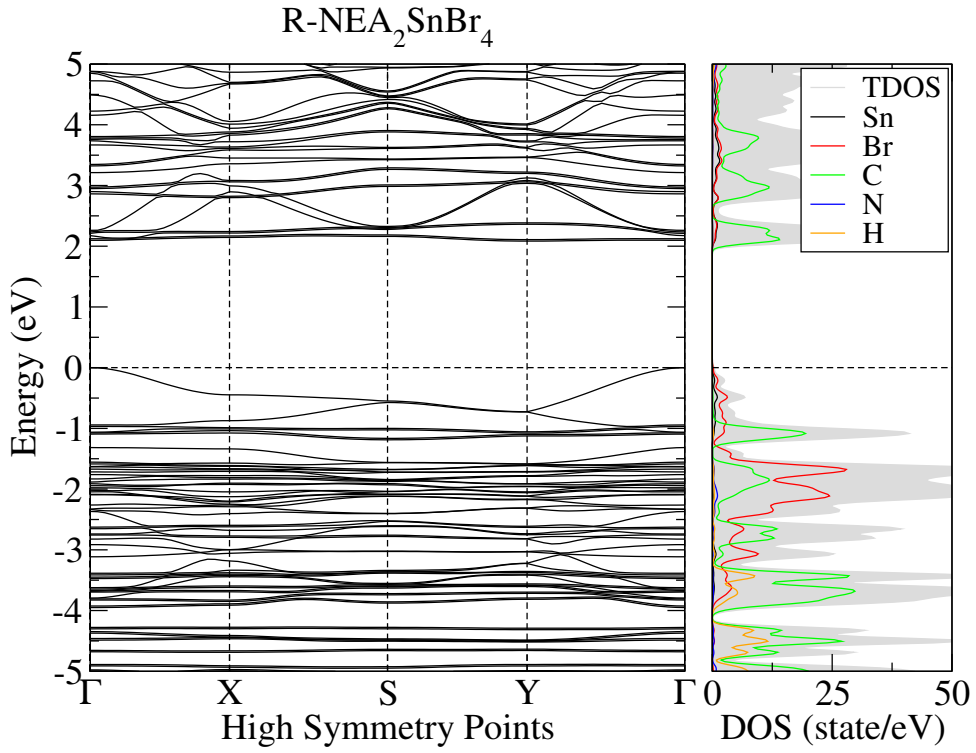

Figure S74: Band structure for $(R\text{-}NEA)_2SnBr_4$ slab with PBE+D3 functional.

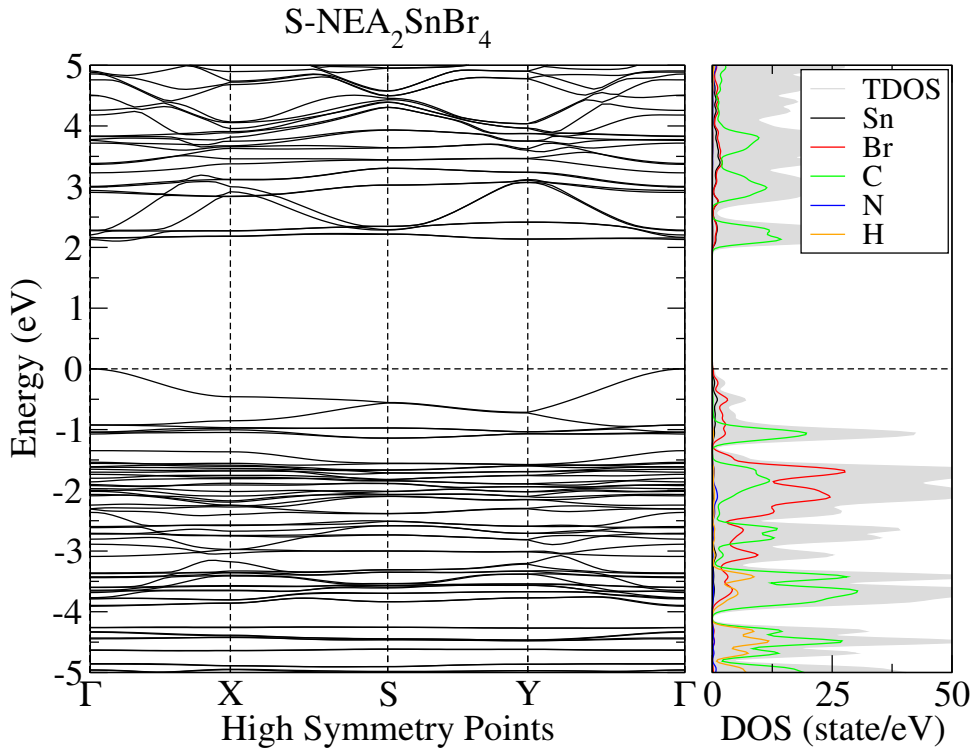

Figure S75: Band structure for $(S\text{-}NEA)_2SnBr_4$ slab with PBE+D3 functional.

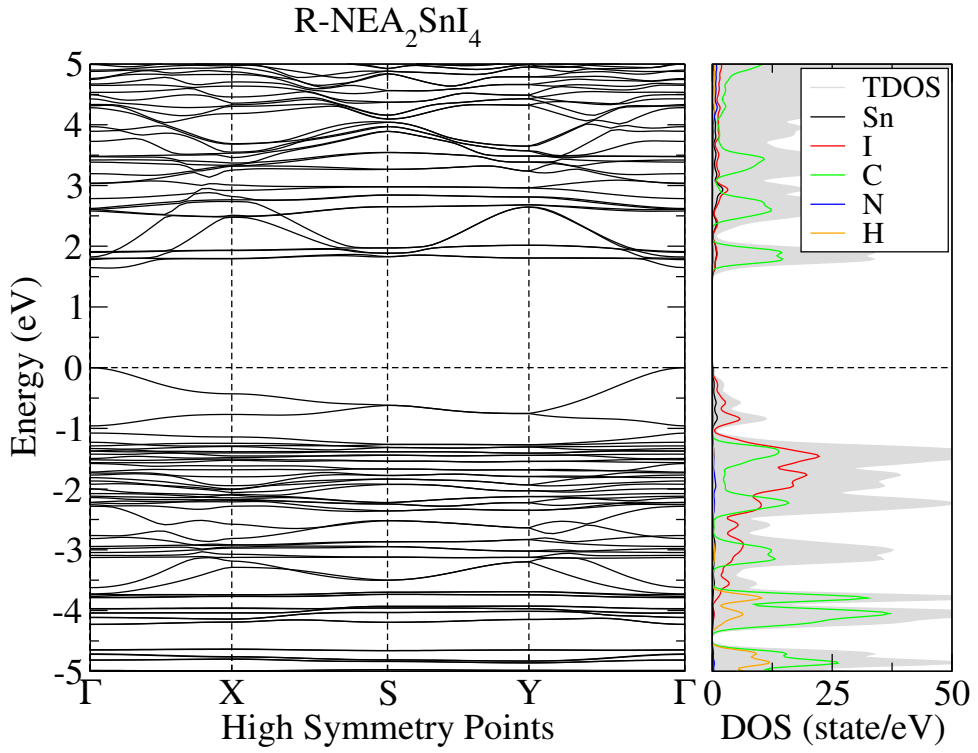

Figure S76: Band structure for $(R\text{-}NEA)_2SnI_4$ slab with PBE+D3 functional.

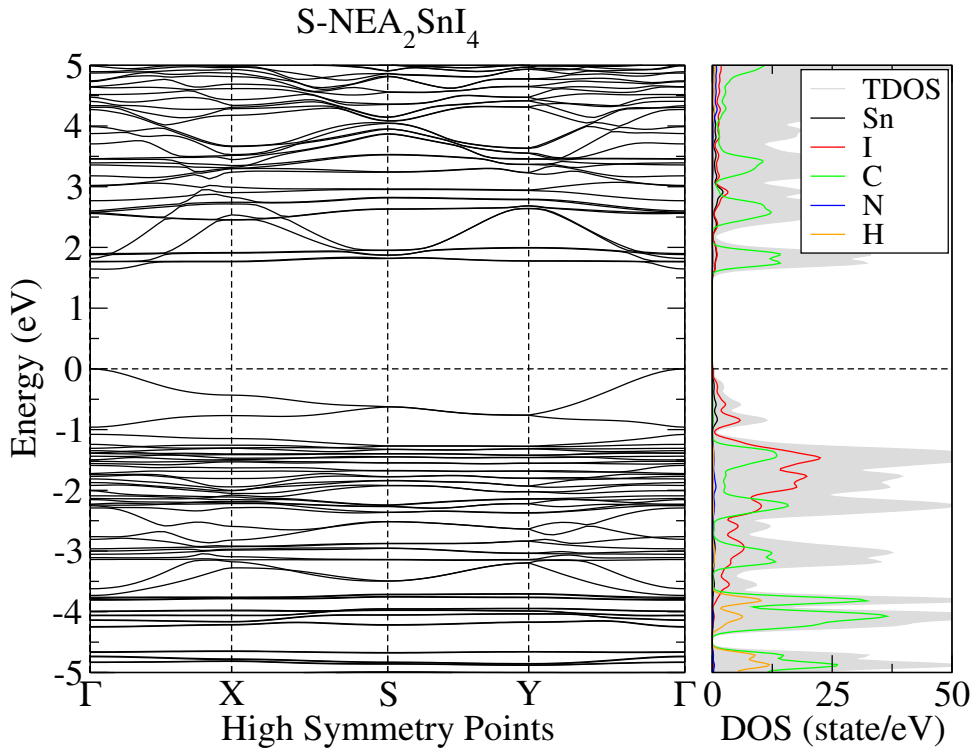

Figure S77: Band structure for $(S\text{-}NEA)_2SnI_4$ slab with PBE+D3 functional.

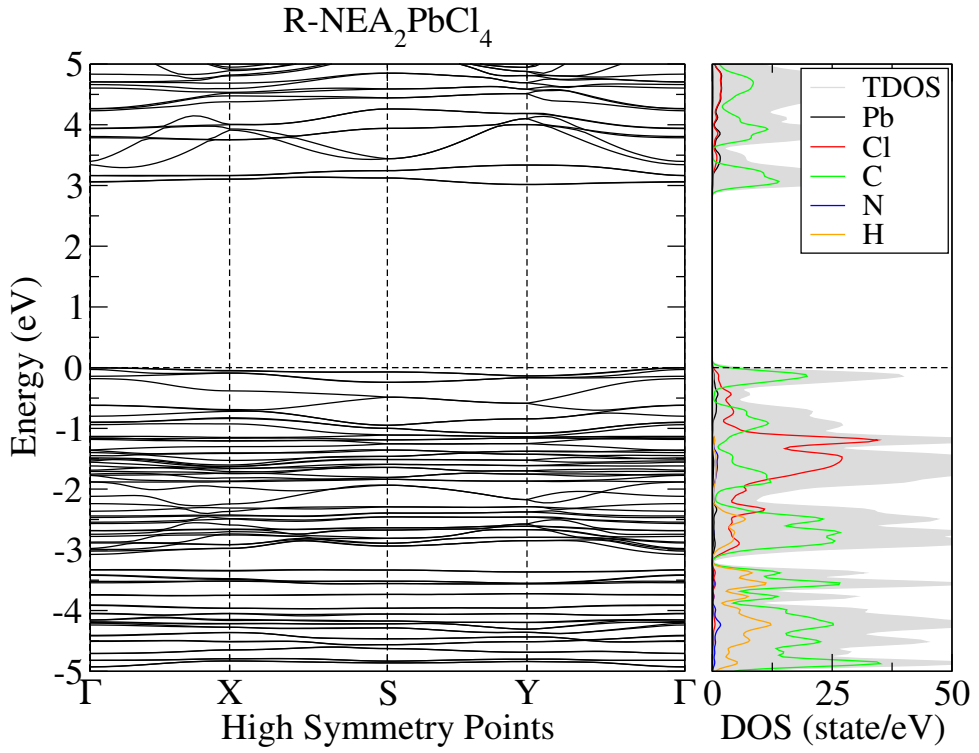

Figure S78: Band structure for $(R\text{-}NEA)_2PbCl_4$ slab with PBE+D3 functional.

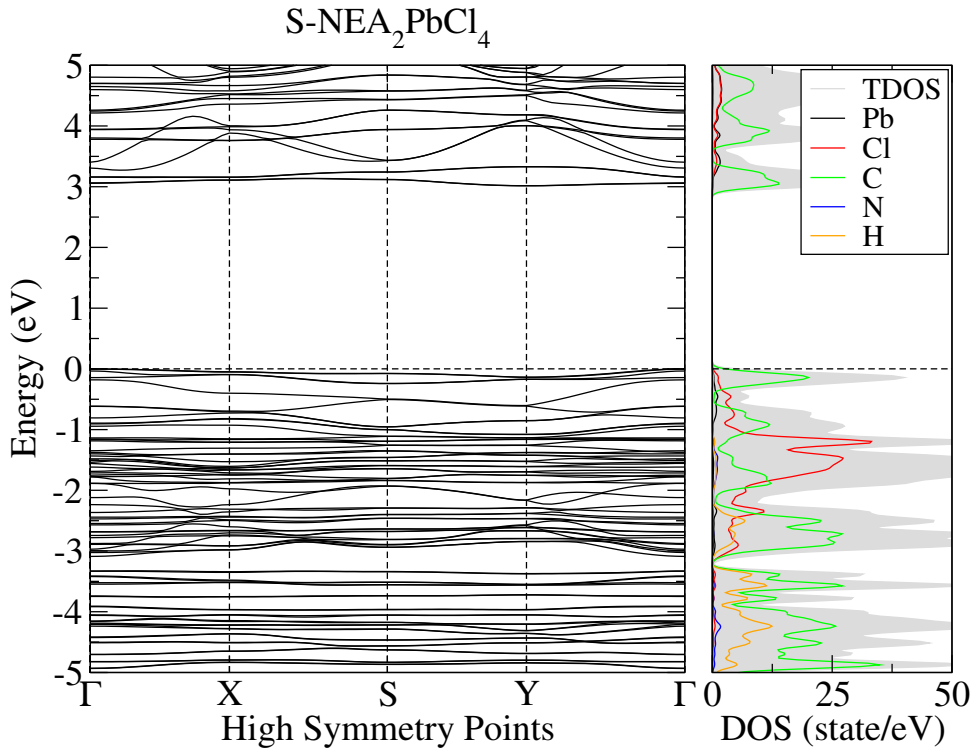

Figure S79: Band structure for $(S\text{-}NEA)_2PbCl_4$ slab with PBE+D3 functional.

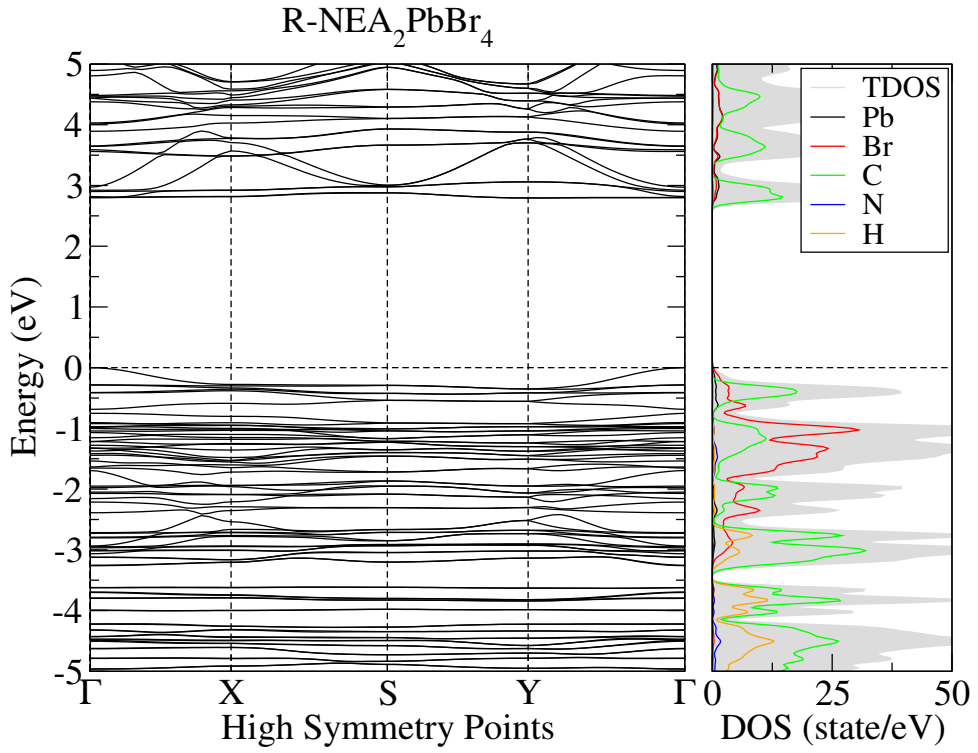

Figure S80: Band structure for $(R\text{-}NEA)_2PbBr_4$ slab with PBE+D3 functional.

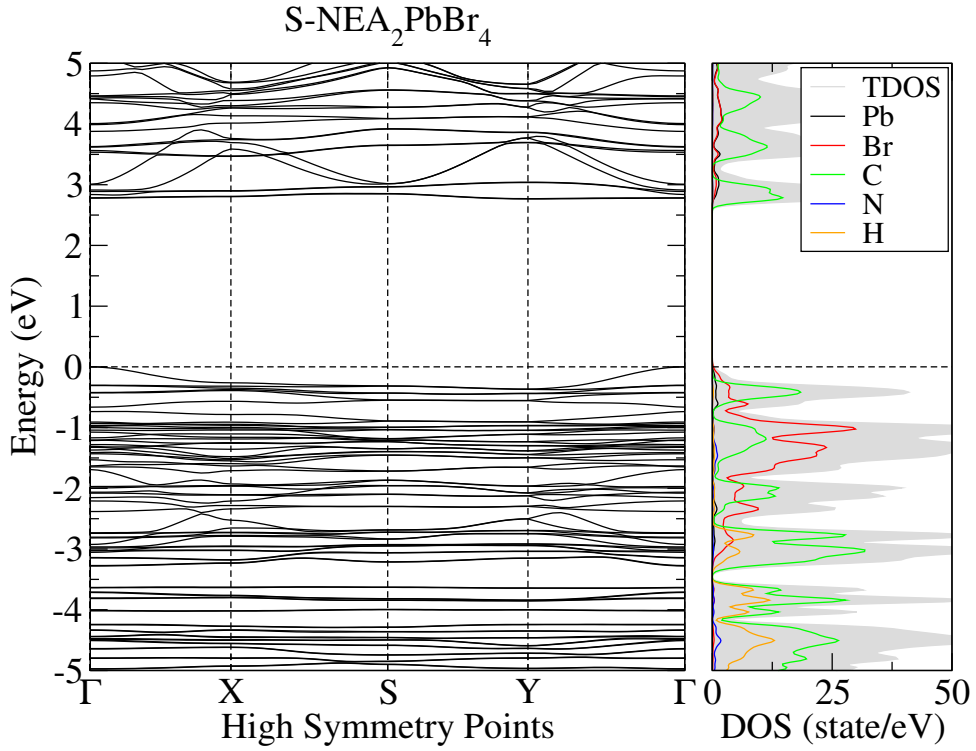

Figure S81: Band structure for $(S\text{-}NEA)_2PbBr_4$ slab with PBE+D3 functional.

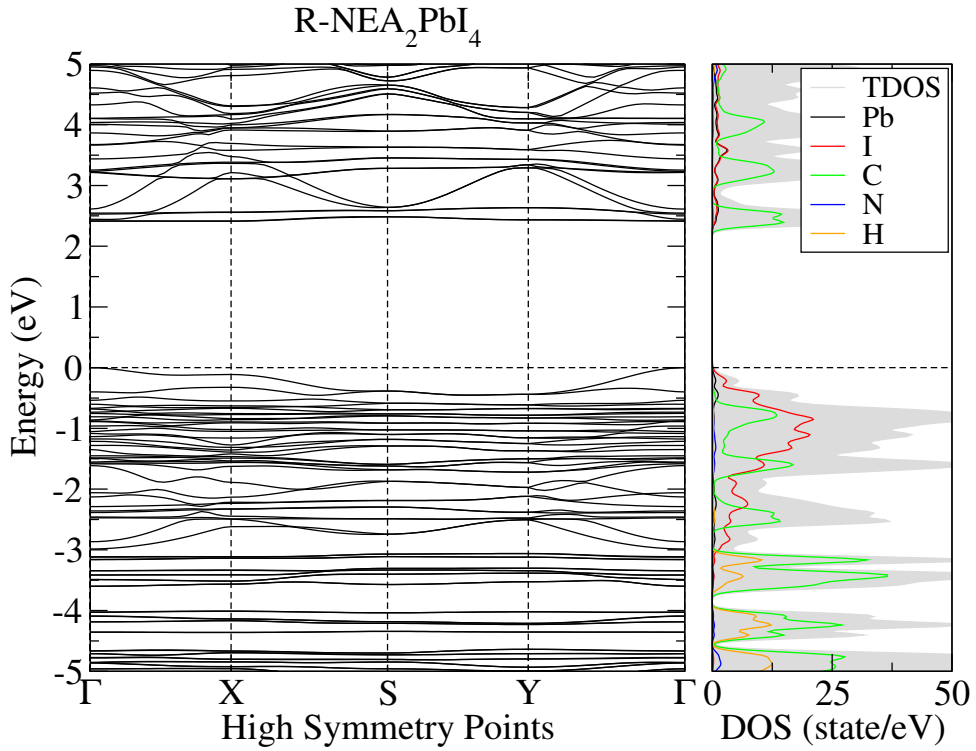

Figure S82: Band structure for $(R\text{-}NEA)_2PbI_4$ slab with PBE+D3 functional.

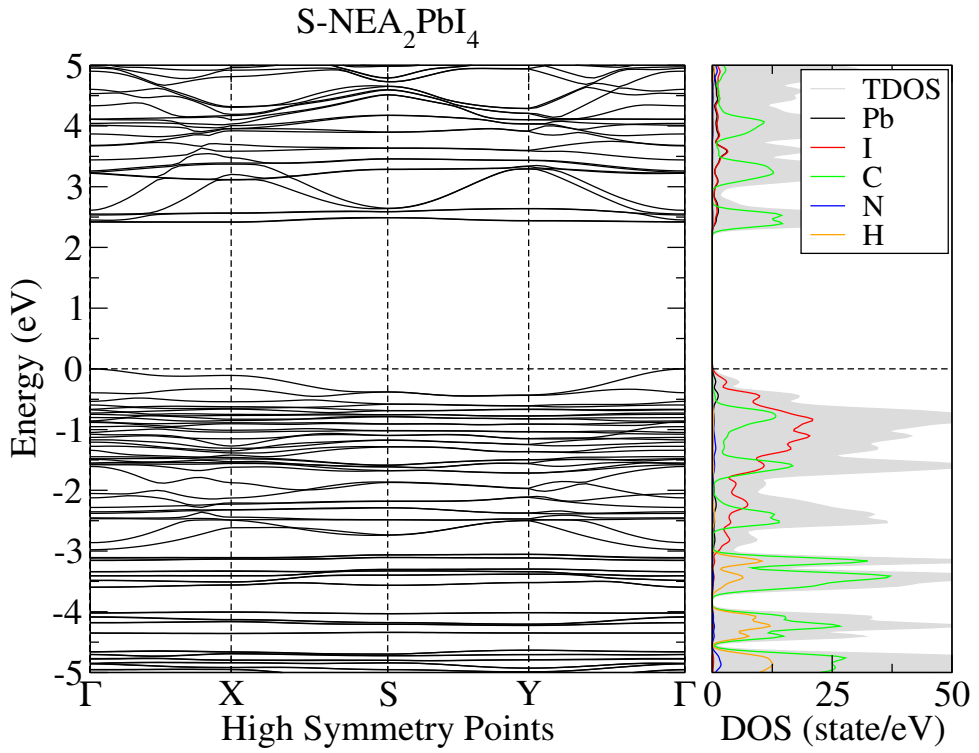

Figure S83: Band structure for $(S\text{-}NEA)_2PbI_4$ slab with PBE+D3 functional.

8 Density of States + Spin Orbit Coupling

8.1 Bulk

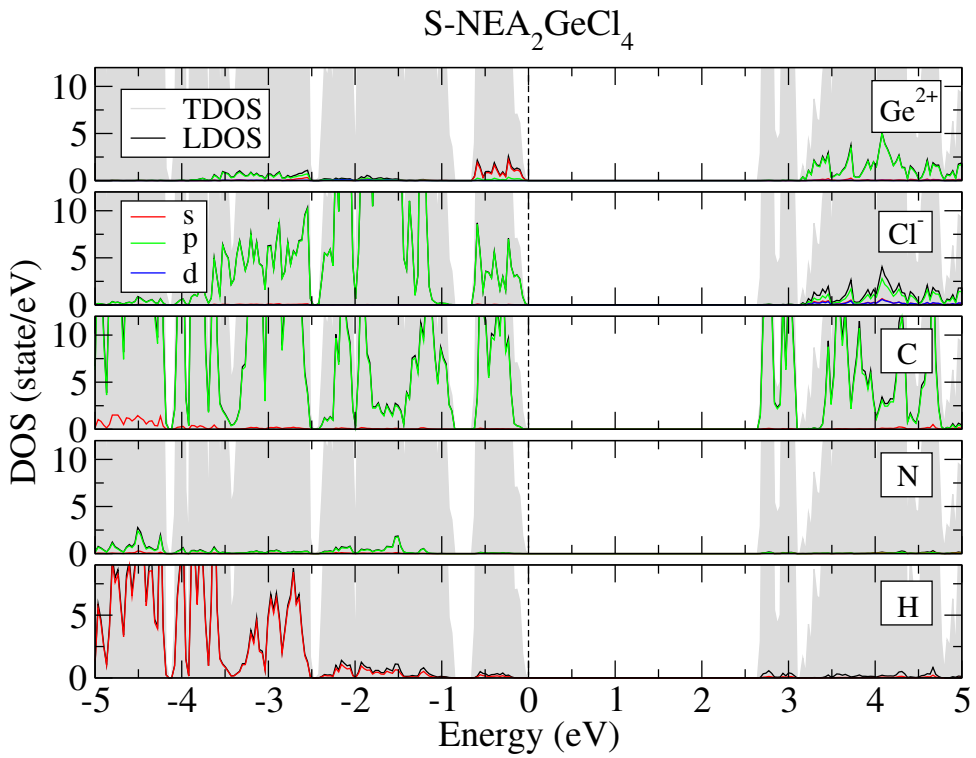

Figure S84: Density of states for $(S\text{-}NEA)_2GeCl_4$ bulk with PBE+D3+Spin Orbit Coupling (SOC) functional.

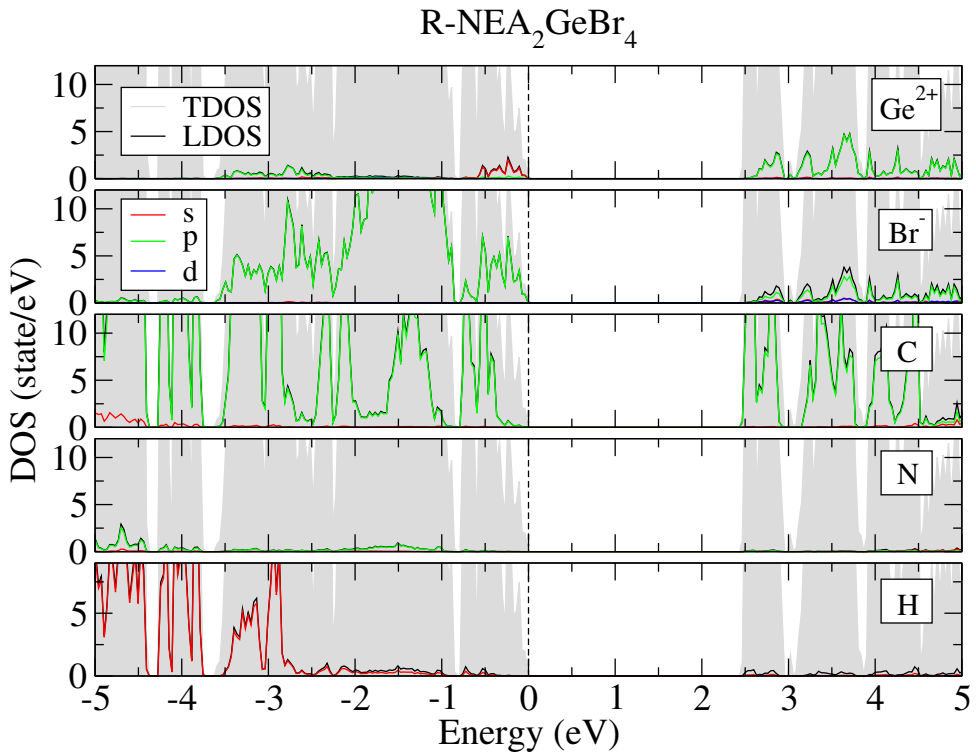

Figure S85: Density of states for $(R\text{-}NEA)_2GeBr_4$ bulk with PBE+D3+SOC functional.

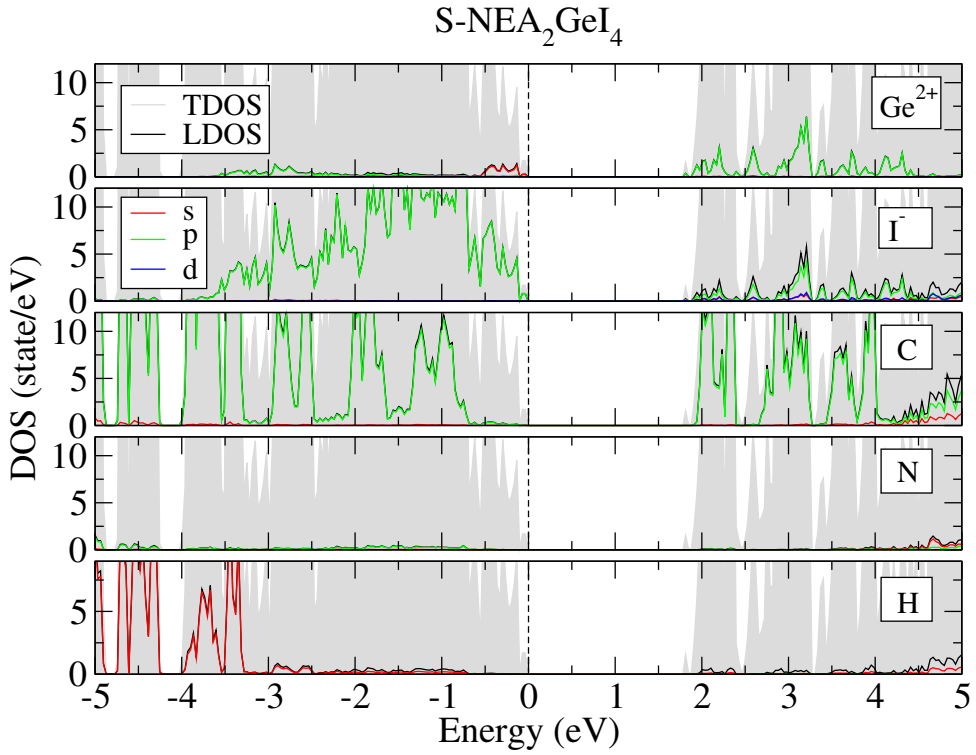

Figure S86: Density of states for $(S\text{-}NEA)_2GeI_4$ bulk with PBE+D3+SOC functional.

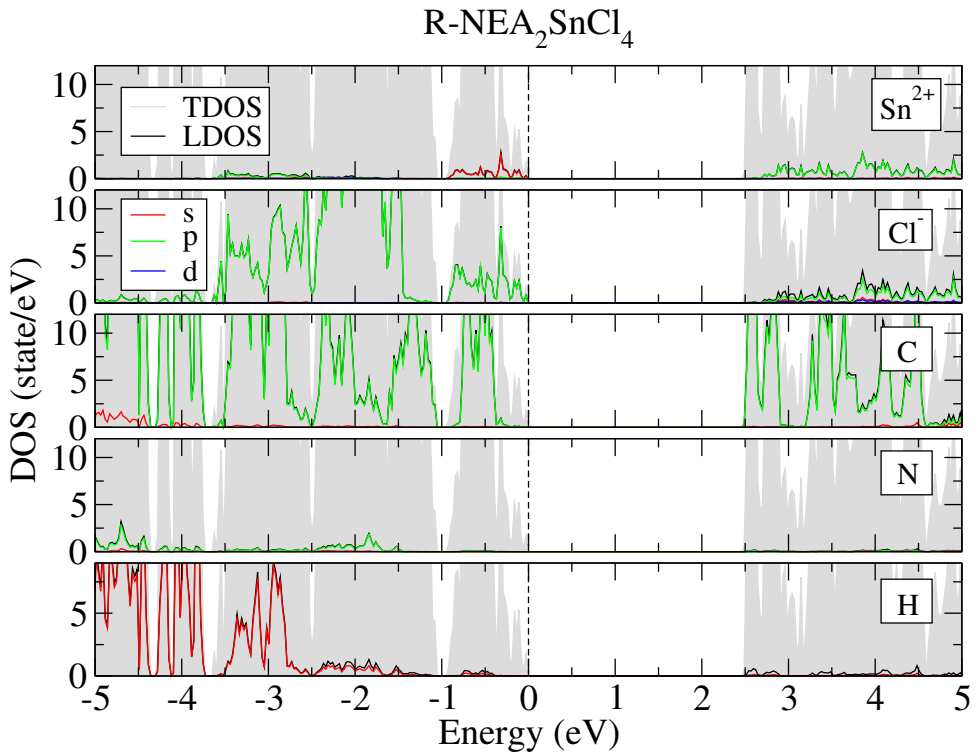

Figure S87: Density of states for $(R\text{-}NEA)_2SnCl_4$ bulk with PBE+D3+SOC functional.

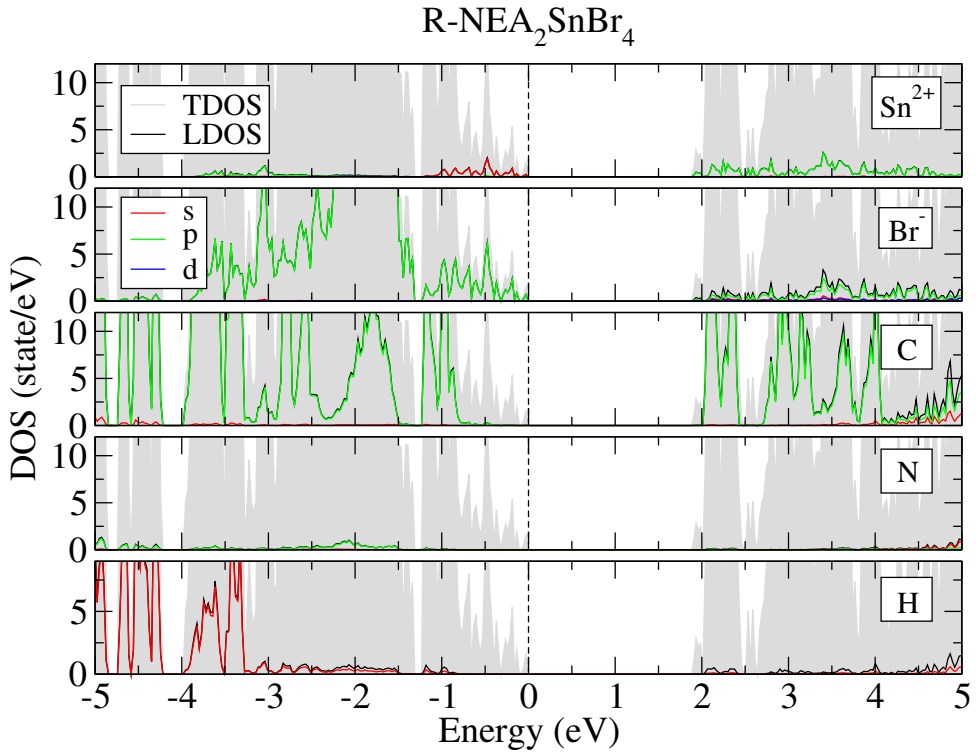

Figure S88: Density of states for $(R\text{-}NEA)_2SnBr_4$ bulk with PBE+D3+SOC functional.

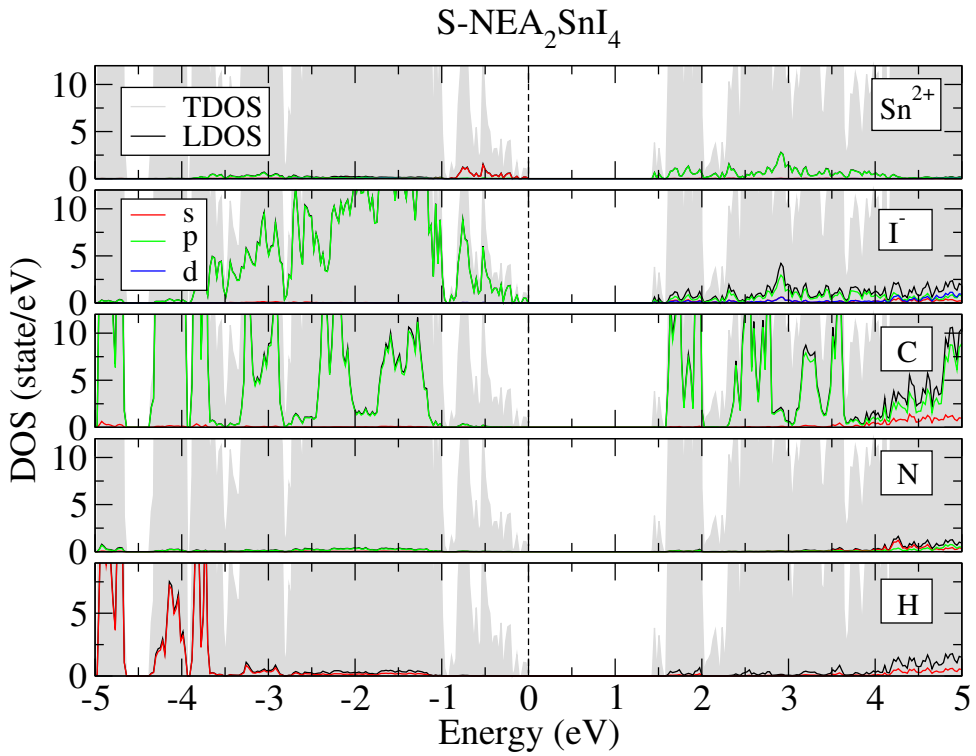

Figure S89: Density of states for $(S\text{-}NEA)_2SnI_4$ bulk with PBE+D3+SOC functional.

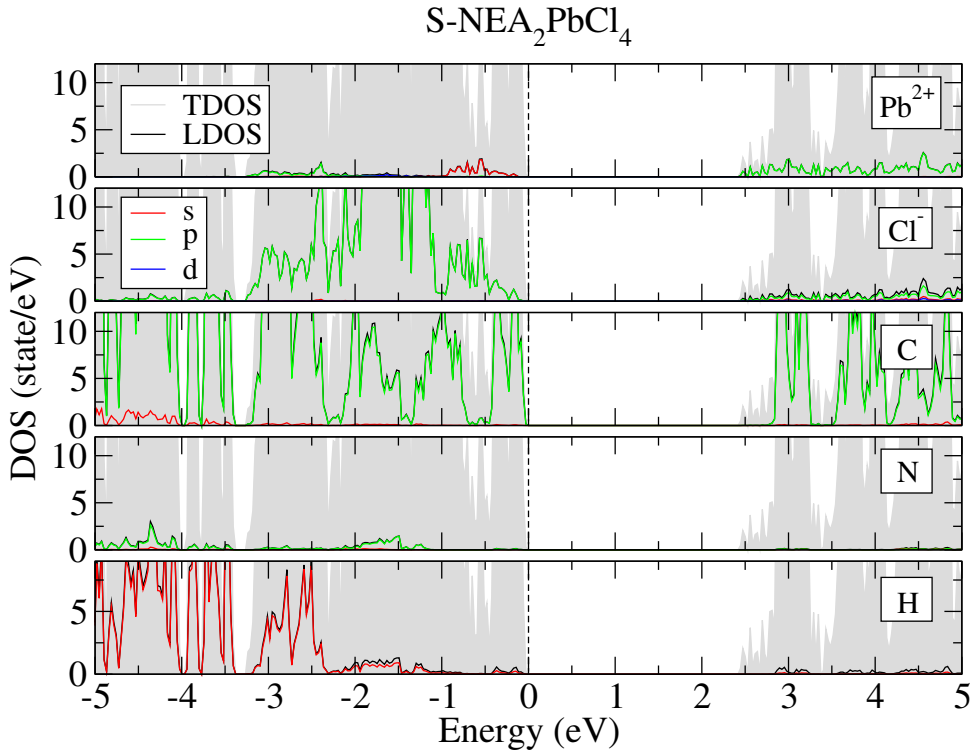

Figure S90: Density of states for $(S\text{-}NEA)_2PbCl_4$ bulk with PBE+D3+SOC functional.

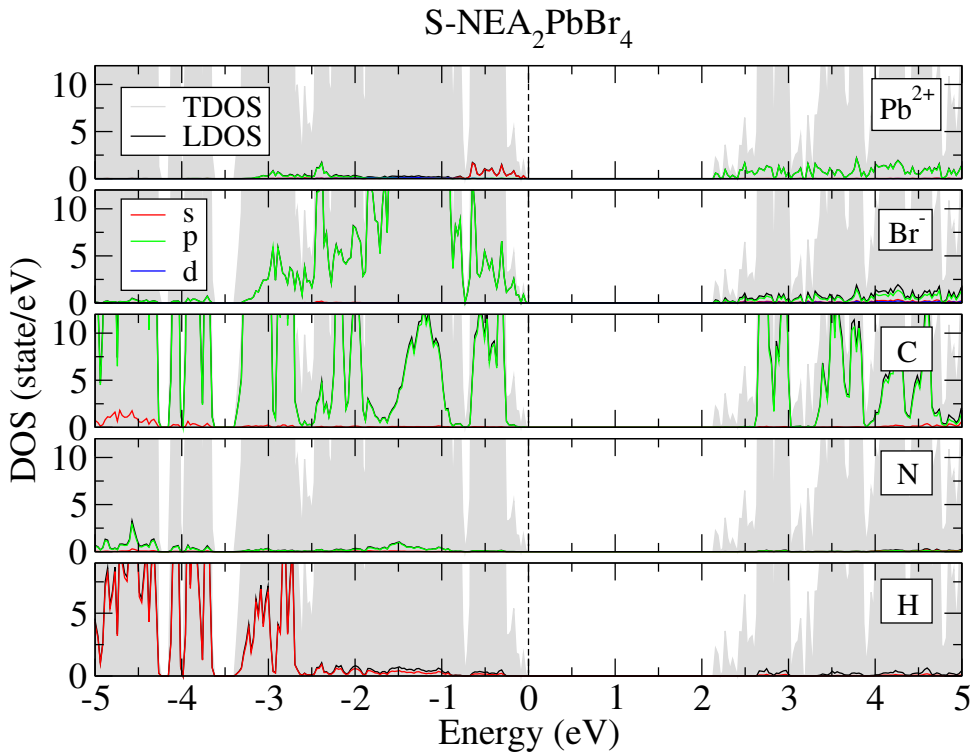

Figure S91: Density of states for $(S\text{-}NEA)_2PbBr_4$ bulk with PBE+D3+SOC functional.

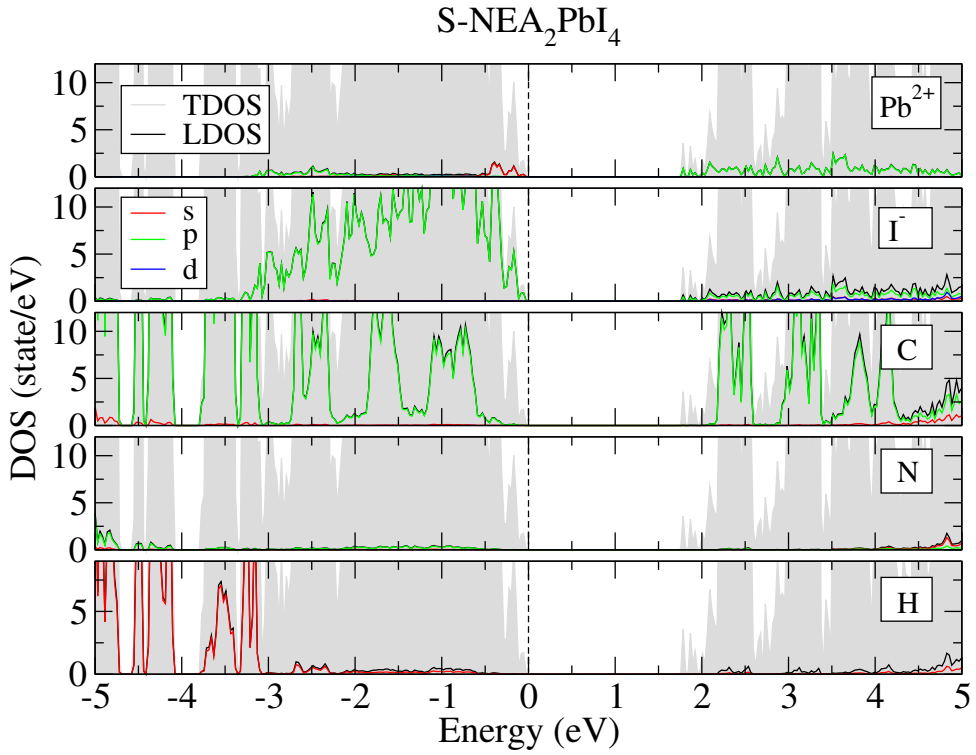

Figure S92: Density of states for $(S\text{-}NEA)_2PbI_4$ bulk with PBE+D3+SOC functional.

8.2 Slab

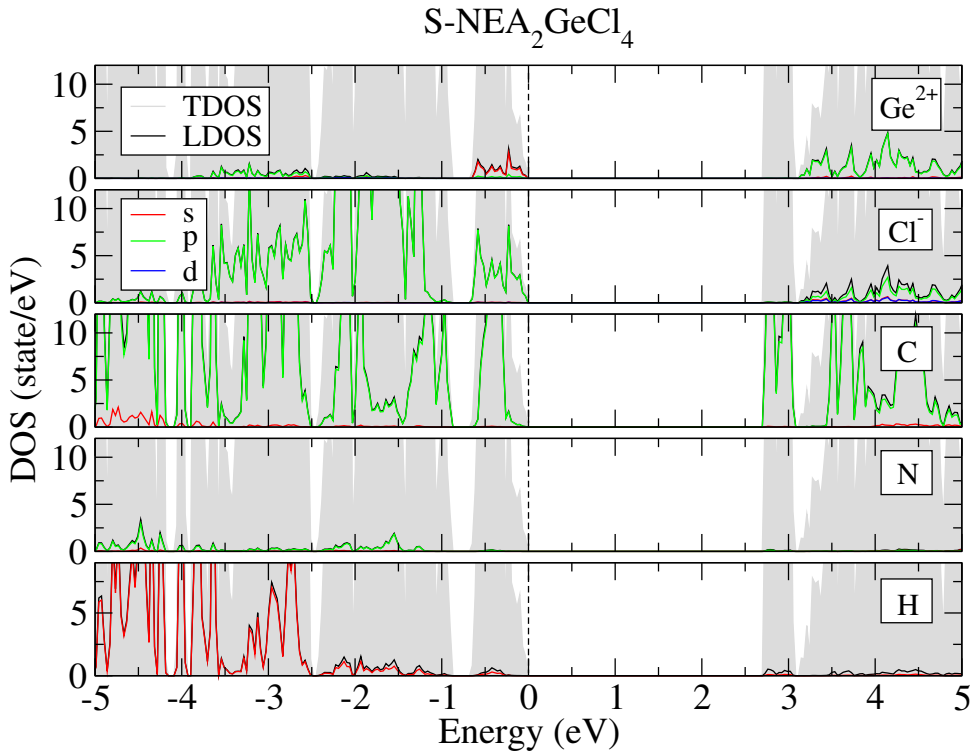

Figure S93: Density of states for $(S\text{-}NEA)_2GeCl_4$ slab with PBE+D3+SOC functional.

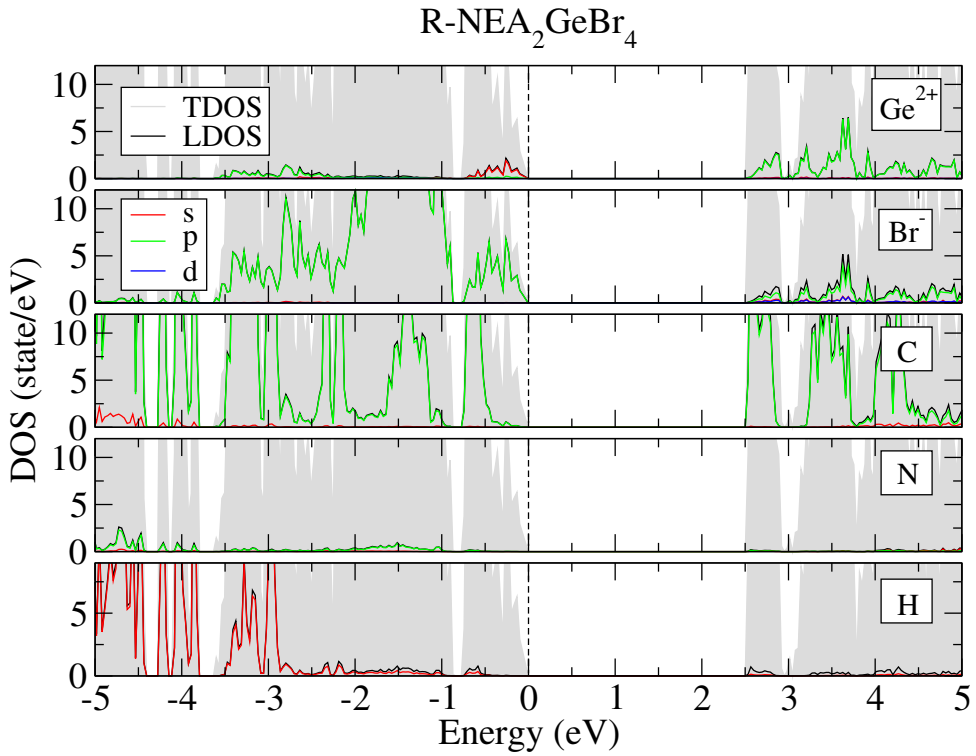

Figure S94: Density of states for $(R\text{-}NEA)_2GeBr_4$ slab with PBE+D3+SOC functional.

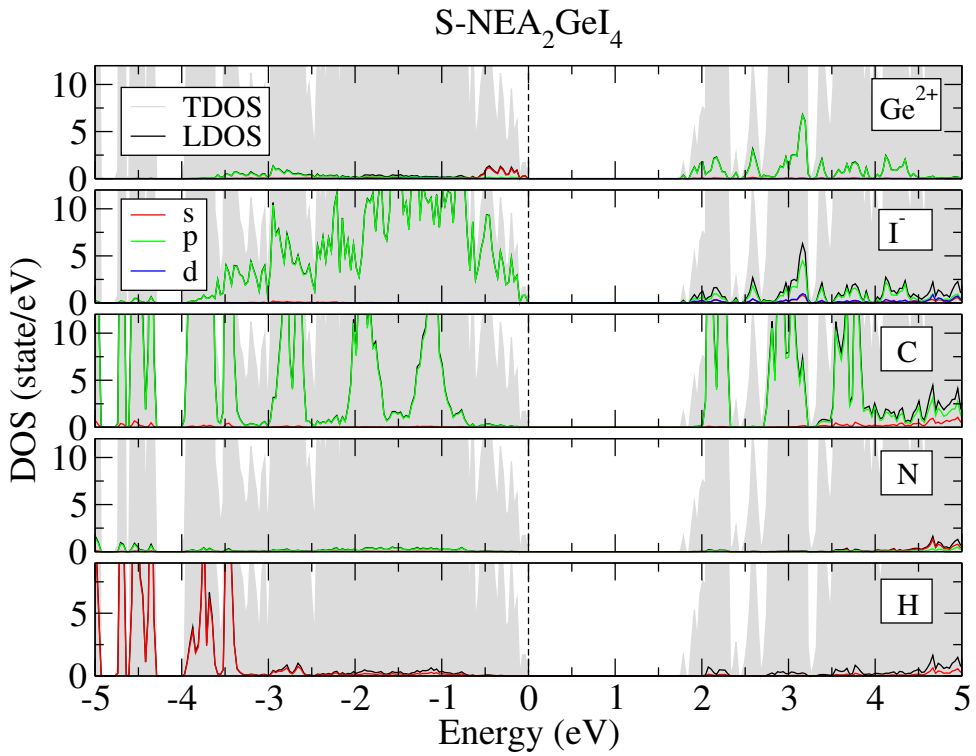

Figure S95: Density of states for $(S\text{-}NEA)_2GeI_4$ slab with PBE+D3+SOC functional.

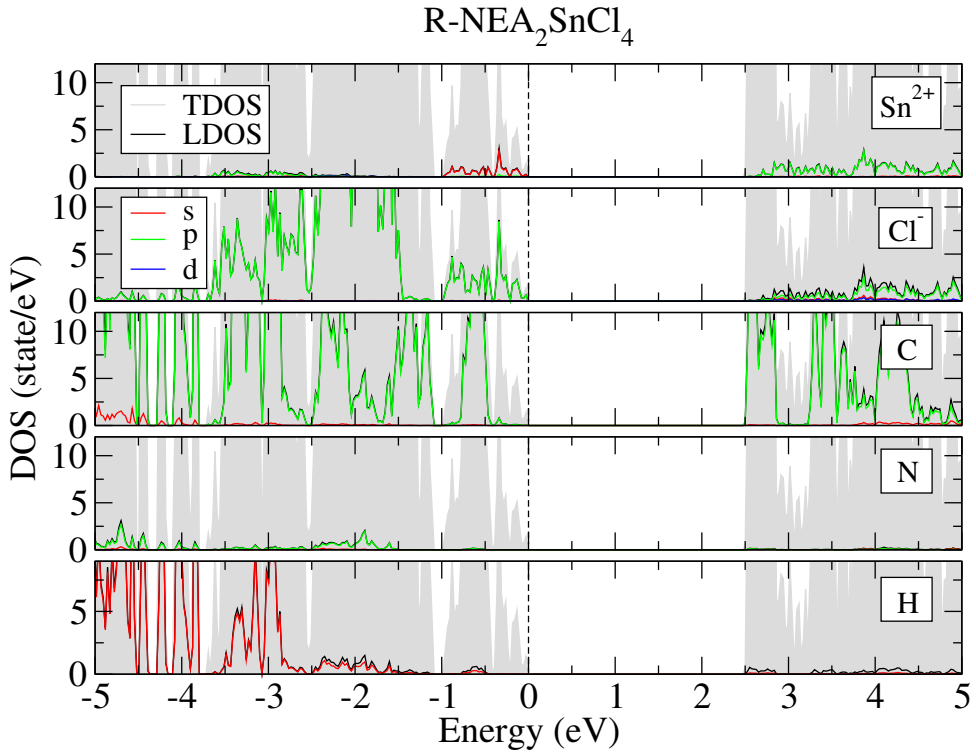

Figure S96: Density of states for $(R\text{-}NEA)_2SnCl_4$ slab with PBE+D3+SOC functional.

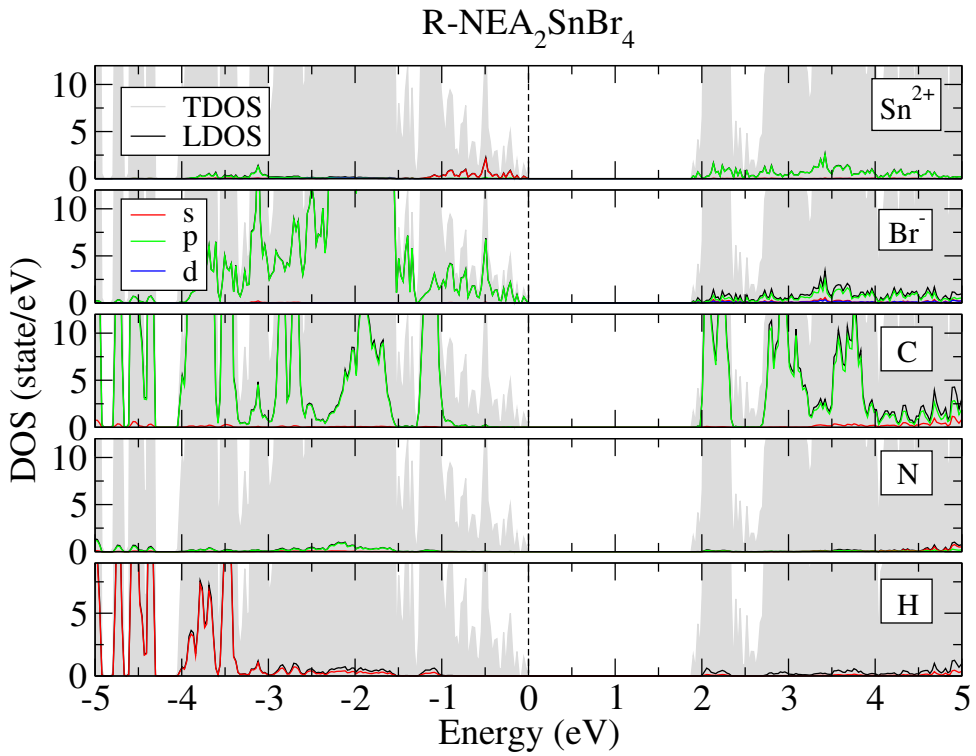

Figure S97: Density of states for $(R\text{-}NEA)_2SnBr_4$ slab with PBE+D3+SOC functional.

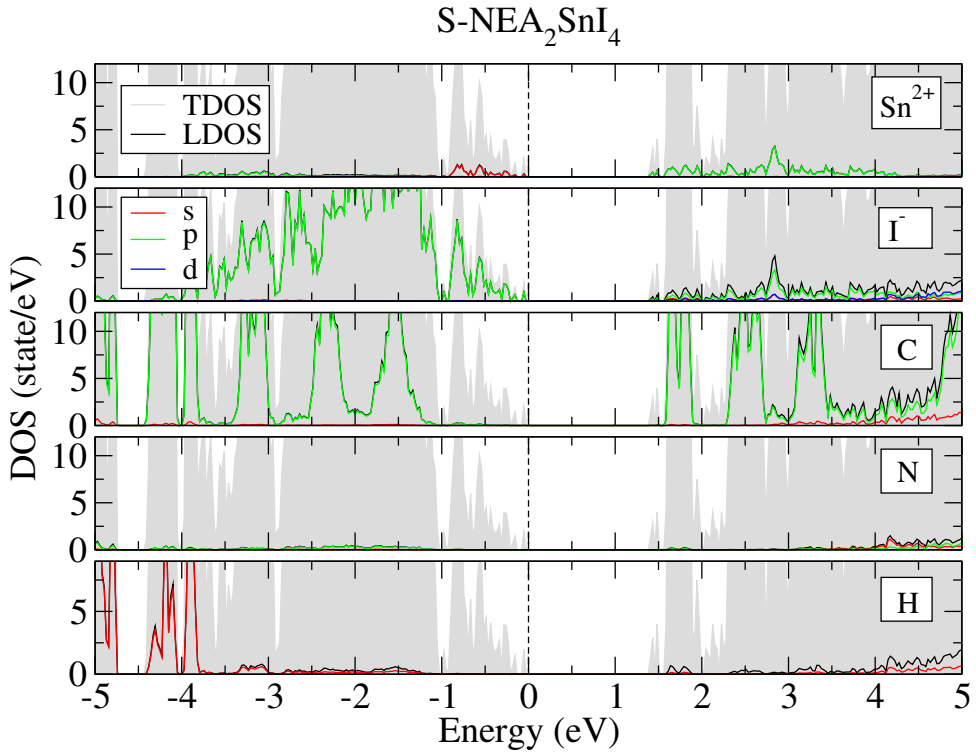

Figure S98: Density of states for $(S\text{-}NEA)_2SnI_4$ slab with PBE+D3+SOC functional.

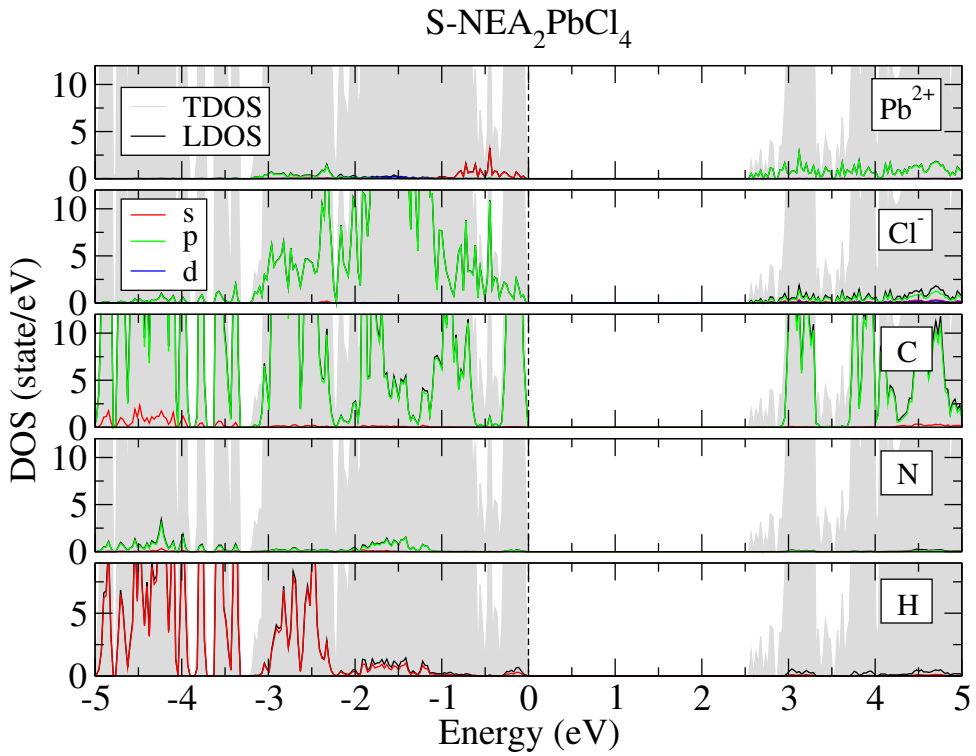

Figure S99: Density of states for $(S\text{-}NEA)_2PbCl_4$ slab with PBE+D3+SOC functional.

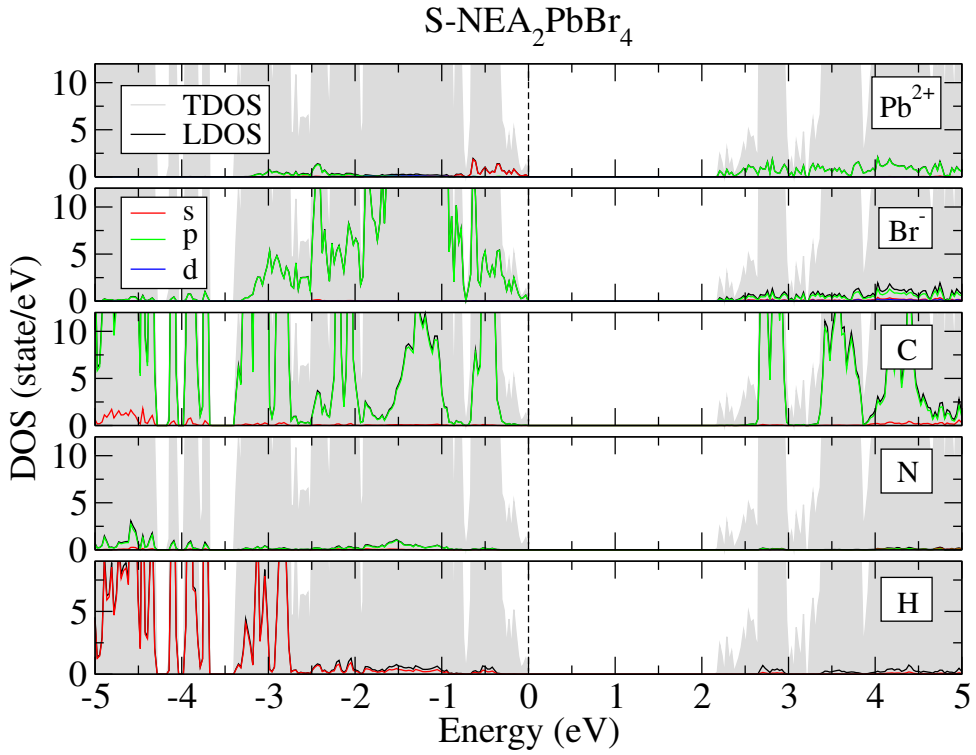

Figure S100: Density of states for $(S\text{-}NEA)_2PbBr_4$ slab with PBE+D3+SOC functional.

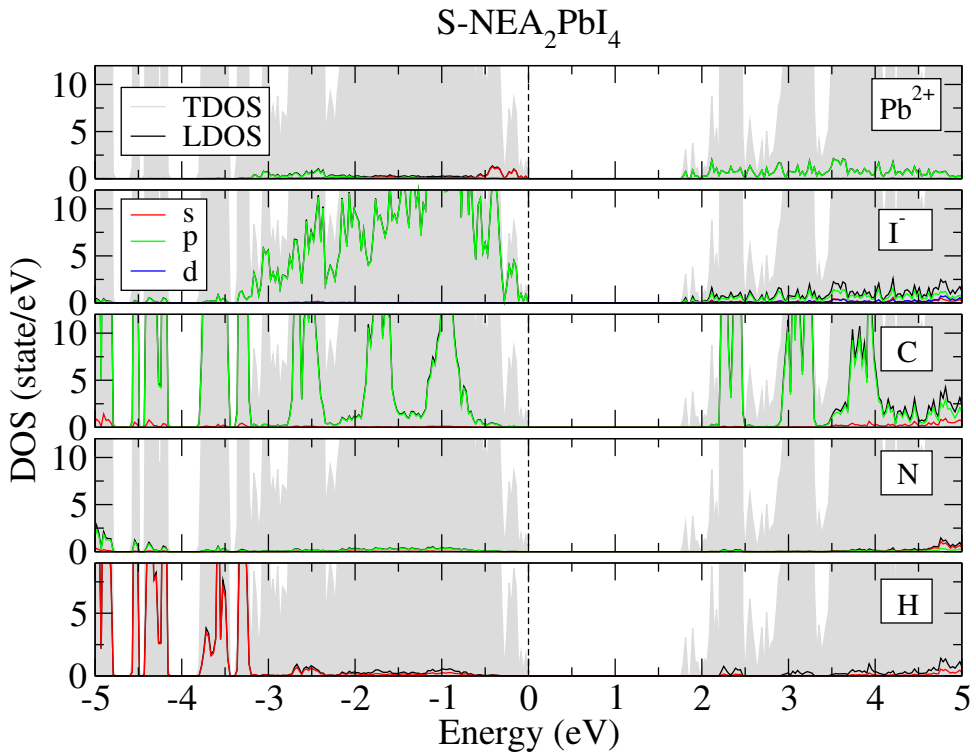

Figure S101: Density of states for $(S\text{-}NEA)_2PbI_4$ slab with PBE+D3+SOC functional.

9 Band Structure + Spin Orbit Coupling

9.1 Bulk

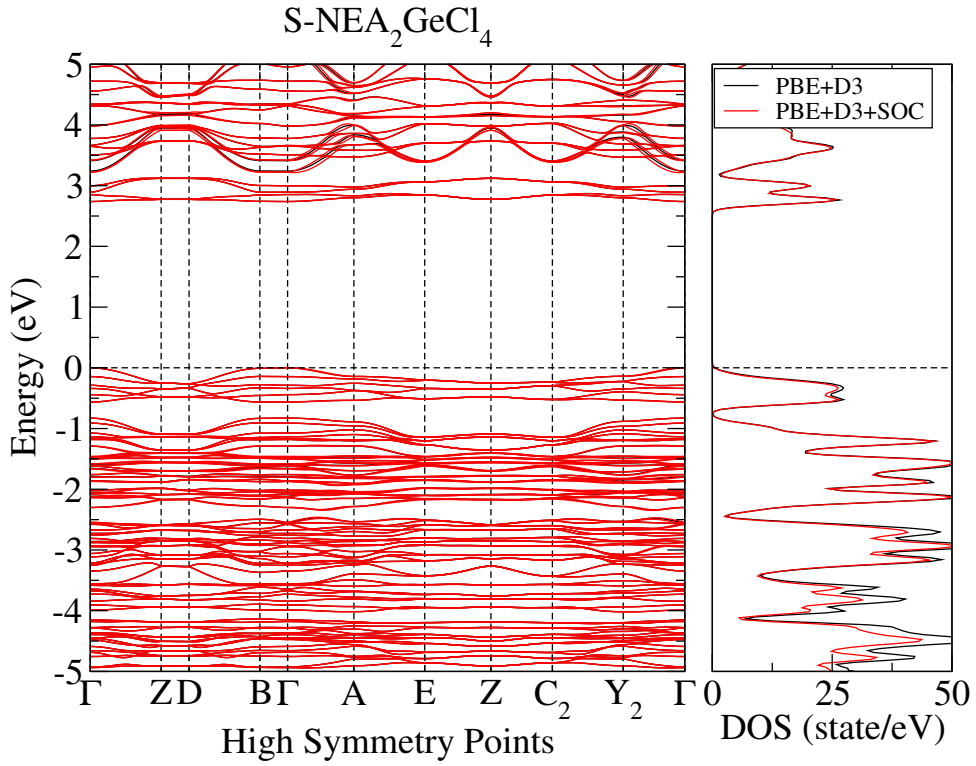

Figure S102: Band structure for $(S\text{-}NEA)_2GeCl_4$ bulk with PBE+D3+SOC functional with PBE+D3 bands in black and PBE+D3+SOC bands in red for comparison of functionals.

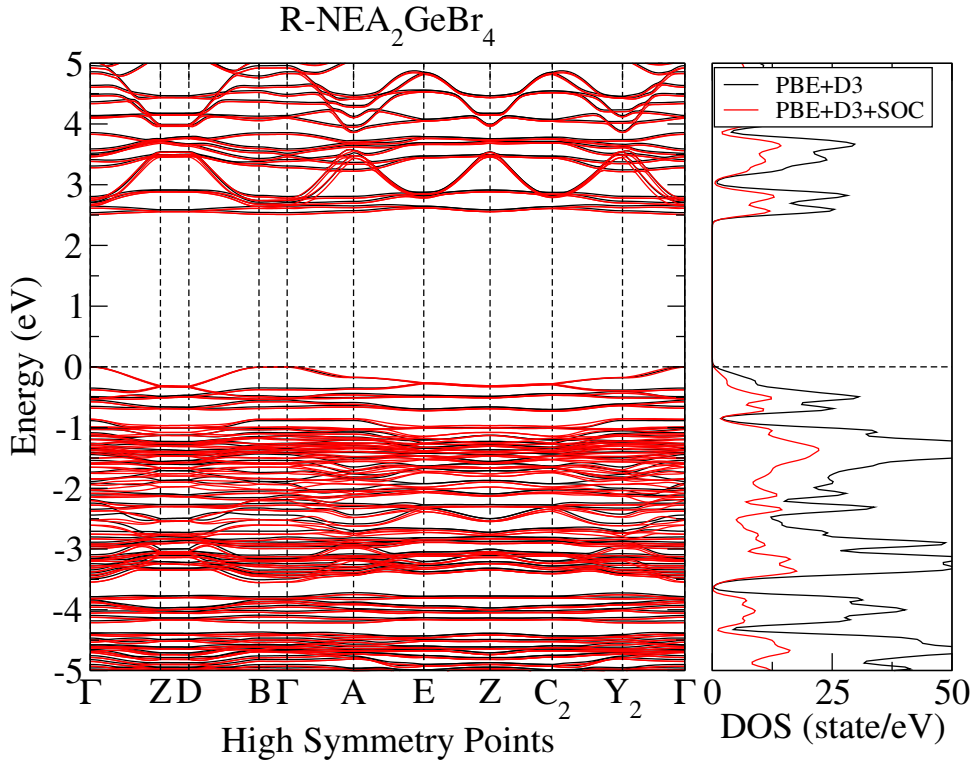

Figure S103: Band structure for $(R\text{-}NEA)_2GeBr_4$ bulk with PBE+D3+SOC functional with PBE+D3 bands in black and PBE+D3+SOC bands in red for comparison of functionals.

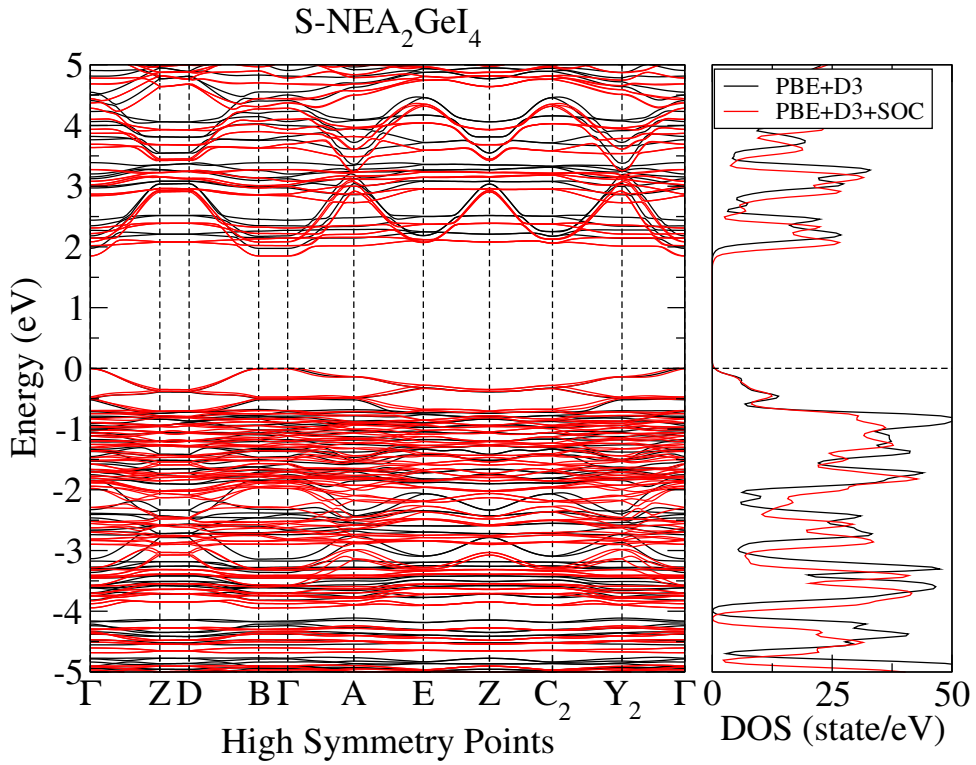

Figure S104: Band structure for $(S\text{-}NEA)_2GeI_4$ bulk with PBE+D3+SOC functional with PBE+D3 bands in black and PBE+D3+SOC bands in red for comparison of functionals.

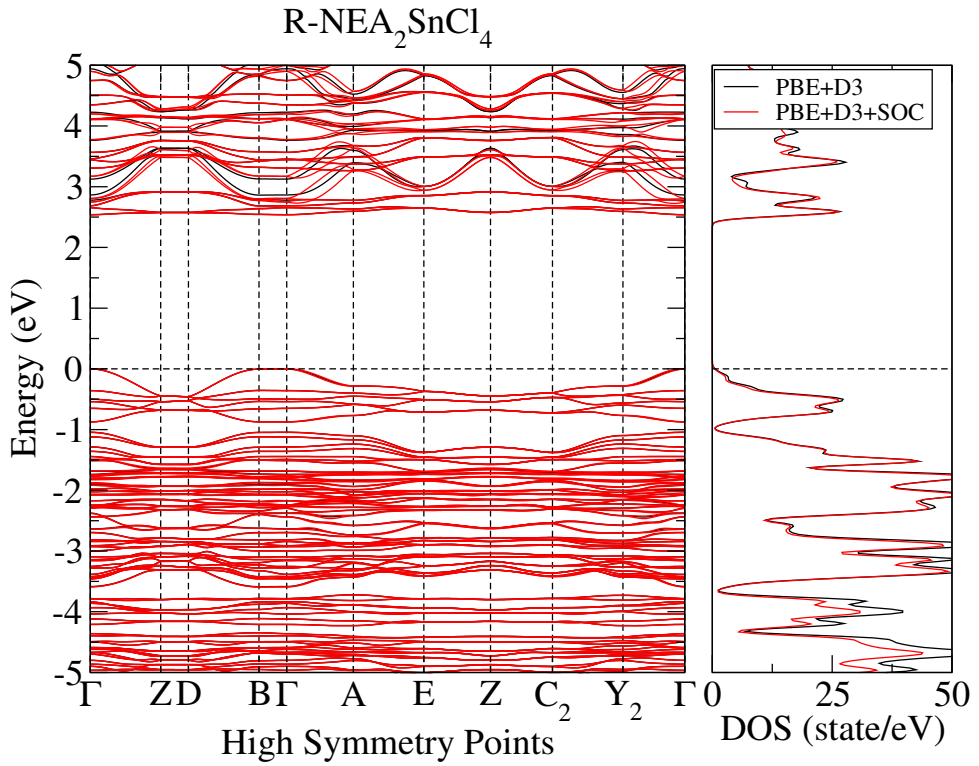

Figure S105: Band structure for $(R\text{-}NEA)_2SnCl_4$ bulk with PBE+D3+SOC functional with PBE+D3 bands in black and PBE+D3+SOC bands in red for comparison of functionals.

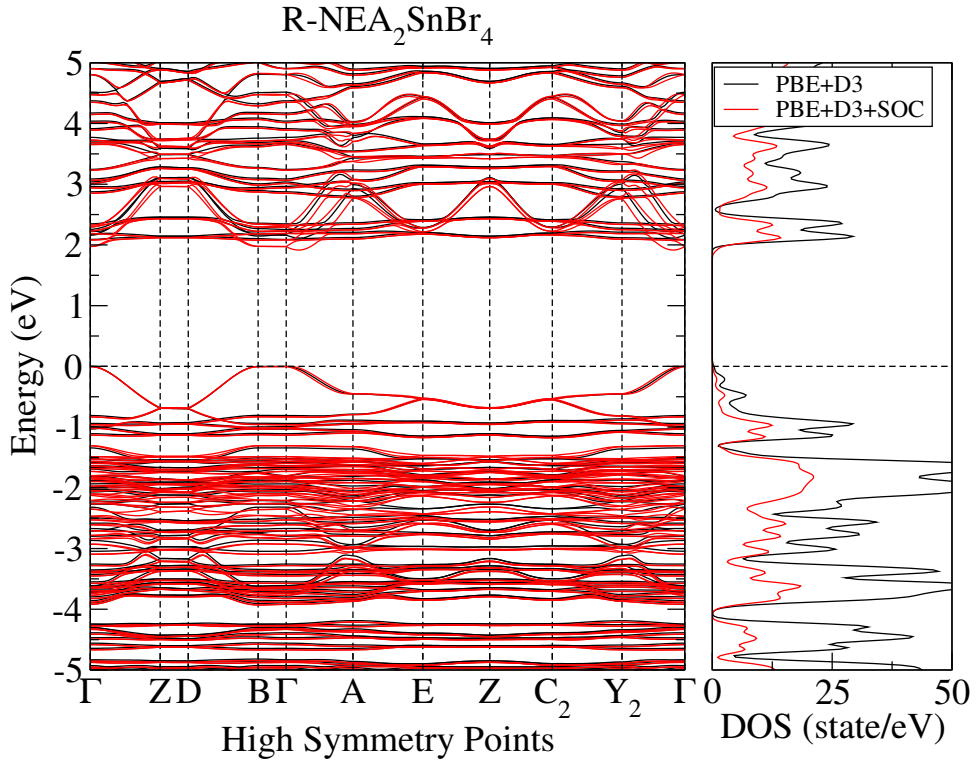

Figure S106: Band structure for $(R\text{-}NEA)_2SnBr_4$ bulk with PBE+D3+SOC functional with PBE+D3 bands in black and PBE+D3+SOC bands in red for comparison of functionals.

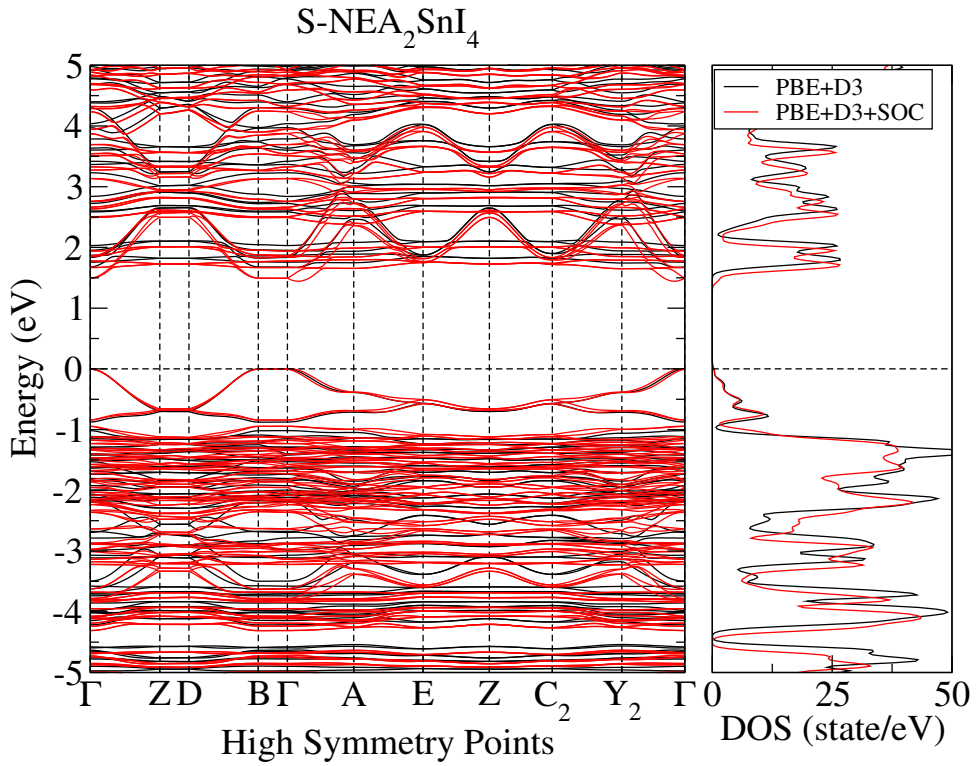

Figure S107: Band structure for $(S\text{-}NEA)_2SnI_4$ bulk with PBE+D3+SOC functional with PBE+D3 bands in black and PBE+D3+SOC bands in red for comparison of functionals.

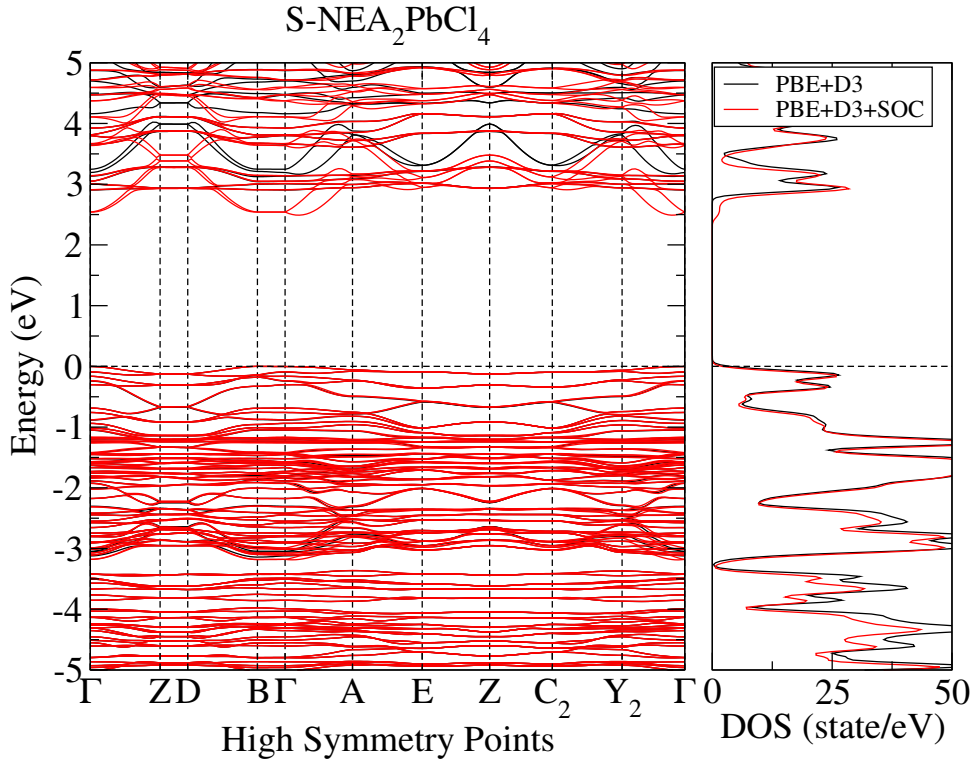

Figure S108: Band structure for $(S\text{-}NEA)_2PbCl_4$ bulk with PBE+D3+SOC functional with PBE+D3 bands in black and PBE+D3+SOC bands in red for comparison of functionals.

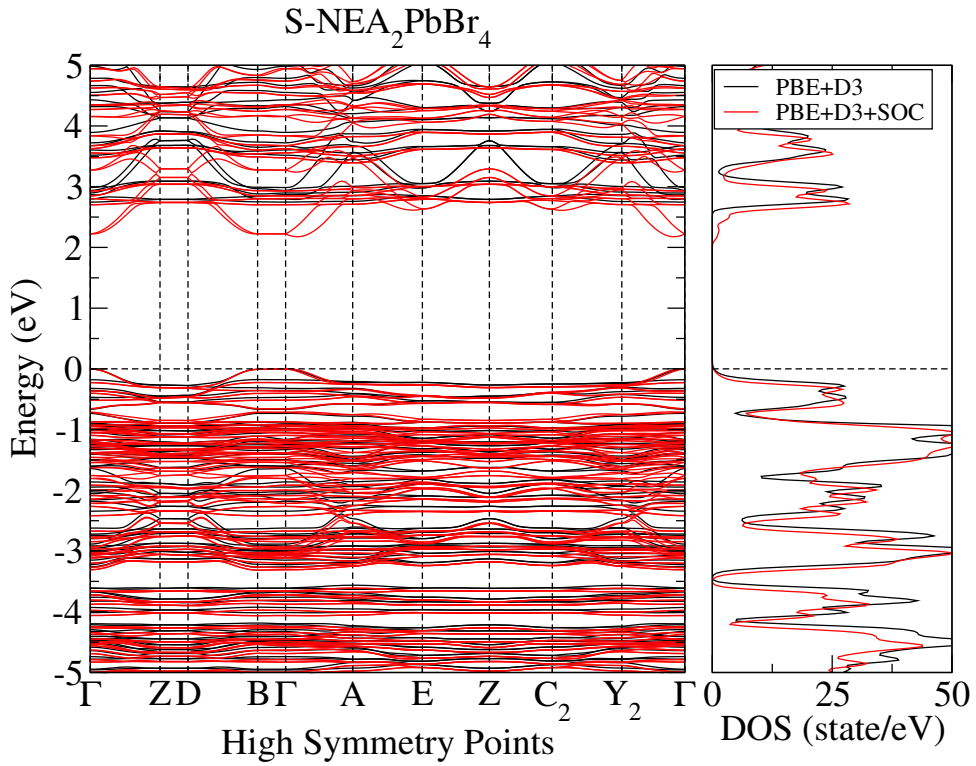

Figure S109: Band structure for $(S\text{-}NEA)_2PbBr_4$ bulk with PBE+D3+SOC functional with PBE+D3 bands in black and PBE+D3+SOC bands in red for comparison of functionals.

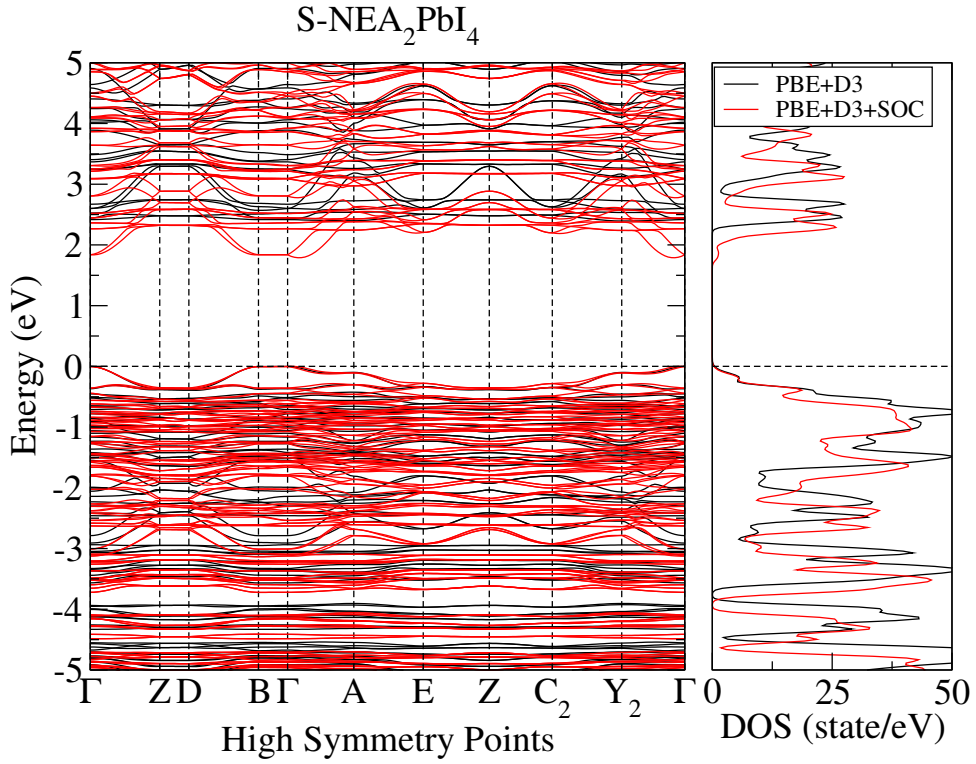

Figure S110: Band structure for $(S\text{-}NEA)_2PbI_4$ bulk with PBE+D3+SOC functional with PBE+D3 bands in black and PBE+D3+SOC bands in red for comparison of functionals.

9.2 Slab

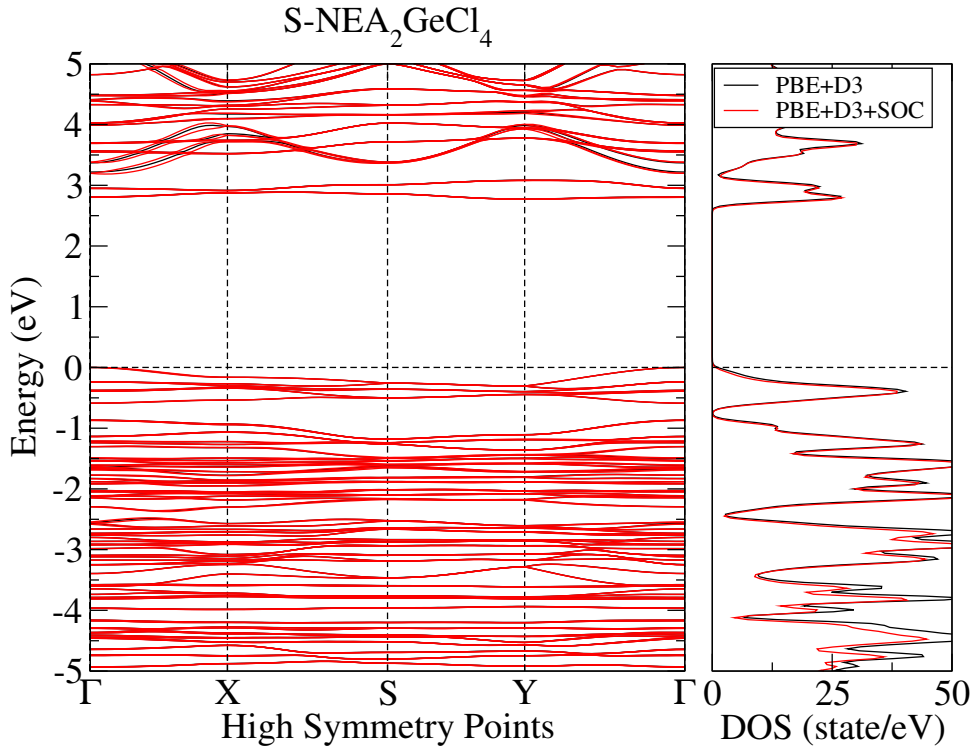

Figure S111: Band structure for $(S\text{-}NEA)_2GeCl_4$ slab with PBE+D3+SOC functional with PBE+D3 bands in black and PBE+D3+SOC bands in red for comparison of functionals.

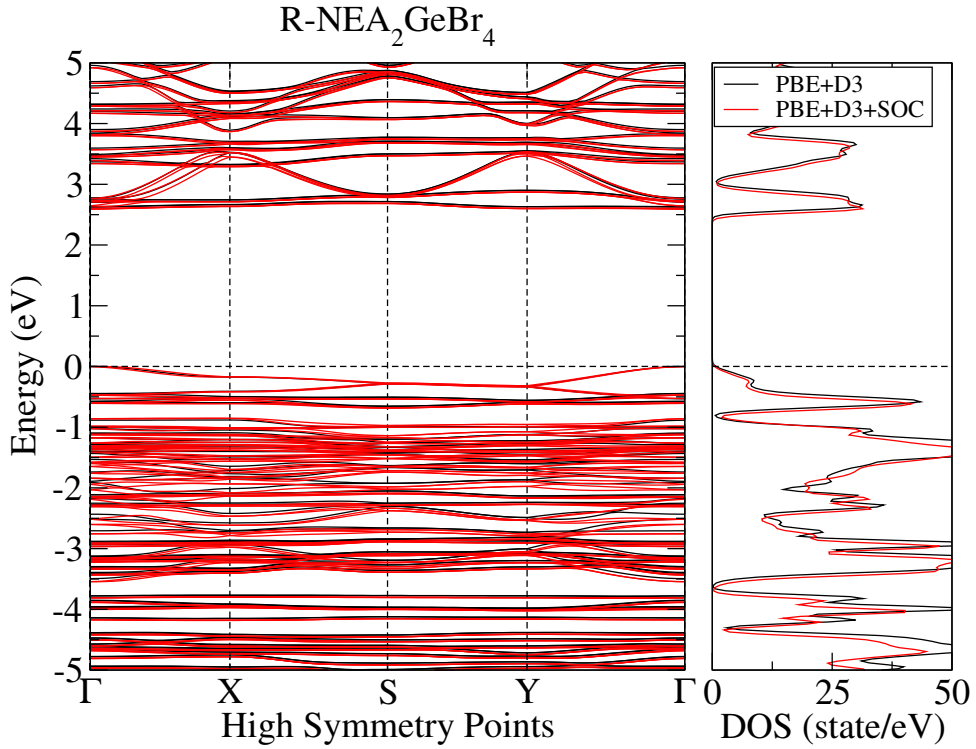

Figure S112: Band structure for $(R\text{-}NEA)_2GeBr_4$ slab with PBE+D3+SOC functional with PBE+D3 bands in black and PBE+D3+SOC bands in red for comparison of functionals.

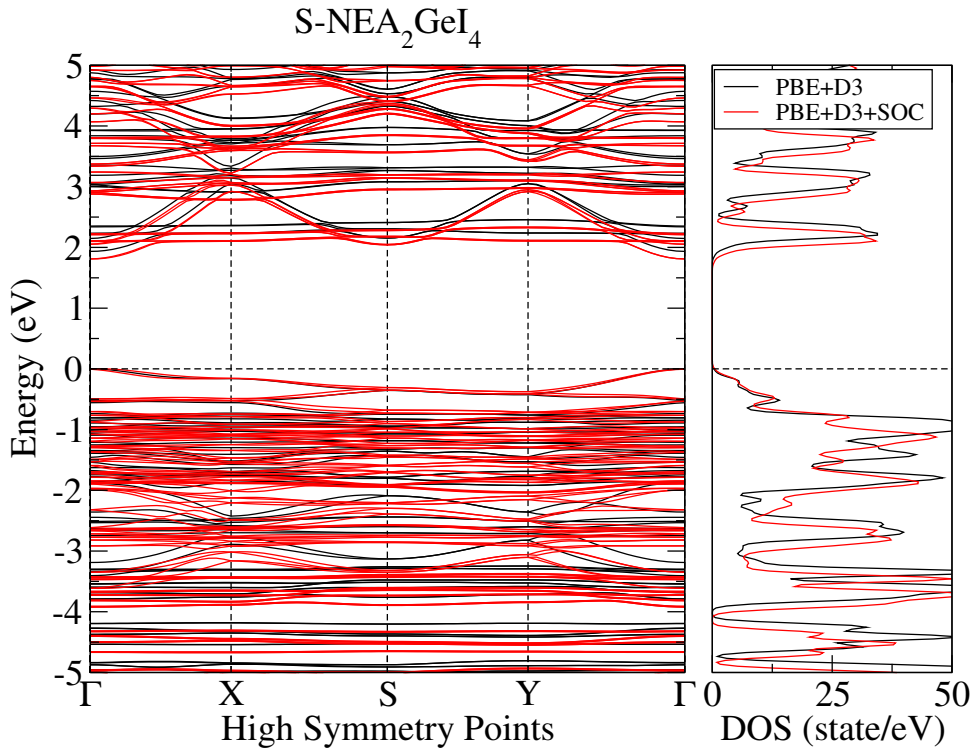

Figure S113: Band structure for $(S\text{-}NEA)_2GeI_4$ slab with PBE+D3+SOC functional with PBE+D3 bands in black and PBE+D3+SOC bands in red for comparison of functionals.

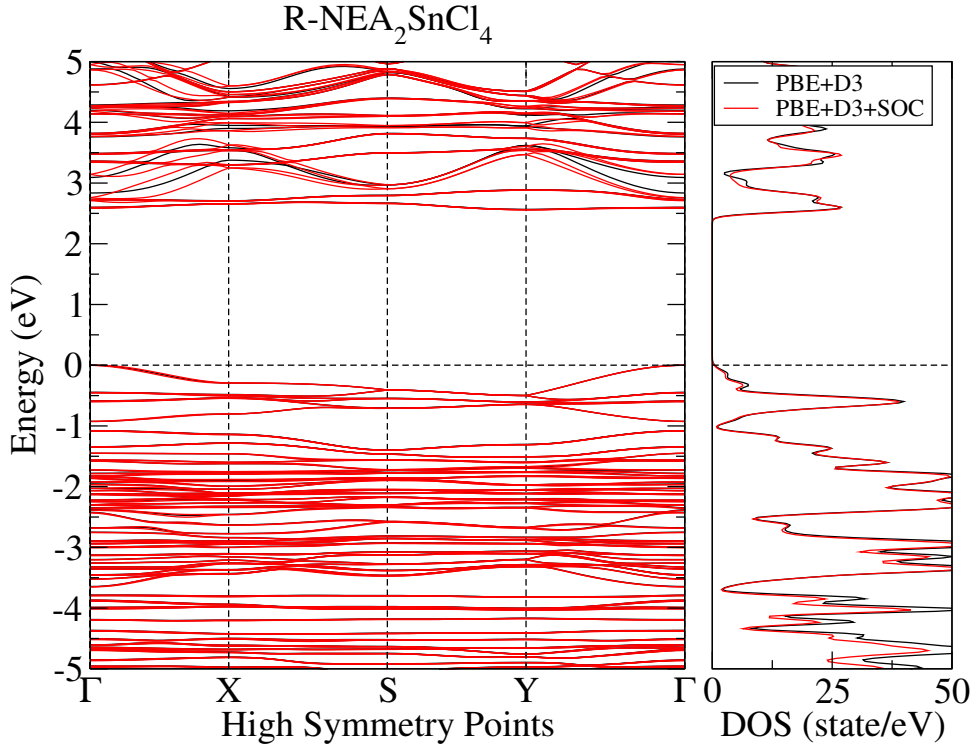

Figure S114: Band structure for $(R\text{-}NEA)_2SnCl_4$ slab with PBE+D3+SOC functional with PBE+D3 bands in black and PBE+D3+SOC bands in red for comparison of functionals.

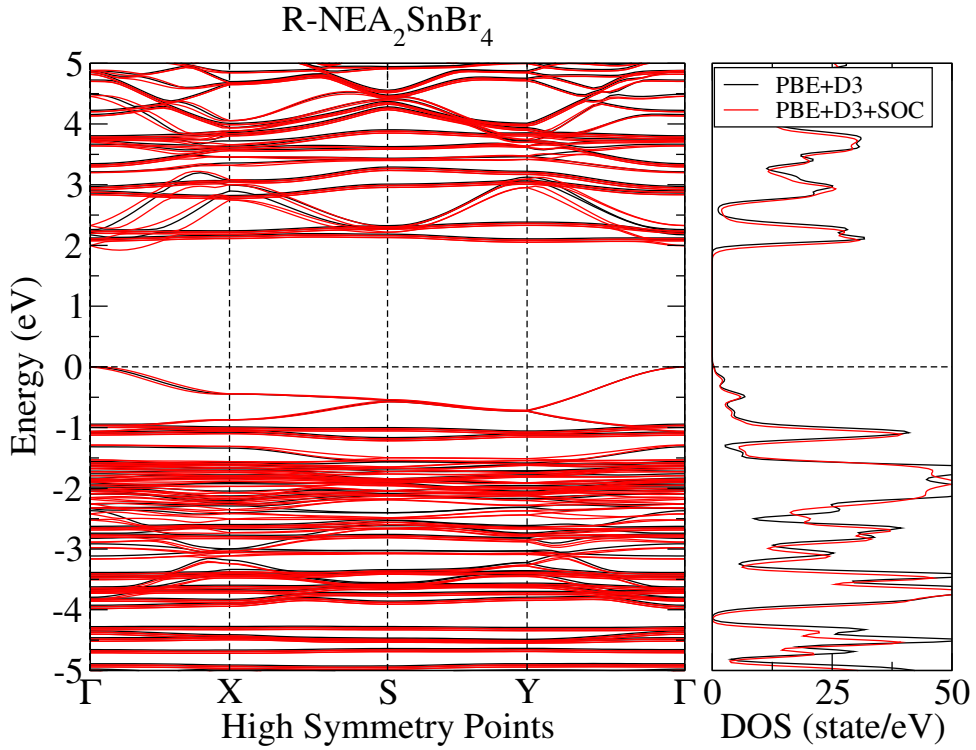

Figure S115: Band structure for $(R\text{-}NEA)_2SnBr_4$ slab with PBE+D3+SOC functional with PBE+D3 bands in black and PBE+D3+SOC bands in red for comparison of functionals.

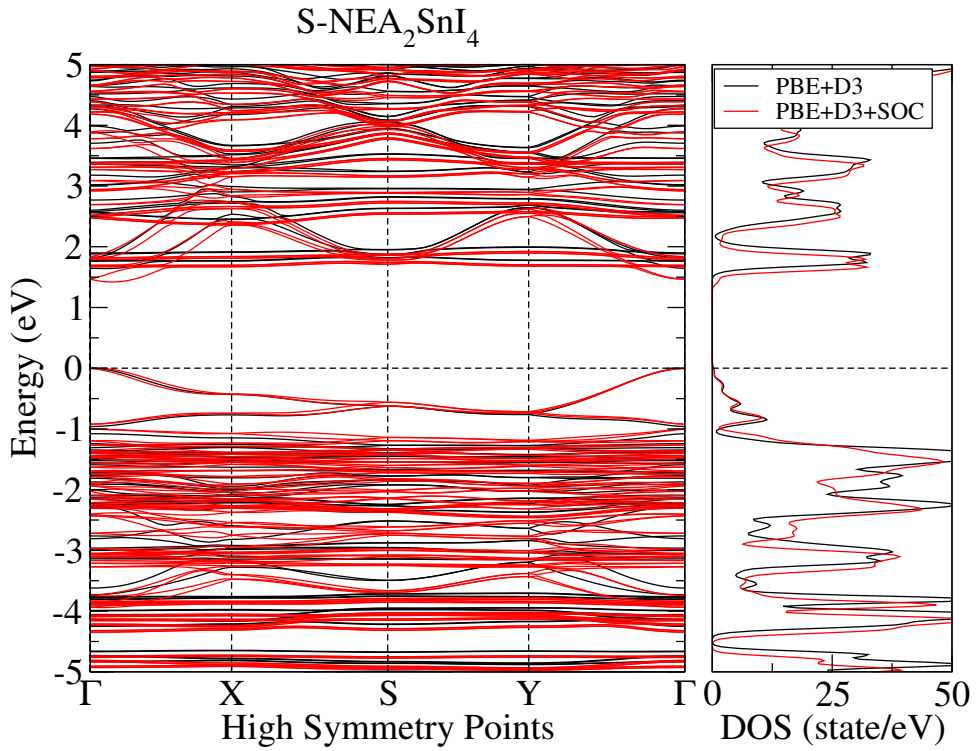

Figure S116: Band structure for $(S\text{-}NEA)_2SnI_4$ slab with PBE+D3+SOC functional with PBE+D3 bands in black and PBE+D3+SOC bands in red for comparison of functionals.

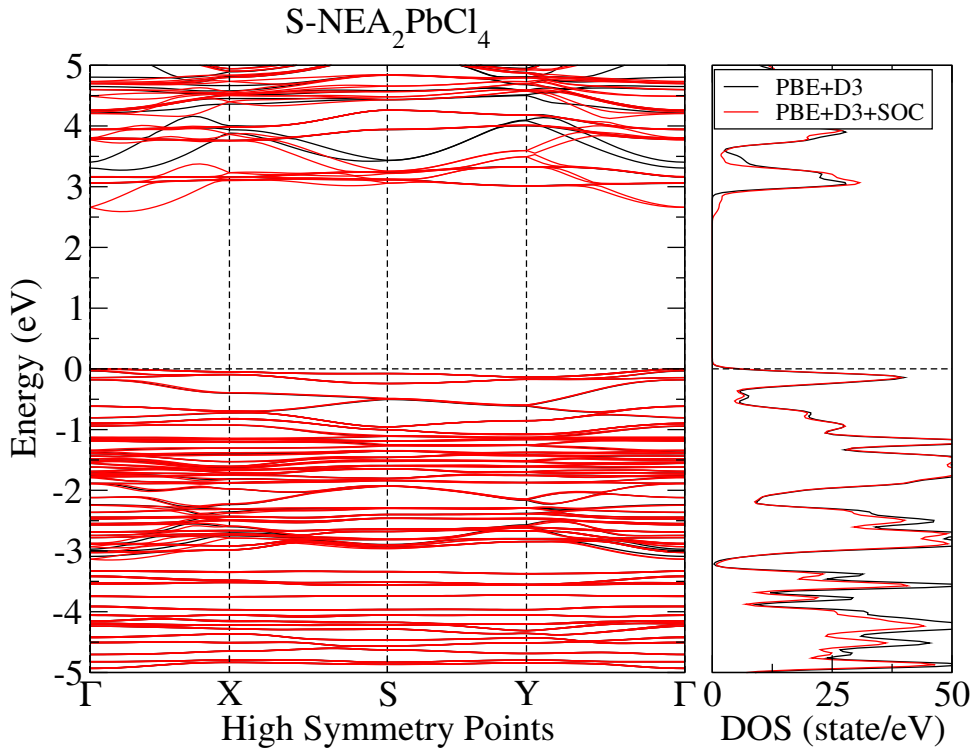

Figure S117: Band structure for $(S\text{-}NEA)_2PbCl_4$ slab with PBE+D3+SOC functional with PBE+D3 bands in black and PBE+D3+SOC bands in red for comparison of functionals.

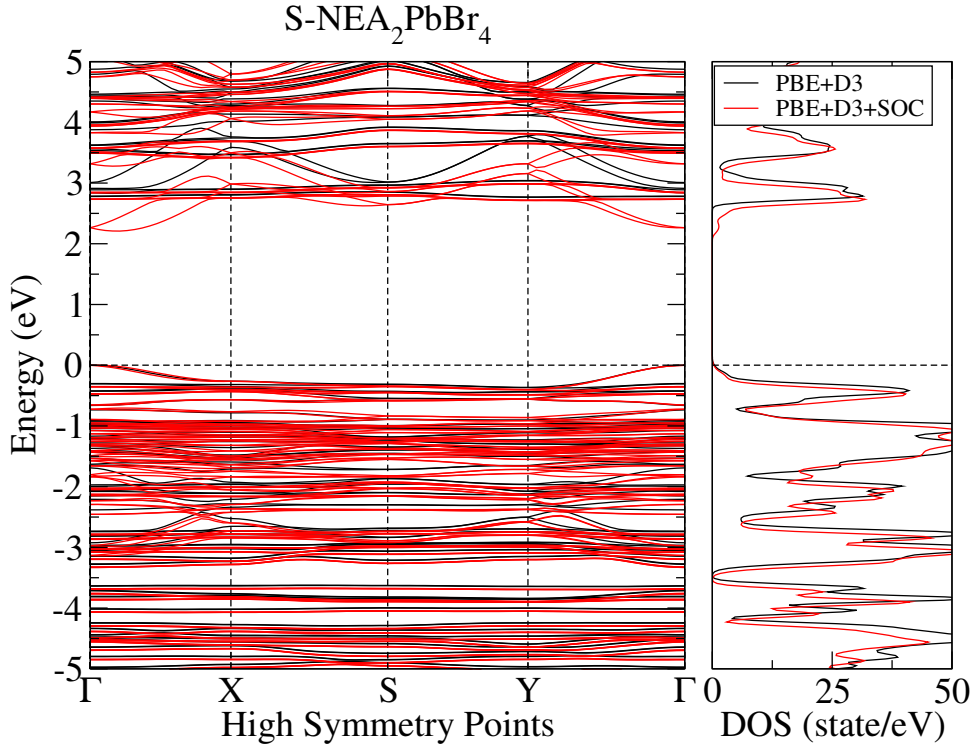

Figure S118: Band structure for $(S\text{-}NEA)_2PbBr_4$ slab with PBE+D3+SOC functional with PBE+D3 bands in black and PBE+D3+SOC bands in red for comparison of functionals.

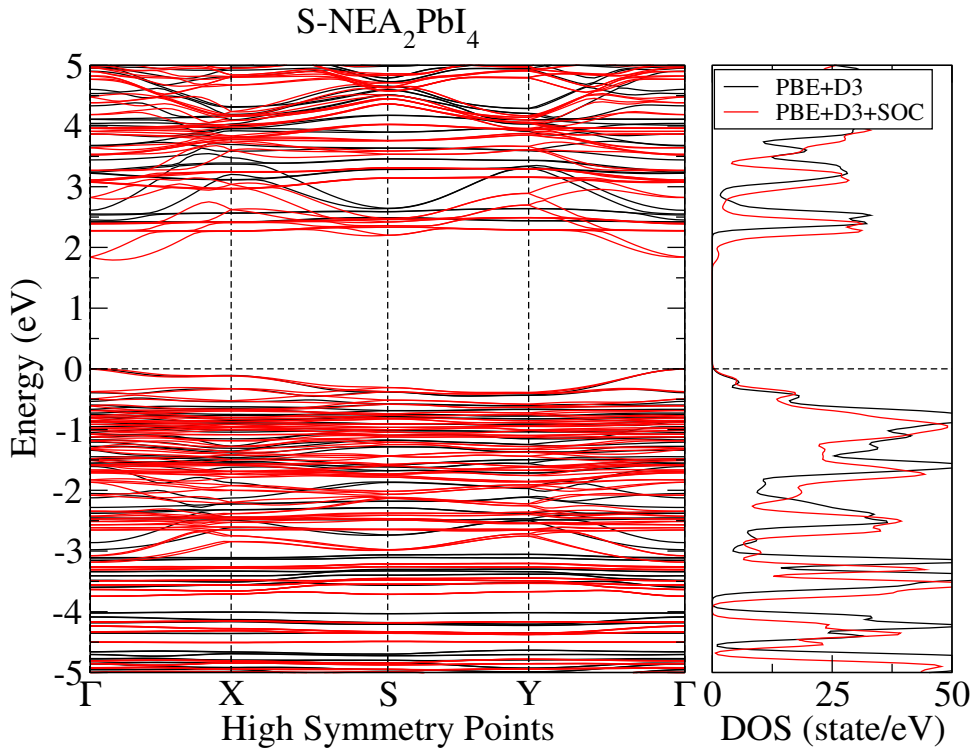

Figure S119: Band structure for $(S\text{-}NEA)_2PbI_4$ slab with PBE+D3+SOC functional with PBE+D3 bands in black and PBE+D3+SOC bands in red for comparison of functionals.

10 Band gap analysis

Table S22: Band gap analysis for orbital contribution of VBM and CBM of PBE+D3 and PBE+D3+SOC functionals for bulk structures.

Structure (bulk)	VBM (PBE+D3)	CBM (PBE+D3)	VBM (PBE+D3+SOC)	CBM (PBE+D3+SOC)
$(S\text{-}NEA)_2GeCl_4$	Cl (p)	C (p)	Cl (p)	C (p)
$(R\text{-}NEA)_2GeBr_4$	Br (p)	C (p)	Br (p)	C (p)
$(S\text{-}NEA)_2GeI_4$	I (p)	Ge (p)	I (p)	Ge (p)
$(R\text{-}NEA)_2SnCl_4$	Cl (p)	C (p)	Cl (p)	C (p)
$(R\text{-}NEA)_2SnBr_4$	Br (p)	C (p)	Br (p)	Sn (p)
$(S\text{-}NEA)_2SnI_4$	I (p)	Sn (p)	I (p)	Sn (p)
$(S\text{-}NEA)_2PbCl_4$	C (p)	C (p)	C (p)	Pb (p)
$(S\text{-}NEA)_2PbBr_4$	Br (p)	C (p)	Br (p)	Pb (p)
$(S\text{-}NEA)_2PbI_4$	I (p)	C (p)	I (p)	Pb (p)

Table S23: Band gap analysis for orbital contribution of VBM and CBM of PBE+D3 and PBE+D3+SOC functionals for slab structures.

Structure (slab)	VBM (PBE+D3)	CBM (PBE+D3)	VBM (PBE+D3+SOC)	CBM (PBE+D3+SOC)
(S-NEA)$_2$GeCl$_4$	Cl (p)	C (p)	Cl (p)	C (p)
(R-NEA)$_2$GeBr$_4$	Br (p)	C (p)	Br (p)	C (p)
(S-NEA)$_2$GeI$_4$	I (p)	Ge (p)	I (p)	Ge (p)
(R-NEA)$_2$SnCl$_4$	Cl (p)	C (p)	Cl (p)	C (p)
(R-NEA)$_2$SnBr$_4$	Br (p)	C (p)	Br (p)	Sn (p)
(S-NEA)$_2$SnI$_4$	I (p)	Sn (p)	I (p)	Sn (p)
(S-NEA)$_2$PbCl$_4$	C (p)	C (p)	C (p)	Pb (p)
(S-NEA)$_2$PbBr$_4$	Br (p)	C (p)	Br (p)	Pb (p)
(S-NEA)$_2$PbI$_4$	I (p)	C (p)	I (p)	Pb (p)

Table S24: Band gap analysis for chiral hybrid perovskites with NEA cation with PBE+D3 functional with vacuum level, valence band maximum (VBM), conduction band minimum (CBM), ionization potential (IP) as result of VBM relative to the vacuum level (Vacuum − VBM) and electron affinity (EA) as result of CBM relative to the vacuum level (Vacuum − CBM).

Structure	Vacuum level (eV)	VBM (eV)	CBM (eV)	IP (eV)	EA (eV)
(R-NEA)$_2$GeCl$_4$	3.10	−1.63	1.16	4.73	1.93
(S-NEA)$_2$GeCl$_4$	3.10	−1.60	1.17	4.71	1.93
(R-NEA)$_2$GeBr$_4$	3.03	−1.52	1.10	4.55	1.93
(S-NEA)$_2$GeBr$_4$	3.03	−1.51	1.10	4.55	1.93
(R-NEA)$_2$GeI$_4$	3.28	−0.91	1.01	4.19	2.26
(S-NEA)$_2$GeI$_4$	3.27	−0.90	1.03	4.18	2.24
(R-NEA)$_2$SnCl$_4$	3.23	−1.26	1.29	4.50	1.93
(S-NEA)$_2$SnCl$_4$	3.24	−1.21	1.30	4.45	1.93
(R-NEA)$_2$SnBr$_4$	3.18	−0.85	1.23	4.04	1.95
(S-NEA)$_2$SnBr$_4$	3.17	−0.90	1.20	4.07	1.97
(R-NEA)$_2$SnI$_4$	3.35	−0.39	1.24	3.75	2.11
(S-NEA)$_2$SnI$_4$	3.36	−0.37	1.26	3.73	2.09
(R-NEA)$_2$PbCl$_4$	3.23	−1.71	1.30	4.94	1.92
(S-NEA)$_2$PbCl$_4$	3.23	−1.70	1.31	4.94	1.92
(R-NEA)$_2$PbBr$_4$	3.14	−1.57	1.22	4.72	1.92
(S-NEA)$_2$PbBr$_4$	3.14	−1.54	1.21	4.69	1.93
(R-NEA)$_2$PbI$_4$	3.31	−1.07	1.33	4.38	1.97
(S-NEA)$_2$PbI$_4$	3.32	−1.07	1.34	4.39	1.98

Table S25: Band gap analysis for chiral hybrid perovskites with NEA cation with PBE+D3+SOC functional with vacuum level, valence band maximum (VBM), conduction band minimum (CBM), ionization potential (IP) as result of VBM relative to the vacuum level (Vacuum − VBM) and electron affinity (EA) as result of CBM relative to the vacuum level (Vacuum − CBM).

Structure	Vacuum level (eV)	VBM (eV)	CBM (eV)	IP (eV)	EA (eV)	IP^{corr} (eV)	EA^{corr} (eV)
$(S\text{-}NEA)_2GeCl_4$	3.10	−1.60	1.17	4.70	1.93	5.20	1.47
$(R\text{-}NEA)_2GeBr_4$	3.03	−1.48	1.10	4.52	1.93	4.98	1.53
$(S\text{-}NEA)_2GeI_4$	3.28	−0.77	1.03	4.06	2.24	4.40	2.00
$(R\text{-}NEA)_2SnCl_4$	3.23	−1.26	1.29	4.50	1.93	4.94	1.47
$(R\text{-}NEA)_2SnBr_4$	3.19	−0.82	1.09	4.01	2.09	4.35	1.72
$(S\text{-}NEA)_2SnI_4$	3.37	−0.29	1.13	3.66	2.24	3.91	2.01
$(S\text{-}NEA)_2PbCl_4$	3.23	−1.70	0.88	4.93	2.35	5.33	1.89
$(S\text{-}NEA)_2PbBr_4$	3.14	−1.50	0.70	4.64	2.43	5.10	2.07
$(S\text{-}NEA)_2PbI_4$	3.31	−0.92	0.86	4.24	2.45	4.60	2.17

Table S26: Band gap analysis for chiral hybrid perovskites with NEA cation with PBE+D3 functional with vacuum level, valence band maximum on Γ-point (VBM), conduction band minimum on Γ-point (CBM), ionization potential on Γ-point (IP) as result of VBM relative to the vacuum level (Vacuum − VBM) and electron affinity (EA) on Γ-point as result of CBM relative to the vacuum level (Vacuum − CBM).

Structure	Vacuum level (eV)	VBM^{Γ} (eV)	CBM^{Γ} (eV)	IP^{Γ} (eV)	EA^{Γ} (eV)
$(S\text{-}NEA)_2GeCl_4$	3.10	−1.60	1.20	4.70	1.90
$(R\text{-}NEA)_2GeBr_4$	3.03	−1.51	1.10	4.54	1.93
$(S\text{-}NEA)_2GeI_4$	3.27	−0.90	1.03	4.17	2.24
$(R\text{-}NEA)_2SnCl_4$	3.23	−1.26	1.32	4.49	1.91
$(R\text{-}NEA)_2SnBr_4$	3.18	−0.85	1.24	4.03	1.94
$(S\text{-}NEA)_2SnI_4$	3.36	−0.37	1.27	3.73	2.09
$(S\text{-}NEA)_2PbCl_4$	3.23	−1.70	1.35	4.93	1.88
$(S\text{-}NEA)_2PbBr_4$	3.14	−1.54	1.22	4.68	1.92
$(S\text{-}NEA)_2PbI_4$	3.32	−1.07	1.34	4.39	1.98

Table S27: Band gap analysis for chiral hybrid perovskites with NEA cation with HSE06+D3 functional with vacuum level, valence band maximum on Γ-point (VBM), conduction band minimum on Γ-point (CBM), ionization potential on Γ-point (IP) as result of VBM relative to the vacuum level (Vacuum − VBM) and electron affinity (EA) on Γ-point as result of CBM relative to the vacuum level (Vacuum − CBM).

Structure	Vacuum level (eV)	VBM^{Γ} (eV)	CBM^{Γ} (eV)	IP^{Γ} (eV)	EA^{Γ} (eV)	χIP^{Γ} (eV)	χEA^{Γ} (eV)
$(S\text{-}NEA)_2GeCl_4$	3.06	−2.14	1.62	5.20	1.44	0.50	−0.46
$(R\text{-}NEA)_2GeBr_4$	2.99	−2.01	1.46	5.00	1.53	0.46	−0.40
$(S\text{-}NEA)_2GeI_4$	3.23	−1.28	1.23	4.51	2.00	0.34	−0.24
$(R\text{-}NEA)_2SnCl_4$	3.19	−1.74	1.74	4.93	1.45	0.44	−0.46
$(R\text{-}NEA)_2SnBr_4$	3.14	−1.23	1.57	4.37	1.57	0.34	−0.37
$(S\text{-}NEA)_2SnI_4$	3.31	−0.67	1.45	3.98	1.86	0.25	−0.23
$(S\text{-}NEA)_2PbCl_4$	3.19	−2.14	1.77	5.33	1.42	0.40	−0.46
$(S\text{-}NEA)_2PbBr_4$	3.10	−2.04	1.54	5.14	1.56	0.46	−0.36
$(S\text{-}NEA)_2PbI_4$	3.27	−1.48	1.57	4.75	1.70	0.36	−0.28

Table S28: Band gap analysis for chiral hybrid perovskites with NEA cation with PBE+D3, PBE+D3+SOC, HSE06+D3 and PBE+D3+SOC+χ functionals with ionic potential (IP) and electronic affinity (EA).

	PBE+D3		PBE+D3+SOC		HSE06+D3		PBE+D3+SOC+χ	
Structure	IP^{Γ}	EA^{Γ}	IP	EA	IP^{Γ}	EA^{Γ}	IP^{corr}	EA^{corr}
$(S\text{-}NEA)_2GeCl_4$	4.70	1.90	4.70	1.93	5.20	1.44	5.20	1.47
$(R\text{-}NEA)_2GeBr_4$	4.54	1.93	4.52	1.93	5.00	1.53	4.98	1.53
$(S\text{-}NEA)_2GeI_4$	4.17	2.24	4.06	2.24	4.51	2.00	4.40	2.00
$(R\text{-}NEA)_2SnCl_4$	4.49	1.91	4.50	1.93	4.93	1.45	4.94	1.47
$(R\text{-}NEA)_2SnBr_4$	4.03	1.94	4.01	2.09	4.37	1.57	4.35	1.72
$(S\text{-}NEA)_2SnI_4$	3.73	2.09	3.66	2.24	3.98	1.86	3.91	2.01
$(S\text{-}NEA)_2PbCl_4$	4.93	1.88	4.93	2.35	5.33	1.42	5.33	1.89
$(S\text{-}NEA)_2PbBr_4$	4.68	1.92	4.64	2.43	5.14	1.56	5.10	2.07
$(S\text{-}NEA)_2PbI_4$	4.39	1.98	4.24	2.45	4.75	1.70	4.60	2.17

Table S29: Band gap analysis for bulk of chiral hybrid perovskites with NEA cation with PBE+D3 functional with band gap, its **k**-point VBM → CBM and Γ-band gap.

Structure (bulk)	Band gap (eV)	**k**-point	E_g^{Γ} (eV)
(R-NEA)$_2$GeCl$_4$	2.73	Γ	2.73
(S-NEA)$_2$GeCl$_4$	2.73	Γ	2.73
(R-NEA)$_2$GeBr$_4$	2.53	Γ	2.53
(S-NEA)$_2$GeBr$_4$	2.54	Γ	2.54
(R-NEA)$_2$GeI$_4$	1.94	Γ	1.94
(S-NEA)$_2$GeI$_4$	1.97	Γ	1.97
(R-NEA)$_2$SnCl$_4$	2.54	Γ	2.54
(S-NEA)$_2$SnCl$_4$	2.55	Γ	2.55
(R-NEA)$_2$SnBr$_4$	2.09	Γ → Y_2-Γ	2.09
(S-NEA)$_2$SnBr$_4$	2.04	Γ → Γ-A	2.06
(R-NEA)$_2$SnI$_4$	1.66	Γ → Y_2-Γ	1.67
(S-NEA)$_2$SnI$_4$	1.67	Γ → Y_2-Γ	1.67
(R-NEA)$_2$PbCl$_4$	2.90	B → Γ	2.90
(S-NEA)$_2$PbCl$_4$	2.90	B → Γ	2.90
(R-NEA)$_2$PbBr$_4$	2.73	Γ	2.73
(S-NEA)$_2$PbBr$_4$	2.74	Γ	2.74
(R-NEA)$_2$PbI$_4$	2.39	Γ → Y_2	2.39
(S-NEA)$_2$PbI$_4$	2.39	Γ → Y_2	2.39

Table S30: Band gap analysis for bulk of chiral hybrid perovskites with NEA cation with PBE+D3+SOC functional with band gap, its **k**-point VBM → CBM and Γ-band gap.

Structure (bulk)	Band gap (eV)	**k**-point	E_g^{Γ} (eV)
(S-NEA)$_2$GeCl$_4$	2.73	Γ-A → Γ	2.73
(R-NEA)$_2$GeBr$_4$	2.50	Γ-A → B-Γ	2.50
(S-NEA)$_2$GeI$_4$	1.85	Γ-A → B-Γ	1.85
(R-NEA)$_2$SnCl$_4$	2.53	Γ-A → B-Γ	2.53
(R-NEA)$_2$SnBr$_4$	1.91	Γ-A → Γ-A	1.92
(S-NEA)$_2$SnI$_4$	1.44	Y_2-Γ → Y_2-Γ	1.45
(S-NEA)$_2$PbCl$_4$	2.48	B → Γ-A	2.49
(S-NEA)$_2$PbBr$_4$	2.17	Y_2-Γ → Γ-A	2.18
(S-NEA)$_2$PbI$_4$	1.78	Y_2-Γ → Y_2-Γ	1.79

Table S31: Band gap analysis for slabs of chiral hybrid perovskites with NEA cation with PBE+D3 functional with band gap, its **k**-point VBM → CBM and Γ-band gap.

Structure (slab)	Band gap (eV)	**k**-point	E_g^{Γ} (eV)
(R-NEA)$_2$GeCl$_4$	2.79	$\Gamma \rightarrow Y$-Γ	2.82
(S-NEA)$_2$GeCl$_4$	2.77	$\Gamma \rightarrow Y$-Γ	2.80
(R-NEA)$_2$GeBr$_4$	2.62	Γ	2.62
(S-NEA)$_2$GeBr$_4$	2.62	Γ	2.62
(R-NEA)$_2$GeI$_4$	1.93	Γ	1.93
(S-NEA)$_2$GeI$_4$	1.93	Γ	1.93
(R-NEA)$_2$SnCl$_4$	2.56	$\Gamma \rightarrow Y$	2.59
(S-NEA)$_2$SnCl$_4$	2.51	$\Gamma \rightarrow Y$	2.55
(R-NEA)$_2$SnBr$_4$	2.08	$\Gamma \rightarrow Y$	2.09
(S-NEA)$_2$SnBr$_4$	2.10	$\Gamma \rightarrow \Gamma$-$X$	2.12
(R-NEA)$_2$SnI$_4$	1.64	$\Gamma \rightarrow \Gamma$-$X$	1.64
(S-NEA)$_2$SnI$_4$	1.64	$\Gamma \rightarrow \Gamma$-$X$	1.64
(R-NEA)$_2$PbCl$_4$	3.01	$\Gamma \rightarrow Y$	3.05
(S-NEA)$_2$PbCl$_4$	3.01	$\Gamma \rightarrow Y$	3.05
(R-NEA)$_2$PbBr$_4$	2.79	$\Gamma \rightarrow Y$-Γ	2.79
(S-NEA)$_2$PbBr$_4$	2.76	$\Gamma \rightarrow Y$	2.77
(R-NEA)$_2$PbI$_4$	2.41	$\Gamma \rightarrow \Gamma$-$X$	2.41
(S-NEA)$_2$PbI$_4$	2.41	$\Gamma \rightarrow X$	2.41

Table S32: Band gap analysis for slabs of chiral hybrid perovskites with NEA cation with PBE+D3+SOC functional with band gap, its **k**-point VBM → CBM and Γ-band gap.

Structure (slab)	Band gap (eV)	**k**-point	E_g^{Γ} (eV)
(S-NEA)$_2$GeCl$_4$	2.77	Γ-$X \rightarrow Y$	2.80
(R-NEA)$_2$GeBr$_4$	2.59	Γ-$X \rightarrow \Gamma$	2.59
(S-NEA)$_2$GeI$_4$	1.81	Γ-$X \rightarrow \Gamma$	1.81
(R-NEA)$_2$SnCl$_4$	2.56	Γ-$X \rightarrow Y$	2.58
(R-NEA)$_2$SnBr$_4$	1.92	Γ-$X \rightarrow \Gamma$-X	1.94
(S-NEA)$_2$SnI$_4$	1.41	Γ-$X \rightarrow \Gamma$-X	1.43
(S-NEA)$_2$PbCl$_4$	2.58	$\Gamma \rightarrow \Gamma$-$X$	2.59
(S-NEA)$_2$PbBr$_4$	2.20	Γ-$X \rightarrow \Gamma$-X	2.22
(S-NEA)$_2$PbI$_4$	1.79	Γ-$X \rightarrow \Gamma$-X	1.79

Table S33: Gamma-point band gap analysis for bulk chiral hybrid perovskites with NEA cation with different functionals (PBE+D3, PBE+D3+SOC, HSE06+D3), the scissor operator (χ) defined by $\chi = E_g^{\Gamma-\text{HSE06+D3}} - E_g^{\Gamma-\text{PBE+D3}}$ and the corrected Γ band gap ($E_g^{\Gamma-\text{corr}}$) defined by $E_g^{\Gamma-\text{corr}} = E_g^{\text{PBE+SOC}} + \chi$. All results are in eV.

Structure	$E_g^{\Gamma-\text{PBE+D3}}$	$E_g^{\Gamma-\text{PBE+D3+SOC}}$	$E_g^{\Gamma-\text{HSE06+D3}}$	χ	$E_g^{\Gamma-\text{corr}}$
(S-NEA)$_2$GeCl$_4$	2.73	2.73	3.70	0.97	3.70
(R-NEA)$_2$GeBr$_4$	2.53	2.50	3.43	0.90	3.40
(S-NEA)$_2$GeI$_4$	1.97	1.85	2.56	0.59	2.44
(R-NEA)$_2$SnCl$_4$	2.54	2.53	3.44	0.90	3.43
(R-NEA)$_2$SnBr$_4$	2.09	1.92	2.79	0.70	2.62
(S-NEA)$_2$SnI$_4$	1.67	1.45	2.16	0.49	1.94
(S-NEA)$_2$PbCl$_4$	2.90	2.49	3.75	0.85	3.34
(S-NEA)$_2$PbBr$_4$	2.74	2.18	3.54	0.80	2.98
(S-NEA)$_2$PbI$_4$	2.39	1.79	3.05	0.66	2.45

Table S34: Gamma-point band gap (E_g^{Γ}) analysis for slab chiral hybrid perovskites with NEA cation with different functionals (PBE+D3, PBE+D3+SOC, HSE06+D3), the scissor operator (χ) defined by $\chi = E_g^{\Gamma-\text{HSE06+D3}} - E_g^{\Gamma-\text{PBE+D3}}$ and the corrected Γ band gap ($E_g^{\Gamma-\text{corr}}$) defined by $E_g^{\Gamma-\text{corr}} = E_g^{\text{PBE+SOC}} + \chi$. All results are in eV.

Structure	$E_g^{\Gamma-\text{PBE+D3}}$	$E_g^{\Gamma-\text{PBE+D3+SOC}}$	$E_g^{\Gamma-\text{HSE06+D3}}$	χ	$E_g^{\Gamma-\text{corr}}$
(S-NEA)$_2$GeCl$_4$	2.80	2.80	3.77	0.97	3.77
(R-NEA)$_2$GeBr$_4$	2.62	2.59	3.48	0.84	3.43
(S-NEA)$_2$GeI$_4$	1.93	1.81	2.52	0.59	2.40
(R-NEA)$_2$SnCl$_4$	2.59	2.58	3.48	0.89	3.47
(R-NEA)$_2$SnBr$_4$	2.09	1.94	2.81	0.72	2.66
(S-NEA)$_2$SnI$_4$	1.64	1.43	2.12	0.48	1.91
(S-NEA)$_2$PbCl$_4$	3.05	2.59	3.92	0.87	3.46
(S-NEA)$_2$PbBr$_4$	2.77	2.22	3.58	0.81	3.03
(S-NEA)$_2$PbI$_4$	2.41	1.79	3.05	0.64	2.43

11 Band offsets

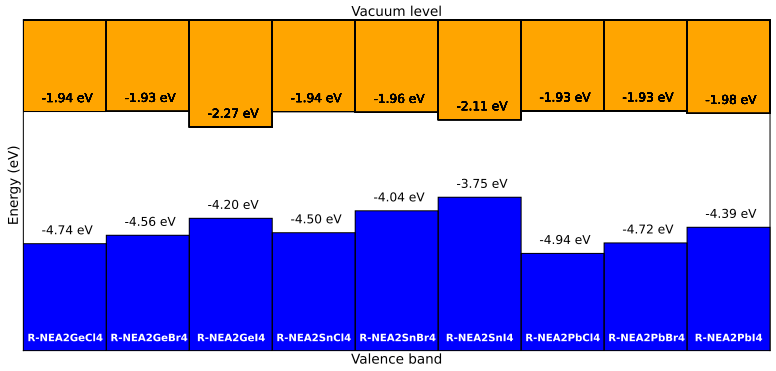

Figure S120: Band offset for R – NEA 2D perovskites with PBE+D3 functional.

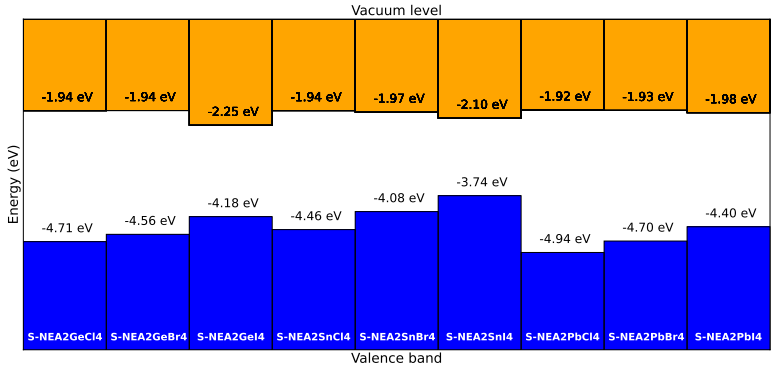

Figure S121: Band offset for S – NEA 2D perovskites with PBE+D3 functional.

12 Spin-splitting

Table S35: Spin-splitting values with k_0 (Å^{-1}) is **k**-point value on lowest energy level of the splitting, E^- and E^+ (eV) are the correspondent energy for splitting, and α_{eff} (eV Å) is the quantization for the splitting[3] which is calculated by $\alpha_{\text{eff}} = \frac{\Delta E^{\pm}}{2k_0}$. Furthermore, $\Delta\theta$ (°) are shown for comparison.

Structure	k_0	E^-	E^+	α_{eff}	$\Delta\theta$
(S-NEA)$_2$GeCl$_4$	0.052632	3.1854	3.2267	0.392350	9.10
(R-NEA)$_2$GeBr$_4$	0.052632	2.6364	2.6746	0.362900	4.43
(S-NEA)$_2$GeI$_4$	0.000000	1.8106	1.8106	–	0.87
(R-NEA)$_2$SnCl$_4$	0.078947	2.6797	2.8755	1.240067	18.11
(R-NEA)$_2$SnBr$_4$	0.105263	1.9224	2.1840	1.242600	16.52
(S-NEA)$_2$SnI$_4$	0.078947	1.4195	1.5762	0.992433	14.12
(S-NEA)$_2$PbCl$_4$	0.105263	2.5896	2.8368	1.174200	21.84
(S-NEA)$_2$PbBr$_4$	0.105263	2.2097	2.4392	1.090125	18.42
(S-NEA)$_2$PbI$_4$	0.078947	1.7921	1.9612	1.070967	16.21

13 Absorption Coefficient

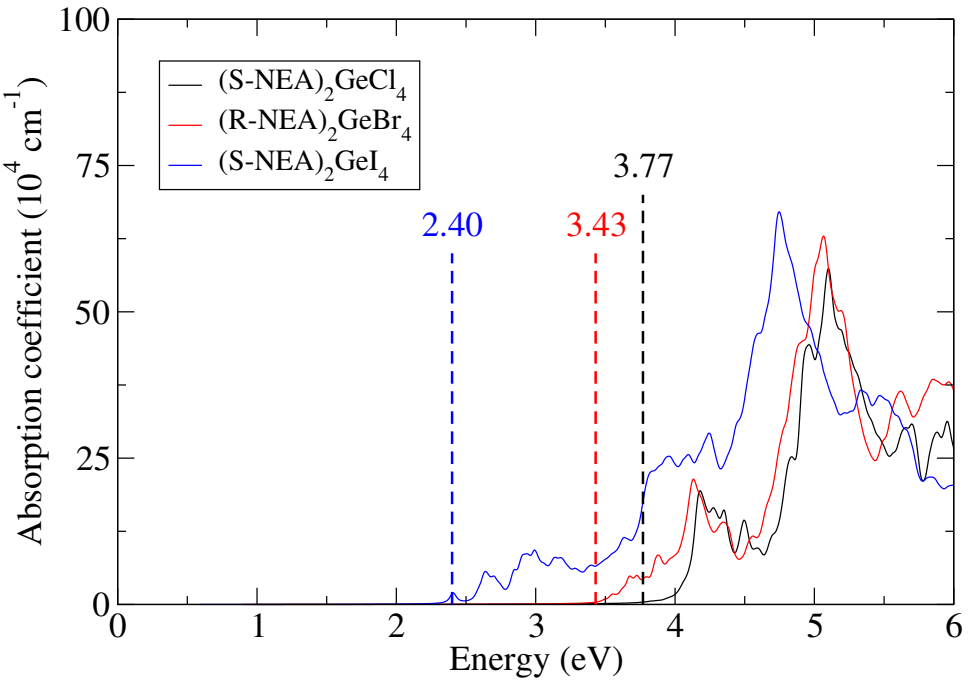

Figure S122: Absorption spectrum calculations for Ge 2D perovskites with PBE+D3+SOC+χ functional. The dashed line represents the direct fundamental band gap values.

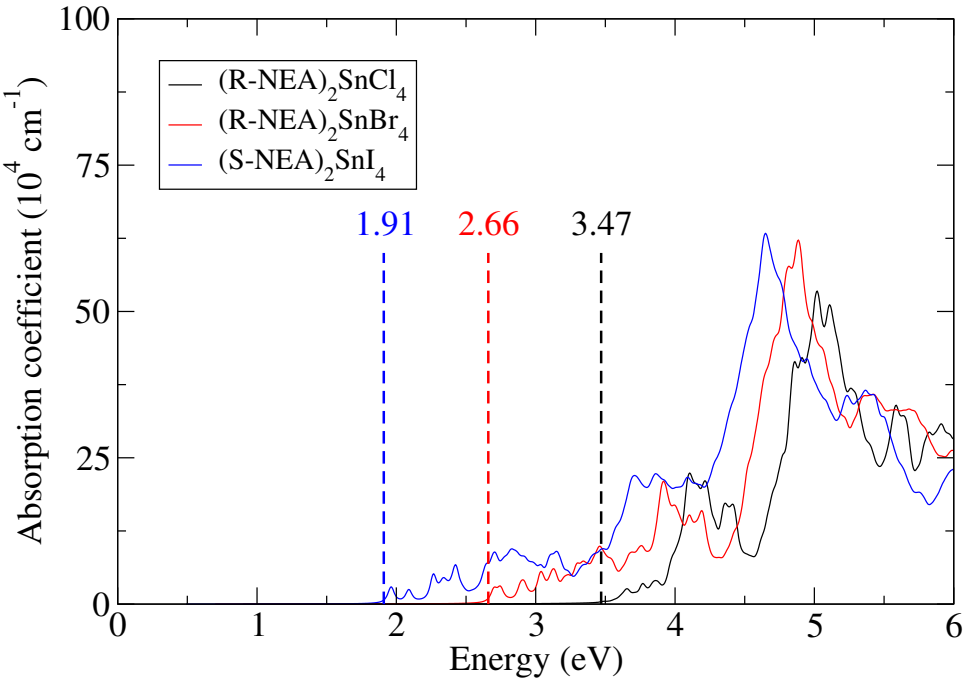

Figure S123: Absorption spectrum calculations for Sn 2D perovskites with PBE+D3+SOC+χ functional. The dashed line represents the direct fundamental band gap values.

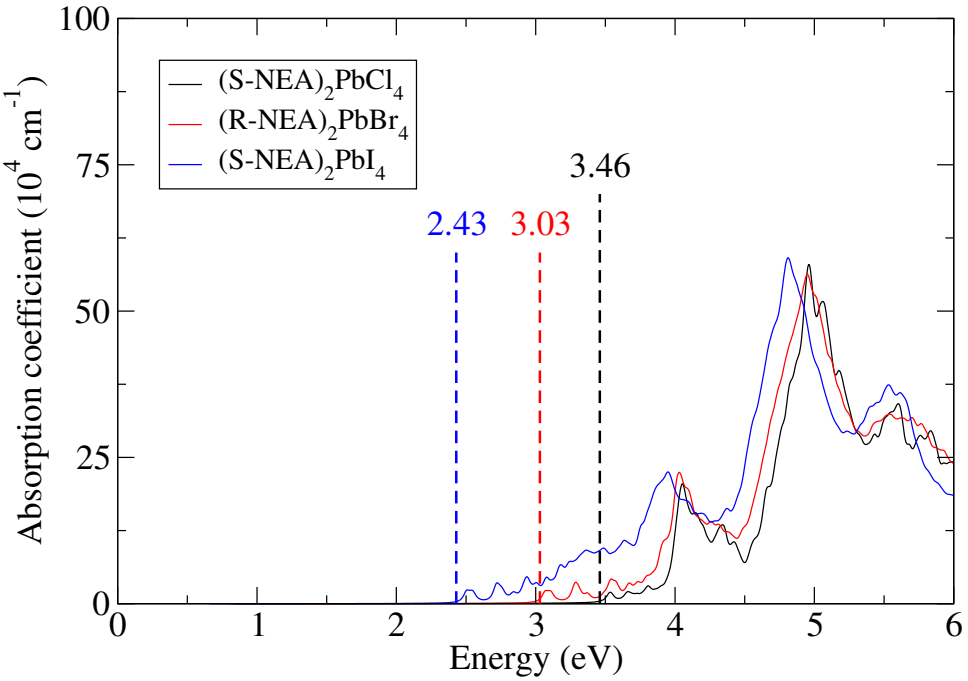

Figure S124: Absorption spectrum calculations for Pb 2D perovskites with PBE+D3+SOC+χ functional. The dashed line represents the direct fundamental band gap values.

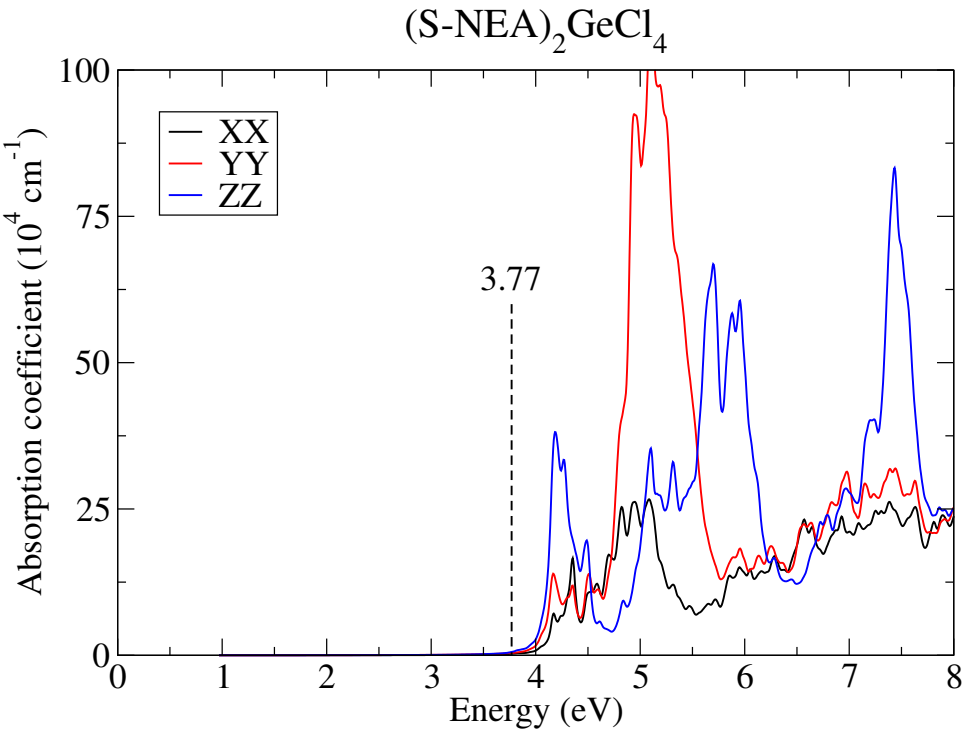

Figure S125: Absorption spectrum on XX, YY and ZZ directions for $(S-NEA)_2GeCl_4$ 2D perovskites with PBE+D3+SOC+χ functional. The dashed line represents the direct fundamental band gap value.

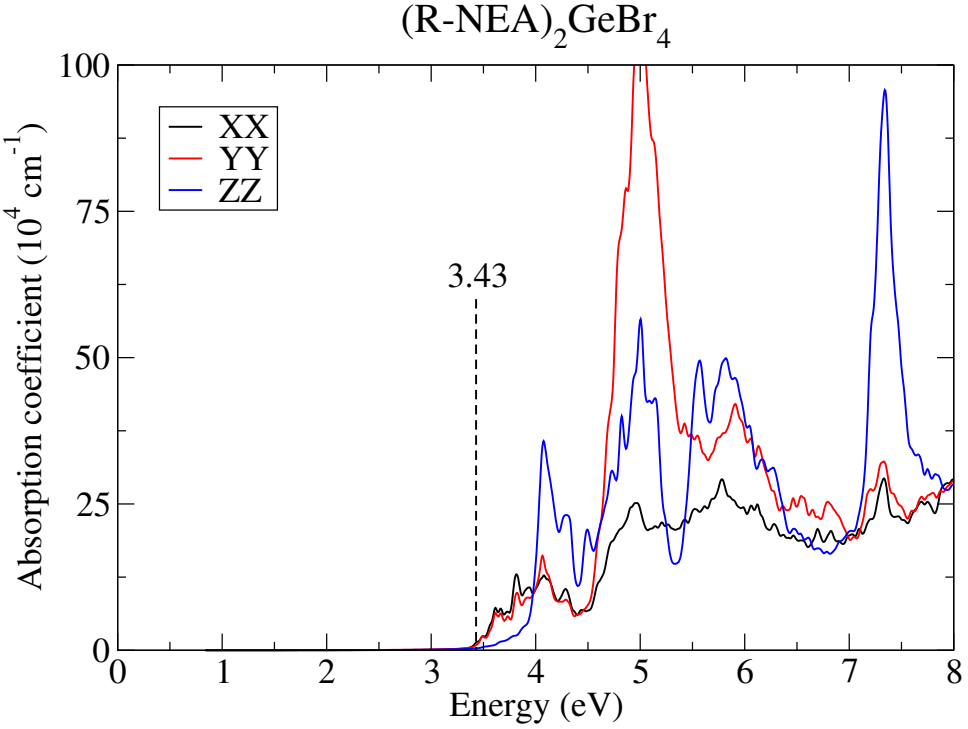

Figure S126: Absorption spectrum on XX, YY and ZZ directions for $(R-NEA)_2GeBr_4$ 2D perovskites with PBE+D3+SOC+χ functional. The dashed line represents the direct fundamental band gap value.

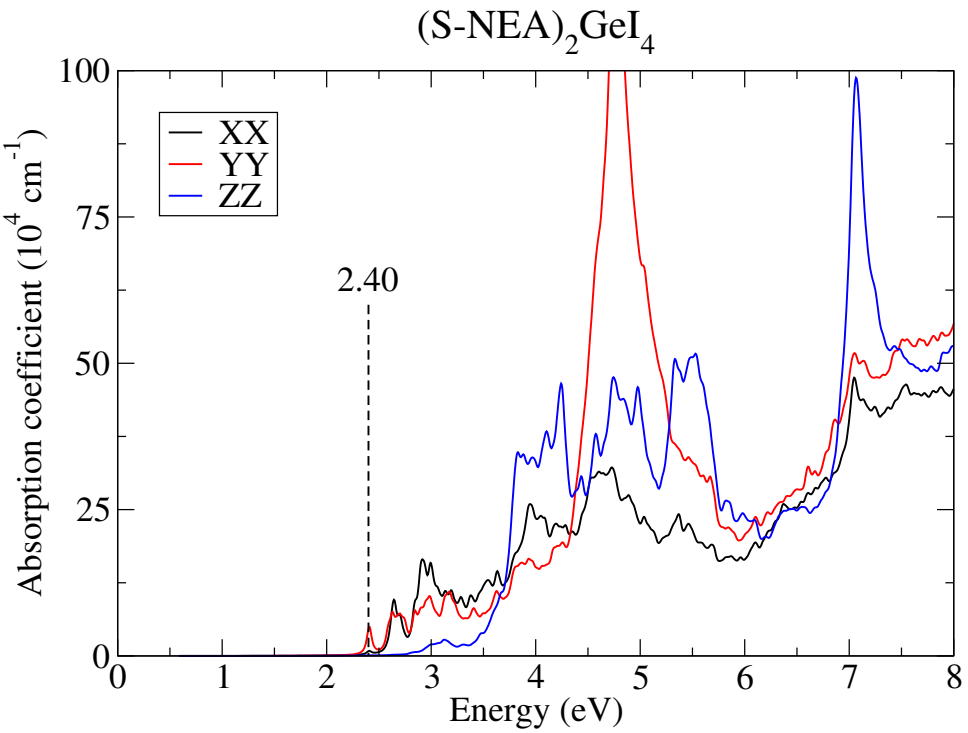

Figure S127: Absorption spectrum on XX, YY and ZZ directions for $(S-NEA)_2GeI_4$ 2D perovskites with PBE+D3+SOC+χ functional. The dashed line represents the direct fundamental band gap value.

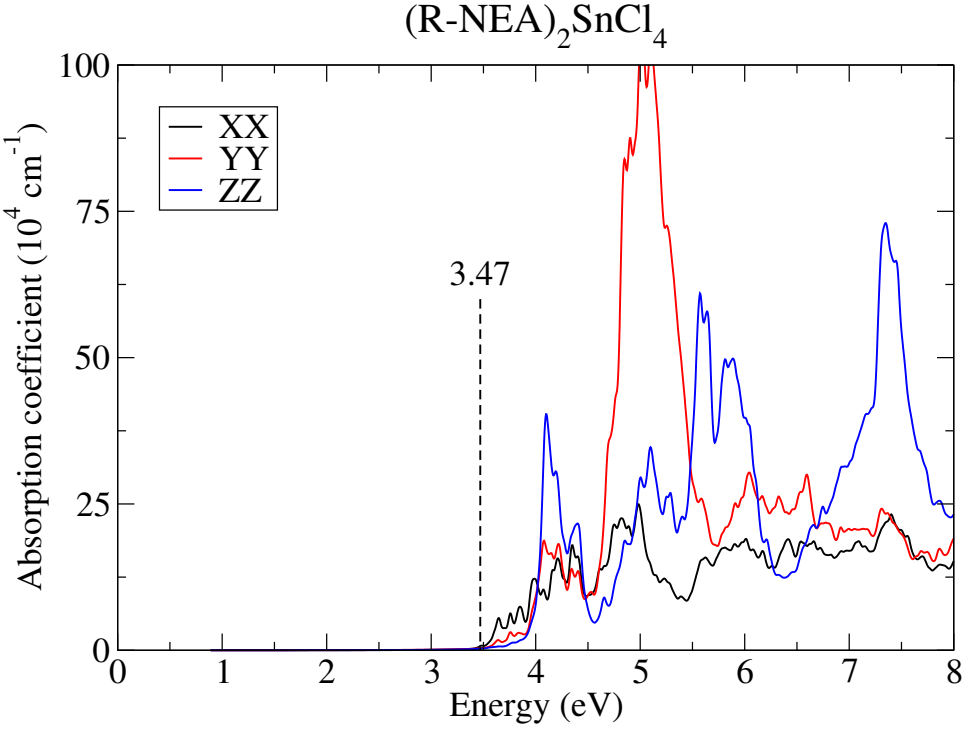

Figure S128: Absorption spectrum on XX, YY and ZZ directions for $(R-NEA)_2SnCl_4$ 2D perovskites with PBE+D3+SOC+χ functional. The dashed line represents the direct fundamental band gap value.

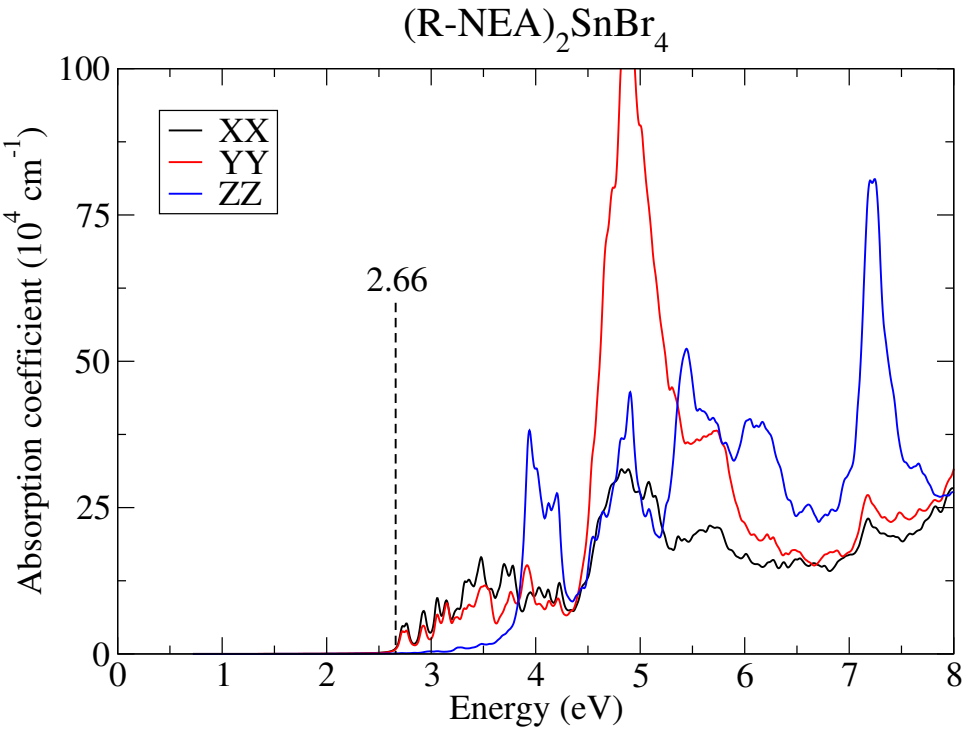

Figure S129: Absorption spectrum on XX, YY and ZZ directions for $(R-NEA)_2SnBr_4$ 2D perovskites with PBE+D3+SOC+χ functional. The dashed line represents the direct fundamental band gap value.

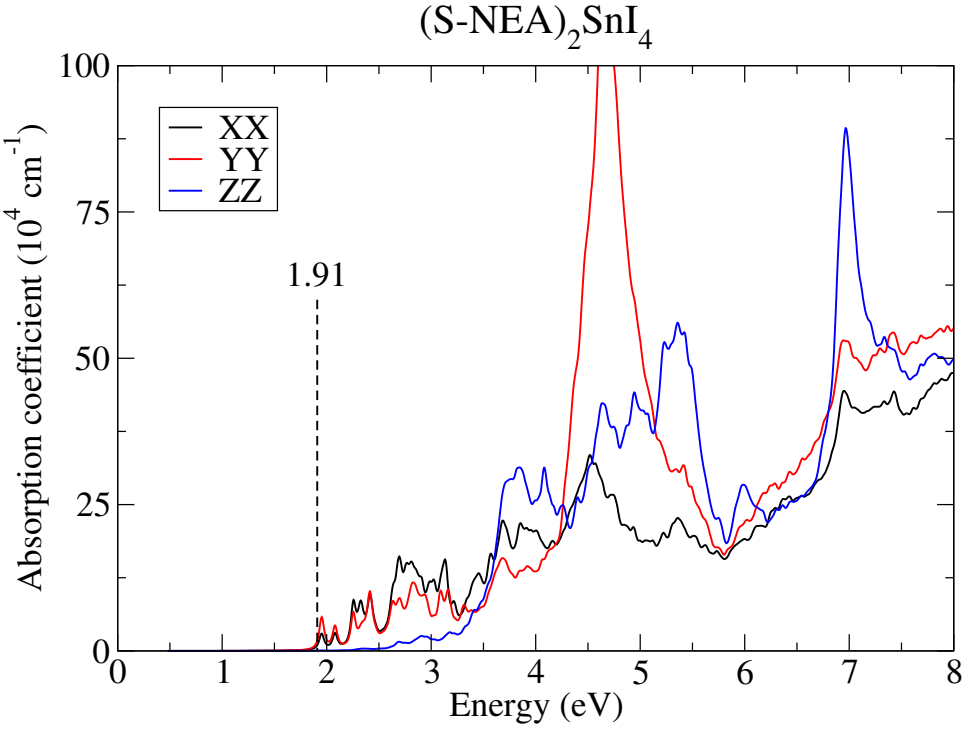

Figure S130: Absorption spectrum on XX, YY and ZZ directions for $(S-NEA)_2SnI_4$ 2D perovskites with PBE+D3+SOC+χ functional. The dashed line represents the direct fundamental band gap value.

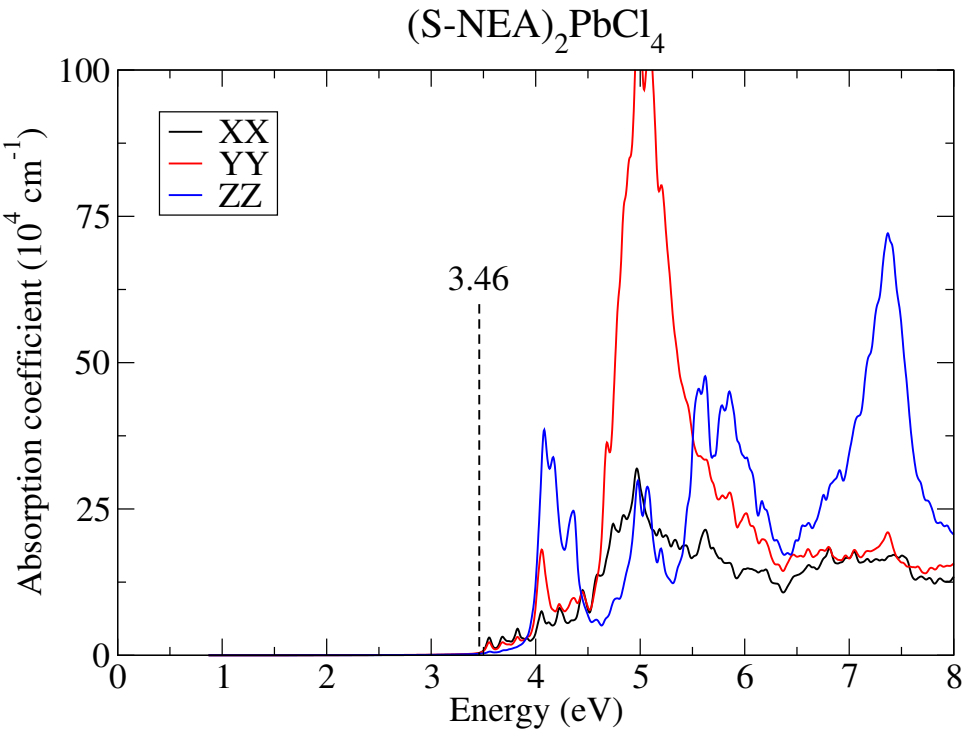

Figure S131: Absorption spectrum on XX, YY and ZZ directions for $(S-NEA)_2PbCl_4$ 2D perovskites with PBE+D3+SOC+χ functional. The dashed line represents the direct fundamental band gap value.

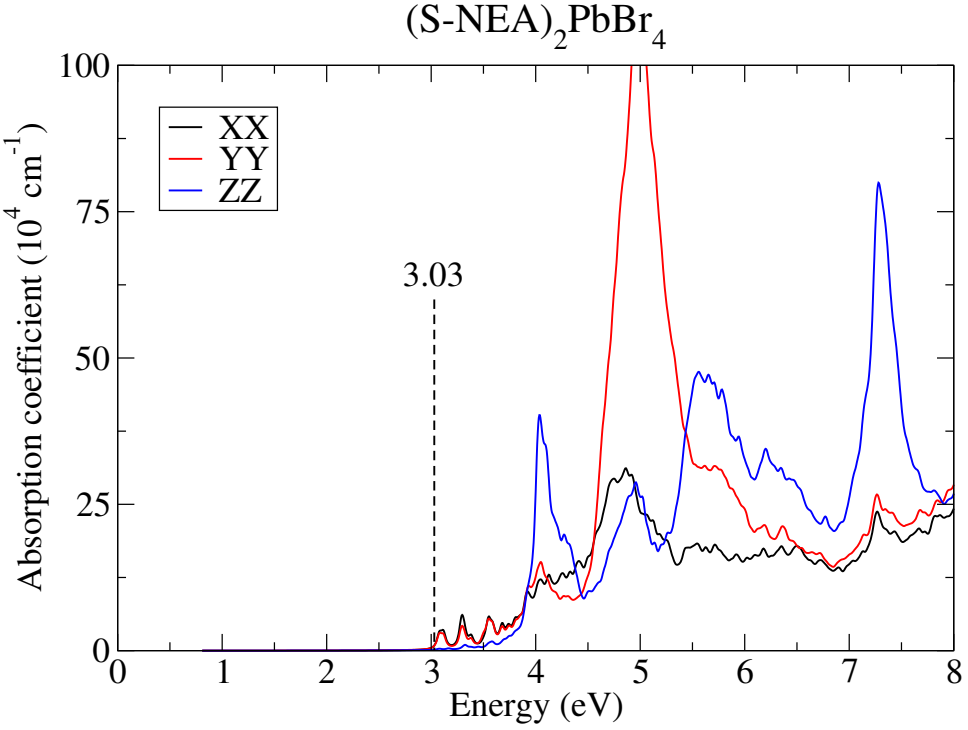

Figure S132: Absorption spectrum on XX, YY and ZZ directions for $(S-NEA)_2PbBr_4$ 2D perovskites with PBE+D3+SOC+χ functional. The dashed line represents the direct fundamental band gap value.

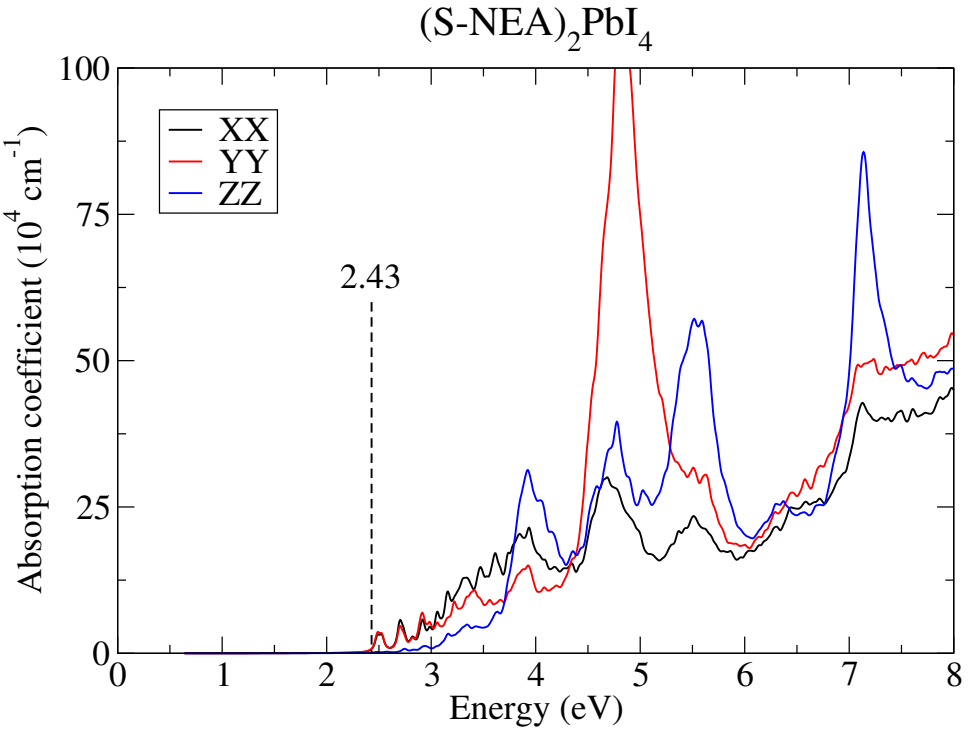

Figure S133: Absorption spectrum on XX, YY and ZZ directions for $(S-NEA)_2PbI_4$ 2D perovskites with PBE+D3+SOC+χ functional. The dashed line represents the direct fundamental band gap value.

References

1 Jana, M. K.; Song, R.; Liu, H.; Khanal, D. R.; Janke, S. M.; Zhao, R.; Liu, C.; Vardeny, Z. V.; Blum, V.; Mitzi, D. B. Organic-to-Inorganic Structural Chirality Transfer in a 2D Hybrid Perovskite and Impact on Rashba-Dresselhaus Spin-Orbit Coupling. *Nat. Commun.* **2020**, *11*, DOI: 10.1038/s41467-020-18485-7.

2 Momma, K.; Izumi, F. *VESTA 3* for Three-Dimensional Visualization of Crystal, Volumetric and Morphology Data. *J. Appl. Crystallogr.* **2011**, *44*, 1272–1276, DOI: 10.1107/s0021889811038970.

3 Jana, M. K.; Song, R.; Xie, Y.; Zhao, R.; Sercel, P. C.; Blum, V.; Mitzi, D. B. Structural Descriptor for Enhanced Spin-Splitting in 2D Hybrid Perovskites. *Nat. Commun.* **2021**, *12*, DOI: 10.1038/s41467-021-25149-7.